

**DOCUMENTATION AND EVALUATION OF THE GEOS-CHEM SIMULATION  
FOR 2002 PROVIDED TO THE VISTAS GROUP**

**Final Report**

Principal Investigator: Daniel J. Jacob, Harvard University  
([djacob@fas.harvard.edu](mailto:djacob@fas.harvard.edu))

Co-Investigators: Rokjin Park and Jennifer A. Logan, Harvard University

June 24, 2005

## TABLE OF CONTENTS

1. PROJECT OBJECTIVE AND PRODUCTS DELIVERED	3
2. DESCRIPTION OF GEOS-CHEM SIMULATIONS FOR VISTAS	3
2.1 The GEOS-Chem Model	3
2.2 Model configuration used for VISTAS	4
2.3 PM sources used in VISTAS simulations	5
2.3.1 Sulfate-nitrate ammonium	5
2.3.3 Carbonaceous aerosols	6
2.3.4 Soil dust	6
2.3.5 Sea salt	6
2.4 Biomass burning emission inventory for 2002	7
2.4.1 The United States and Canada	7
2.4.2 Russia and Kazakhstan	8
2.4.3 Summary	9
3. MODEL PERFORMANCE EVALUATION	9
4. REFERENCES	11
FIGURES	13

Appendix A: Rokjin J. Park, Daniel J. Jacob, Mian Chin, and Randall V. Martin (2003), Sources of carbonaceous aerosols over the United States and implications for natural visibility, *J. Geophys. Res.*, 108(D12), 4355, doi:10.1029/2002JD003190. 22

Appendix B: Rokjin J. Park, Daniel J. Jacob, Brendan D. Field, Robert M. Yantosca, and Mian Chin (2004), Natural and transboundary pollution influences on sulfate-nitrate-ammonium aerosols in the United States: implications for policy, *J. Geophys. Res.*, 109, D15204, doi:10.1029/2003JD004473. 48

## 1. PROJECT OBJECTIVE AND PRODUCTS DELIVERED

The objective of this project was to provide chemical boundary conditions with synoptic-scale resolution from the GEOS-Chem global chemical transport model (CTM) to serve as continental-scale CMAQ regional simulations for 2002 conducted by the VISTAS group. The GEOS-Chem simulations were to include a detailed representation of ozone-NO<sub>x</sub>-VOC-PM chemistry as described by Park et al. [2003, 2004] (appended to this report). They were to replicate the Park et al. [2003, 2004] simulations but with coarser resolution (4°x5° horizontal resolution vs. 2°x2.5°), updated anthropogenic emissions from the EPA NEI 1999, and 2002-specific biomass burning emissions. They were also to include preliminary simulations of soil dust and sea salt. We conducted three full-year simulations for 2002:

1. A *baseline* simulation with best estimates of 2002 emissions;
2. A *background* simulation modified from the baseline by shutting off U.S. anthropogenic<sup>1</sup> emissions;
3. A *natural* simulation modified from the baseline by shutting off anthropogenic emissions worldwide.

3-D concentration fields with 3-hour temporal resolution were archived from each simulation to serve as boundary conditions for CMAQ. A model performance evaluation (MPE) was conducted through comparisons of the baseline simulation to IMPROVE and CASTNET observations in the United States, using the same metrics as in Park et al. [2003, 2004].

## 2. DESCRIPTION OF GEOS-CHEM SIMULATIONS FOR VISTAS

### 2.1. The GEOS-Chem model

The GEOS-Chem model (<http://www-as.harvard.edu/chemistry/trop/geos>) is a cooperative global CTM used by 21 institutions in North America and Europe, and centrally managed by Daniel Jacob's group at Harvard. It is driven by assimilated meteorological observations from the Global Earth Observation System (GEOS) of the NASA Global Modeling and Assimilation Office (GMAO). It is presently being applied to a wide range of atmospheric composition problems including greenhouse gases, oxidants, PM, mercury, and other species. The coupled ozone-NO<sub>x</sub>-VOC-PM version of GEOS-Chem is described in Park et al. [2004] (appendix B). The GEOS-Chem model is documented in over 100 papers in the refereed literature (see above web site for the

---

<sup>1</sup> "Anthropogenic" here includes all fuel, industrial, and agricultural sources; it does not include biomass burning. See Park et al. [2004] for detail on source specifications.

publication list). Evaluations of the global PM simulation are presented in Park et al. [2003, 2004, 2005ab], Li et al. [2005], Alexander et al. [2005], and Heald et al. [2005].

## **2.2. Model configuration used for VISTAS**

The GEOS-Chem simulations for VISTAS used GEOS meteorological observations for the year 2002. These were obtained from GMAO as a 6-hourly archive (3-hour for surface quantities such as mixing depths). The data through August 2002 are from the GEOS-3 assimilation, with horizontal resolution of  $1^\circ \times 1^\circ$  and 55 vertical layers. The data after August 2002 are from the updated GEOS-4 assimilation, with horizontal resolution of  $1^\circ \times 1.25^\circ$  and 48 vertical layers.

GEOS-Chem simulations can be conducted either with the native resolution of the GEOS meteorological data, or with degraded horizontal resolution to reduce computational expense. The Park et al. [2003, 2004] simulations used a  $2^\circ \times 2.5^\circ$  horizontal resolution. Continental-scale simulations for North America have been conducted with the native  $1^\circ \times 1^\circ$  resolution of the GEOS-3 data [Li et al., 2005; Park et al., 2005b]. The VISTAS simulations used a coarser horizontal resolution of  $4^\circ$  latitude  $\times$   $5^\circ$  longitude, as this was considered sufficient to provide boundary conditions outside of North America for use in continental-scale CMAQ simulations. In Fiore et al. [2003], we previously compared ozone simulations for North America using GEOS-Chem with  $4^\circ \times 5^\circ$  and  $2^\circ \times 2.5^\circ$  resolution, and the MAQSIP regional model with  $36 \times 36 \text{ km}^2$  resolution. We found that using the  $4^\circ \times 5^\circ$  resolution of GEOS-Chem significantly degraded the ability of the model to reproduce the observed variability of concentrations over North America, but still maintained the synoptic-scale structure and did not incur a significant continental-scale mean bias.

Significant modifications to the representation of PM sources were made in the VISTAS simulations relative to the work of Park et al. [2003, 2004] and are described in more detail below. They include (1) use of U.S. anthropogenic emissions from the EPA NEI 1999 inventory; (2) use of forest fire information specific to 2002; (3) inclusion of the secondary organic aerosol (SOA) formation mechanism from Chung and Seinfeld [2002]; (4) inclusion of prototype soil dust and sea salt simulations. An additional modification was the application of surface emissions and dry deposition to the GEOS-diagnosed mixed layer column rather than to the surface layer of the model. This was introduced to correct for the effect of 1-hour operator splitting between transport and chemistry (including emissions and dry deposition) in the model, when dealing with a very shallow surface layer (only 10-m deep in GEOS-3). The effect is significant for fast-depositing gases such as  $\text{HNO}_3$  and  $\text{NH}_3$ ; correcting it is an objective model improvement that has since been implemented in the standard version of GEOS-Chem.

Other aspects of the simulation (transport, chemistry, deposition) are as described in Park et al. [2004]. Briefly, transport uses the advection scheme of Lin and Rood [1998], with instantaneous vertical mixing through the local mixing depth, and convective transport computed from GEOS-3 archived convective mass fluxes by replicating the convection algorithm of the parent GEOS general circulation model

(GCM). Natural sources are calculated within the GEOS-Chem simulation as a function of local values of meteorological variables (temperature, insolation, soil moisture, precipitation, wind speed, convective cloud tops). The description of ozone-NO<sub>x</sub>-VOC-PM chemistry includes ~100 chemical species and ~400 chemical reactions. A full documentation of this mechanism is posted as a pdf document on the GEOS-Chem web site ([http://www.env.leeds.ac.uk/%7Emat/GEOS-CHEM/geoschem\\_mech.pdf](http://www.env.leeds.ac.uk/%7Emat/GEOS-CHEM/geoschem_mech.pdf)). Coupling of PM with ozone-NO<sub>x</sub>-VOC oxidant chemistry takes place through sulfate, nitrate, and SOA formation and thermodynamics, aerosol effects on UV actinic fluxes, and heterogeneous radical chemistry. Wet deposition of soluble gases and PM follows the scheme of Liu et al. [2001] and includes contributions from scavenging in convective updrafts, rainout and washout in convective and large-scale precipitation, and partial or total release during re-evaporation below cloud base. Dry deposition is computed with a standard resistance-in-series scheme [Wang et al., 1998].

All simulations were conducted from September 1, 2001 to December 31, 2002. The first four months were used to achieve proper initialization. Results delivered to VISTAS are from the 12-month 2002 simulation.

### **2.3. PM sources used in VISTAS simulations**

We describe here briefly the PM sources used in the VISTAS simulations. Description of the biomass burning emission inventory for 2002 is presented in section 2.4.

#### **2.3.1. Sulfate-nitrate-ammonium**

Global GEOS-Chem budgets of sulfate, nitrate, and ammonium aerosols, including breakdown by source types of emissions for sulfur, NO<sub>x</sub>, and ammonia, are given by Park et al. [2004]. Anthropogenic emissions are from the Global Emission Inventory Activity (GEIA) with 1°x1° spatial resolution and seasonal temporal resolution, and are scaled for individual countries to the year 1998 on the basis of national emission inventories and fuel use statistics. Park et al. [2004] give global totals for non-U.S. anthropogenic emissions computed in this manner. They used the same procedure also for U.S. emissions. For the VISTAS baseline simulation, we used monthly mean anthropogenic U.S. emissions from the NEI 1999 inventory produced by EPA. An archive of monthly mean NEI 1999 emissions from that inventory with 0.25°x0.25° horizontal resolution was generated for us by Alice Gilliland of EPA/ORD, and was re-gridded to 4°x5° for application to VISTAS. The U.S. emission of ammonia in the NEI99 inventory (3.6 Tg N yr<sup>-1</sup>) is known to be too high [Gilliland et al., 2004]. Therefore we retained for that species the U.S. emission inventory of Park et al. [2004] (2.2 Tg N yr<sup>-1</sup>)

Natural emissions except for biomass burning are as given by Park et al. [2004]. Volcanic sulfur emissions are from the GEIA climatology. Emission of dimethylsulfide (DMS) by phytoplankton uses a global distribution of DMS seawater concentrations from Kettle et al. [1999] and a standard sea-air exchange parameterization driven by the local wind. Soil emissions of NO<sub>x</sub> are from GEIA and are function of local temperature and precipitation history. Lightning emissions of NO<sub>x</sub> are computed globally with a standard

algorithm based on convective cloud tops [Wang et al., 1998] and are scaled to yield a global source of 6 Tg N yr<sup>-1</sup> [Martin et al., 2002]. Emissions of ammonia from soils and oceans are from GEIA.

### **2.3.2. Carbonaceous aerosols**

Detailed discussion of the EC and OC emission source processes in the model is given in Park et al. [2003] (appendix A). Anthropogenic emissions of EC and OC outside the U.S. are from the Cooke et al. [1999] inventory. For the VISTAS baseline simulation we used U.S. anthropogenic emissions from Park et al. [2003], who optimized EC and OC sources using monthly IMPROVE observations for 1998. Both EC and OC have major sources from biomass burning; emission factors are from Andreae and Merlet [2001] and are applied to the 2002 biomass burning inventory described in section 2.4. Secondary organic aerosol (SOA) formation from biogenic hydrocarbons follows the scheme of Chung and Seinfeld [2002] developed for application in global models (the Park et al. [2003] simulations simply scaled the SOA source to 10% of monoterpene emission). The Chung and Seinfeld [2002] describes SOA formation from oxidation of several classes of biogenic hydrocarbons through gas-aerosol partitioning of the semi-volatile products as a function of local temperature and pre-existing OC mass concentration.

### **2.3.3. Soil dust**

We included in the VISTAS simulations a preliminary representation of soil dust using the global dust mobilization scheme of Zender et al. [2003]. Dust particles in four different size classes were transported as separate tracers with different source and settling properties, thus allowing in particular some segregation of PM<sub>2.5</sub> and PM<sub>10-2.5</sub>. A global evaluation of this preliminary dust simulation in GEOS-Chem was presented by Fairlie [2004]. Asian and African dust sources are simulated without obvious bias. There is a large overestimate at many IMPROVE sites in fall due to spurious local dust generation from seasonally dry and vegetation-deprived prairie ecosystems.

### **2.3.4. Sea salt**

The sea salt concentrations in the VISTAS simulations are from a new GEOS-Chem capability developed by Alexander et al. [2005]. The simulation uses the standard source scheme of Monahan [1986] which is function of surface wind speed over the oceans, and transports sea salt PM in two size classes (0.1-1 and 1-10 μm). The resulting global source of sea salt in GEOS-Chem is 5400 Tg yr<sup>-1</sup>, consistent with earlier literature (3500-7600 Tg yr<sup>-1</sup>). Alexander et al. [2005] present further discussion of the global sea salt budget and distributions in GEOS-Chem, including comparisons to observations and previous global models.

## 2.4. Biomass burning emission inventory for 2002

### 2.4.1. The United States and Canada

We developed an inventory for emissions from fires in the United States using data for areas burned that are reported by several federal agencies, by regional interagency coordination centers such as the Pacific Northwest, Western Great Basin, Eastern Great Basin, and Southwest ([www.or.blm.gov/nwcc/](http://www.or.blm.gov/nwcc/), [www.nv.blm.gov/wgbcc/](http://www.nv.blm.gov/wgbcc/), [www.blm.gov/utah/egbcc/](http://www.blm.gov/utah/egbcc/), [www.fs.fed.us/r3/fire/](http://www.fs.fed.us/r3/fire/)) and by various states. We also obtained a data base of fires in the southeastern United States from G. Stella of Alpine Geophysics. In the western half of the U.S. and Alaska, most of the land is federally owned, so the fire information is thought to be comprehensive. Reports from the Bureau of Indian Affairs, Bureau of Land Management (BLM), National Park Service, Fish and Wildlife Service, and U.S. Forest Service are available on-line (<http://famweb.nwcc.gov/weatherfirecd>). These reports give the fire name, start and end date, their location (latitude and longitude), and area burned. We analyzed these data to spatially and temporally allocate the fires. A simple concatenation of data was not possible as different agencies sometimes reported the same fires, so we ensured that duplicate reports for the same fire were eliminated. The Daily Incident Management Reports ([www.cidi.org/wildfire](http://www.cidi.org/wildfire)) of the National Interagency Coordination Center (NICC) were consulted to corroborate incidence, location and sizes of major fires, and to determine whether these fires were surface or crown fires.

Our database of all fires with areas larger than 100 acres gives a total of 1626 fires, of which 338 are located in the southeastern states. These fires consumed  $2.65 \times 10^6$  ha in the United States in 2002. The data provided by Alpine Geophysics for the southeast gave a total area of  $0.044 \times 10^6$  ha. Six states accounted for over 80% of the national area burned, namely Alaska, Oregon, Colorado, California, New Mexico, and Arizona. Alaska accounted for one third of the area burned in the United States, and the seven largest fires in Alaska contributed 55% of the area burned for the state. For the entire United States, the largest 20 fires accounted for half the area burned nationally.

The area burned in the United States in 2002 was the second highest for the previous ten years. To put the area burned in a larger context, the area burned in Canada was similar to that in the United States,  $2.76 \times 10^6$  ha, while  $2.8 \times 10^6$  ha burned in Kazakhstan, and  $11 \times 10^6$  ha in Asiatic Russia. It was also a very high fire year in Russia.

For our initial estimate of the amount of dry matter burned (used in the GEOS-CHEM simulations) we adopted a loading  $2.6 \text{ kg DM/m}^2$  for Alaskan fires, and  $1.8 \text{ kg DM/m}^2$  for the lower states. We found that 47 Tg of dry matter was consumed by fires in the United States, producing CO emissions of 5 Tg in about 3 months. We developed preliminary maps of dry matter burned on a  $1^\circ \times 1^\circ$  grid by month by assuming that each fire burned at the same rate during each day of the burn period.

For Canada, we relied on a product provided by David Lavoue (Environment Canada). He is developing an inventory for Canada using a detailed data-base on the location of the size and position of the fires; that data-base is not yet publicly available. He gave us an interim product that consists of monthly totals of fuel consumed on a map

with resolution of 1°x1° latitude by longitude. Lavoue estimates that 58 Tg of dry matter was consumed by fires in 2002, which gives rise to CO emissions of 7 Tg..

#### 2.4.2. Russia and Kazakhstan

The most detailed fire information was available for eastern Russia. The IFFN report ([http://www.fire.uni-freiburg.de/iffn/iffn\\_28/Russia-1.pdf](http://www.fire.uni-freiburg.de/iffn/iffn_28/Russia-1.pdf)) gives estimates by province of the total areas burned in Asian Russia for the fire season of 2002. The total area burned was 11 x 10<sup>6</sup> ha. The Fire Laboratory of the Sukachev Institute of Forest, Krasnoyarsk, provides maps showing the locations of large fires for 10-day periods derived from NOAA AVHRR data (<http://www.fire.uni-freiburg.de/current/archive/archive.htm>). We used these maps to spatially and temporally apportion the area burned in each province among all of the fires logged for the province; burn scars at the end of the fire season were approximated as rectangles. The areas burned were put on a grid of 1°x1° (lat. x long.) for each 10 day period. The Kamchatka Peninsula was not included on the burning maps for eastern Russia. Areas burned there were confined to June and July (IFFN report). Maps of ATSR fire counts were used to locate the fires.

Most of the burning in Russia was in July-August in the northern province of Yakutia. There was a smaller peak in the burning in May, primarily in the provinces of southern Siberia. We relied on a detailed vegetation map of Russia to determine the dominant vegetation type in each gridbox, and applied appropriate fuel loads to determine the amount of biomass burned.

Table 1. Loadings used for fires in Russia, in kg dry matter (DM) m<sup>-2</sup>

Vegetation Type	kg DM m <sup>-2</sup>
Tundra	1.8
Wooded Tundra	2.0
Taiga	2.5
Boreal Forest	3.0
Grasslands	0.3
Steppe	0.3
Desert	0.3
Farmlands	0.3

Recent work indicates the importance of including the burning of peat as a component of boreal fires. We track peat burning separately from burning of other forest fuels as it has a higher moisture content, hence less efficient combustion, and higher emission factors for CO. The construction of peatland map is in progress for Russia (L. Pozdnyakova, personal communication), there is not one currently available. As a surrogate, we used maps of wetlands and soil drainage to give the distribution of boggy or poorly drained soils, as advised by S. Conard and M. Turetsky. The locations of individual fires given by the remote sensing data were superimposed on this map; burning of peat was confined to the area defined by the perimeter of the fires. Few

experiments have been reported which describe measurements of fuel consumed and emissions from peat fires in boreal forests. We assumed that  $2.2 \text{ kg C m}^{-2}$  was burned.

For western Russia, wildfires other than peat bog fires were not reported in sufficient detail to ascertain their whereabouts. Qualitative descriptions of major peat bog fires in July to September around Moscow, St. Petersburg, Nizhny Novgorod, and other cities were abundant, but few estimates of areas burned and depth of peat burned were found. From the IFFN news and CNN reports, we used quantitative and qualitative information to approximate the areas burned in the peat bogs around four of the major cities. We distributed the burning homogeneously in the oblast (province) that contained each city and applied a fuel consumption estimate for peat burning as above.

Maps of fires for each month and the annual amount burned ( $2.8 \times 10^6 \text{ ha}$ ) were available for Kazakhstan. Here also, ATSR fire counts were used to locate the fires on a monthly basis. We used a vegetation map for Kazakhstan [[http://www.fire.unifreiburg.de/iffn/country/kz/kz\\_2\\_1b.gif](http://www.fire.unifreiburg.de/iffn/country/kz/kz_2_1b.gif)] and an agricultural map of the CIS (Major World Crop Areas and Climatic Profiles) to determine the fuel loads to use. Based on these maps, we postulated that the fires in the southern regions were burning of agricultural residues, for which we adopted a loading of  $1.2 \text{ kg DM m}^{-2}$ ; for the pine forests in the north, we adopted a loading recommended for Kazakhstan's pine forests,  $2 \text{ kg DM m}^{-2}$ .

### **2.4.3. Summary**

We find that 409 Tg dry matter was consumed in Russia, 52 Tg in Kazakhstan, and 47 Tg in the United States. For Canada, Lavoue's estimate of 58 Tg of dry matter consumed in 2002 is low in comparison to our estimate for Russia, given the ratio of areas. Lavoue did not include burning of peat in Canada as he believes it is not an important component of the Canadian fires (personal communication). These estimates were used in the GEOS-CHEM simulations to provide monthly emissions from biomass burning. In other regions we relied on the work of Van der Werf et al. (Science, 2003), based on VIRS satellite data.

## **3. MODEL PERFORMANCE EVALUATION**

Model performance evaluation (MPE) of the baseline VISTAS simulation focused on the annual and seasonal PM concentration statistics previously reported by Park et al. [2003, 2004] using observations from IMPROVE and CASTNET sites. The Park et al. simulations were conducted for 1998 and 2001, whereas the VISTAS simulation was for 2002. We use here observations from 145 IMPROVE sites and 84 CASTNET sites available for 2002.

The limitations of using U.S. concentration data to evaluate a global PM simulation with  $4^\circ \times 5^\circ$  horizontal resolution should be stressed. Any variability on scales less than  $\sim 500 \text{ km}$  cannot be resolved. This compromises the evaluation for individual sites, particularly in urban, industrial, and coastal regions. We focus therefore our evaluation on the large-scale spatial distribution and on seasonal statistics for the national

ensemble of sites. The evaluation figures shown here reproduce similar figures presented by Park et al. [2003, 2004] for their 1998 and 2001 simulations with  $2^{\circ} \times 2.5^{\circ}$  resolution. Direct comparison to these figures can therefore be made to assess the relative quality of the simulations. We use the slopes of the regression lines in the simulated vs. observed scatterplots to diagnose mean biases in the model. Regression lines are computed with the reduced major axis method [Hirsch and Gilroy, 1984].

Figure 1 compares simulated and observed annual mean sulfate concentrations at the ensemble of IMPROVE and CASTNET sites for the year 2002, plotted on the  $4^{\circ} \times 5^{\circ}$  model grid. Values are highest in the industrial midwest, in both model and observations, reflecting the distribution of anthropogenic emissions. Figure 2 shows scatterplots of simulated vs. observed annual and seasonal sulfate concentrations for the ensemble of (left) IMPROVE and (middle) CASTNET sites. The right column in Figure 2 compares simulated and observed sulfate precipitation data for 2002 at NADP sites. The correlation between model and observations is high for the annual mean values ( $R^2 = 0.82$  for the concentration data and  $0.71$  for the deposition data) and also for the seasonal means ( $R^2 = 0.63$ – $0.87$  for the concentration data). An exception is the deposition data in summer, for which correlation between model and observations is low ( $R^2 = 0.18$ ). Overall, the correlations presented here are consistent with those presented by Park et al. [2004] for 2001 (see Figures 3 and 4 of appendix B) although that simulation was more successful in capturing the variance in summer deposition.

Figure 3 compares simulated and observed annual mean concentrations of ammonium at CASTNET sites. Observed concentrations are higher in the east than in the west and are highest in the midwest, reflecting agricultural operations. The model reproduces this spatial distribution. Scatterplots of simulated vs. observed annual and seasonal ammonium concentrations are shown in Figure 4 for the ensemble of sites. The model reproduces the variability of observed ammonium concentrations, both in an annual mean sense ( $R^2 = 0.81$ ) and in different seasons ( $R^2 = 0.72$ – $0.81$ ). The  $R^2$  values are slightly lower than the values from the Park et al. [2004] simulation (Figure 6 of appendix B). That simulation showed a factor of 2 high bias in fall due to too high seasonal ammonia emission. Despite the same ammonia emission, the VISTAS simulation shows much reduced bias (50% for ammonium concentration in fall). This reflects in part the increase in the effective ammonia deposition velocity resulting from application of the dry deposition sink throughout the mixed layer column, as described in section 2.2.

Figure 5 compares simulated and observed annual mean nitrate concentrations at the IMPROVE and CASTNET sites. Maximum concentrations are in the Midwest, reflecting the limitation of ammonium nitrate formation by the availability of ammonia. The model captures the observed spatial distribution of nitrate concentrations but tends to be high on an annual mean basis (slope =  $1.41$ – $1.80$  in Figure 4). This is however also an improvement over Park et al. [2004], which found a factor of 2 high bias (slope =  $1.87$  –  $2.43$  in Figure 6 of appendix B), and reflects the improved treatment of  $\text{HNO}_3$  dry deposition. The high bias in the VISTAS simulation is mainly driven by the fall months, when the model appears to produce too much ammonium nitrate due to too high ammonia emission [Park et al., 2004].

Figure 6 compares simulated and observed annual mean concentrations of EC at IMPROVE sites, and the scatterplots of Figure 7 compare seasonal mean concentrations. The model reproduces about half of the observed spatial variability in different seasons ( $R^2 = 0.42-0.58$ ) except in summer ( $R^2 = 0.18$ ). Simulated concentrations tend to be higher than observed (slope = 1.58-1.74) except in summer (slope = 0.76). The high bias is mostly driven by IMPROVE sites in the northeastern corridor.

Figure 8 compares simulated and observed annual mean concentrations of organic carbon mass (OMC) at IMPROVE sites, and Figure 9 shows the seasonal scatterplots. Although the ability of the model to reproduce variability in the observations is poor, particularly in summer, the simulated seasonal mean concentrations are generally within a factor of two of observations. The simulation is significantly worse than that described by Park et al. [2003]; this reflects the use of the Chung and Seinfeld [2002] SOA parameterization, which appears to underestimate the source from vegetation.

Overall, the MPE conducted for the VISTAS simulation for the U.S. shows the level of agreement that can be expected considering the state of the science in large-scale aerosol modeling and the intrinsic limitations of a simulation with  $4^\circ \times 5^\circ$  horizontal resolution. Simulated concentrations are mainly within a factor of 2 of observations on regional and seasonal scales, and can generally account (except for OC) for most of the observed variability on those scales.

#### 4. REFERENCES

- Alexander, B., R. J. Park, D. J. Jacob, Q. B. Li, R. M. Yantosca, J. Savarino, C. C. W. Lee, and M. H. Thiemens (2005), Sulfate formation in sea-salt aerosols: Constraints from oxygen isotopes, *J. Geophys. Res.*, 110, D10307, doi:10.1029/2004JD005659.
- Andreae, M. O. and P. Merlet (2001), Emission of trace gases and aerosols from biomass burning, *Global Biogeochem. Cycles*, 15(4), 955-966.
- Chung, S. H. and J. H. Seinfeld (2002), Global distribution and climate forcing of carbonaceous aerosols, *J. Geophys. Res.*, 107(D19), 4407, doi:10.1029/2001JD001397.
- Cooke, W.F., C. Liousse, H. Cachier, and J. Feichter (1999), Construction of a  $1^\circ \times 1^\circ$  fossil fuel emission data set for carbonaceous aerosol and implementation and radiative impact in the ECHAM-4 model, *J. Geophys. Res.*, 104, 22,137-22,162.
- Fairlie T. D. (2004), Transpacific Transport of Mineral Dust from Asia During Spring 2001, presented at the American Geophysical Union Spring Meeting in Montreal, May 19, 2004.
- Fiore, A. M., D. J. Jacob, R. Mathur, and R. V. Martin (2003), Application of empirical orthogonal functions to evaluate ozone simulations with regional and global models, *J. Geophys. Res.*, 108, 4431, doi: 10.1029/2002JD003151.
- Heald, C.L., D.J. Jacob, R.J. Park, L.M. Russell, B.J. Huebert, J.H. Seinfeld, H. Liao and R.J. Weber (2005), A large organic aerosol source in the free troposphere missing from current models, submitted to *Geophys. Res. Lett.*
- Hirsch, R. M., and E. J. Gilroy (1984), Methods of fitting a straight line to data: examples in water resources, *Water Res. Bull.*, 20, 705-711.

- Kettle, A. J., et al. (1999), A global database of sea surface dimethylsulfide (DMS) measurements and a procedure to predict sea surface DMS as a function of latitude, longitude, and month, *Glob. Biogeochem. Cycle*, 13(2), 399-444.
- Li, Q., D. J. Jacob, R. Park, Y. Wang, C. L. Heald, R. Hudman, R. M. Yantosca, R. V. Martin, and M. Evans (2005), North American pollution outflow and the trapping of convectively lifted pollution by upper-level anticyclone, *J. Geophys. Res.*, 110, D10301, doi:10.1029/2004JD005039.
- Lin, S.-J., and R. B. Rood (1996), Multidimensional flux-form semi-Lagrangian transport schemes, *Mon. Wea. Rev.*, 124, 2046-2070.
- Liu, H., D. J. Jacob, I. Bey, and R. M. Yantosca (2001), Constraints from  $^{210}\text{Pb}$  and  $^7\text{Be}$  on wet deposition and transport in a global three-dimensional chemical tracer model driven by assimilated meteorological fields, *J. Geophys. Res.*, 106, 12,109-12,128.
- Martin, R.V., K. Chance, D.J. Jacob, T.P. Kurosu, R.J.D. Spurr, E. Bucsela, J.F. Gleason, P.I. Palmer, I. Bey, A.M. Fiore, Q.B. Li, R.M. Yantosca, and R.B.A. Koелеmeijer (2002), An improved retrieval of tropospheric nitrogen dioxide from GOME, *J. Geophys. Res.*, 107(D20), 4437, 10.1029/2001JD001027.
- Monahan, E. C., D. E. Spiel, and K. L. Davidson (1986), A model of marine aerosol generation via whitecaps and wave disruption, in *Oceanic Whitecaps and Their Role in Air-Sea Exchange Processes*, edited by E. C. Monahan and G. M. Niocaill, pp. 167-174, Springer, New York.
- Park, R. J., D. J. Jacob, M. Chin and R. V. Martin (2003), Sources of carbonaceous aerosols over the United States and implications for natural visibility, *J. Geophys. Res.*, 108(D12), 4355, doi:10.1029/2002JD003190.
- Park, R. J., D. J. Jacob, B. D. Field, R. M. Yantosca, and M. Chin (2004), Natural and transboundary pollution influences on sulfate-nitrate-ammonium aerosols in the United States: implications for policy, *J. Geophys. Res.*, D15204, 10.1029/2003JD004473.
- Park, R. J., D.J. Jacob, P.I. Palmer, A.D. Clarke, R.J. Weber, M.A. Zondlo, F.L. Eisele, A.R. Bandy, D.C. Thornton, G.W. Sachse, and T.C. Bond (2005a), Export efficiency of black carbon aerosol in continental outflow: global implications, *J. Geophys. Res.*, 110, D11205, doi:10.1029/2004JD005432.
- Park, R. J., D. J. Jacob, et al. (2005b), Natural and transboundary pollution influences on variability of regional visibility in the United States, manuscript in preparation.
- Wang, Y., D. J. Jacob, and J. A. Logan (1998), Global simulation of tropospheric  $\text{O}_3$ - $\text{NO}_x$ -hydrocarbon chemistry, 1. Model formulation, *J. Geophys. Res.*, 103(D9), 10,713-10,726.
- Zender, C. S., H. Bian, and D. Newman (2003), Mineral Dust Entrainment and Deposition (DEAD) model: Description and 1990s dust climatology, *J. Geophys. Res.*, 108(D14), 4416, doi:10.1029/2002JD002775.

Figure 1. Annual mean concentrations of sulfate in surface air over the United States in 2002. The top panel shows results from the GEOS-CHEM model. The middle and bottom panels show the observations from the IMPROVE and CASTNET networks, respectively, averaged over the model  $4^\circ \times 5^\circ$  grid.

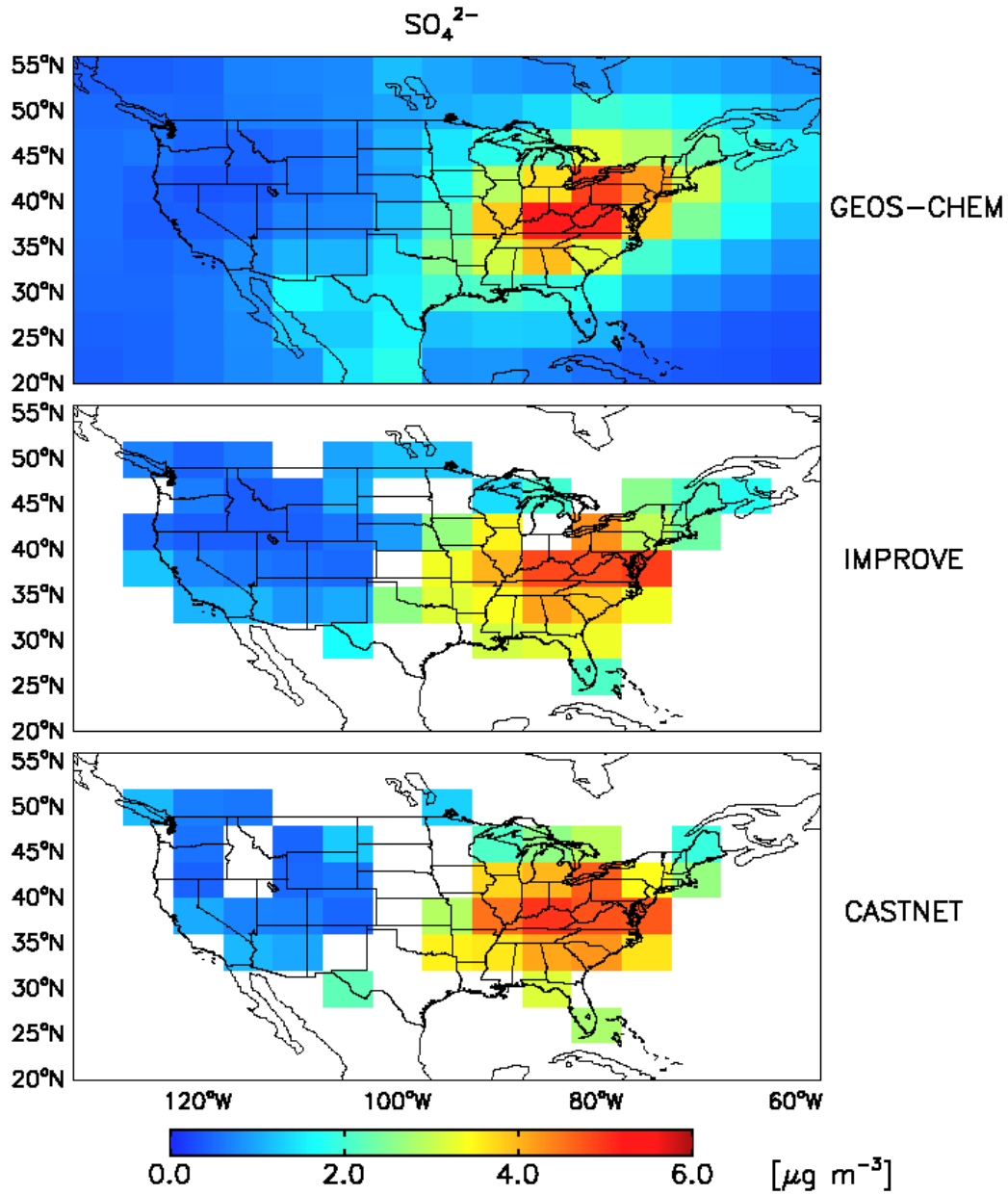


Figure 2. Scatterplot of simulated versus observed sulfate concentrations at the IMPROVE and CASTNET sites, and sulfate deposition fluxes at NADP sites. Values are annual means (top panels) and seasonal means for 2002. Sites in the western and eastern United States (separated at 95°W) are shown as pluses and open circles, respectively. Thick solid lines are reduced major axis regressions for the ensemble of the data; regression equations and  $R^2$  are shown inset. Thin solid lines show the  $y=x$  relationship.

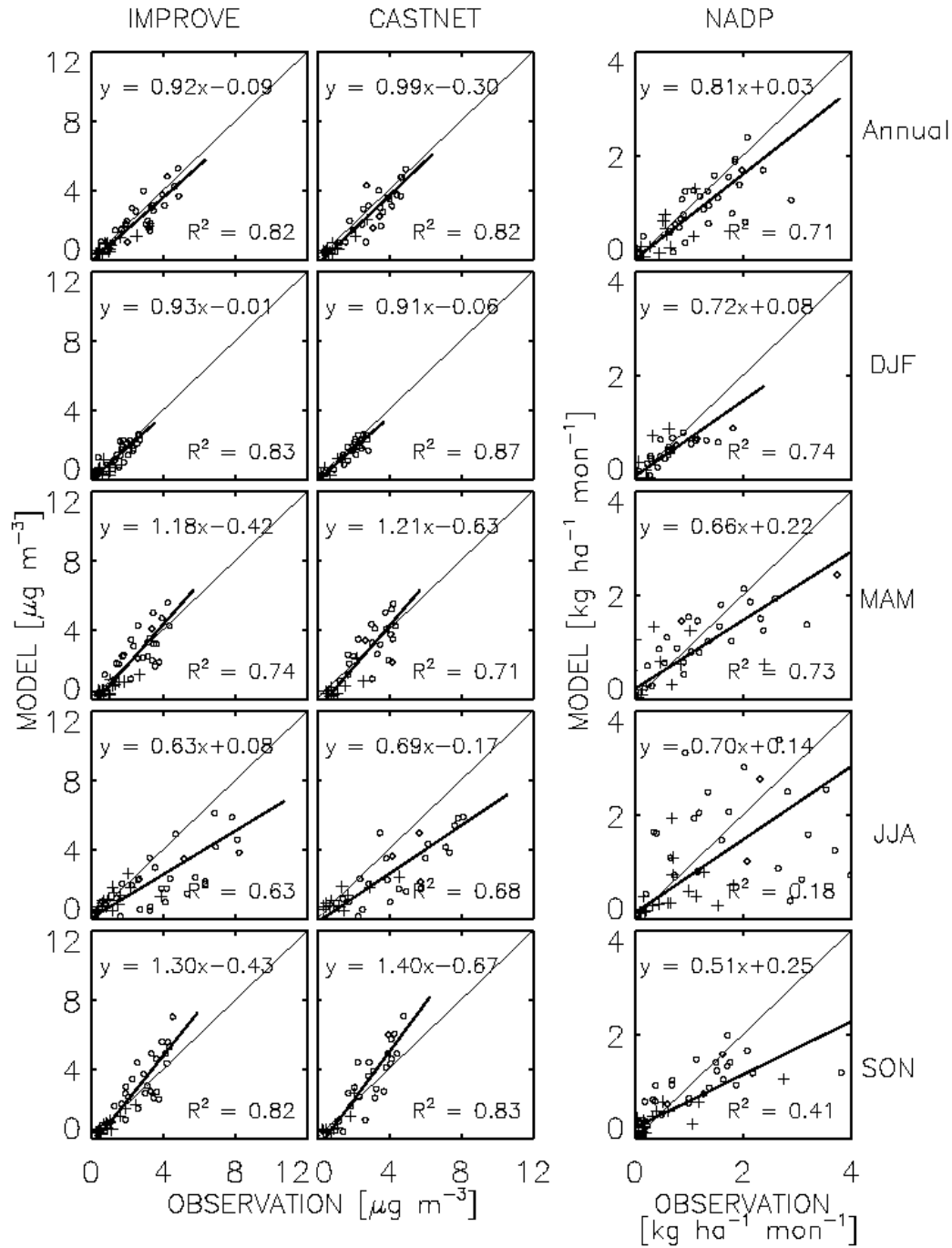


Figure 3. Annual mean concentrations of ammonium in surface air over the United States in 2002. The top panel shows results from the GEOS-CHEM model. The bottom panel shows the observations from the CASTNET network.

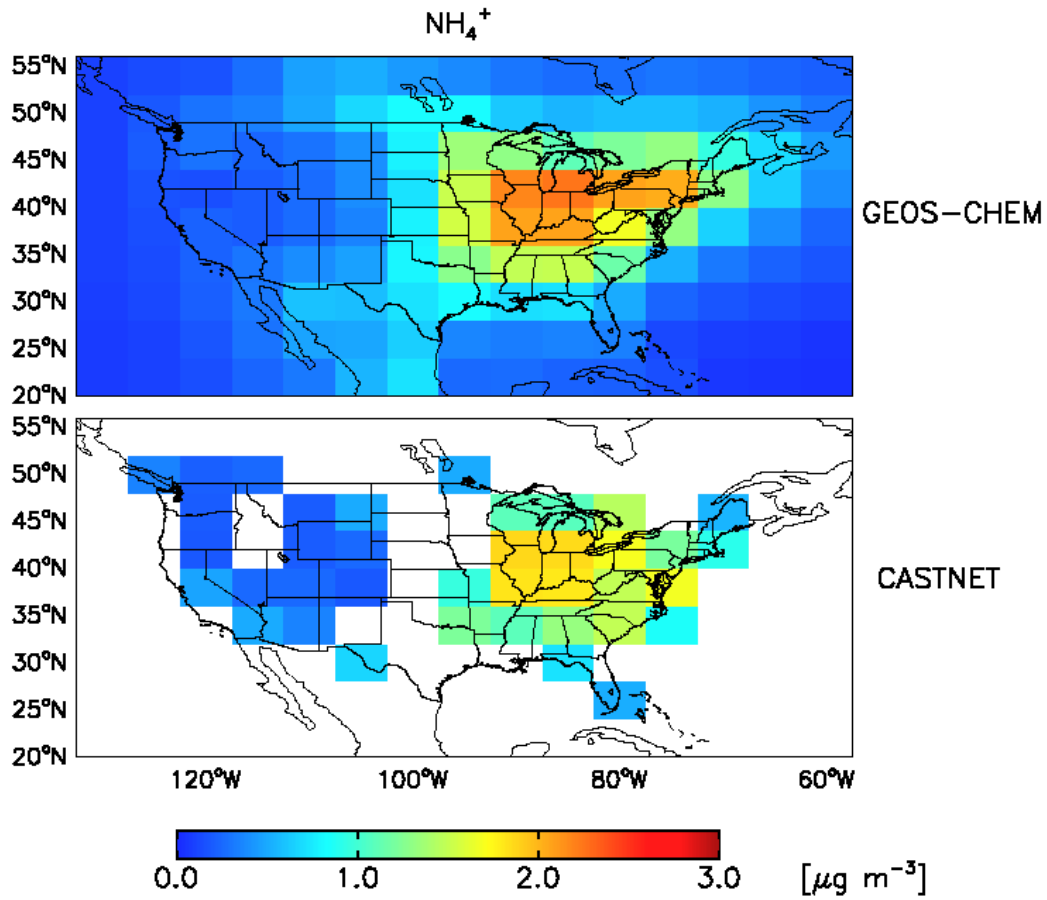


Figure 4. Scatterplot of simulated versus observed ammonium concentrations at the CASTNET sites (left column), and nitrate concentrations at the CASTNET and IMPROVE sites (right two columns). Values are annual means (top panels) and seasonal means for 2002. Sites in the western and eastern United States (separated at 95°W) are shown as pluses and open circles, respectively. Thick solid lines are reduced major axis regressions for the ensemble of the data; regression equations and  $R^2$  are shown inset. Thin solid lines show the  $y=x$  relationship.

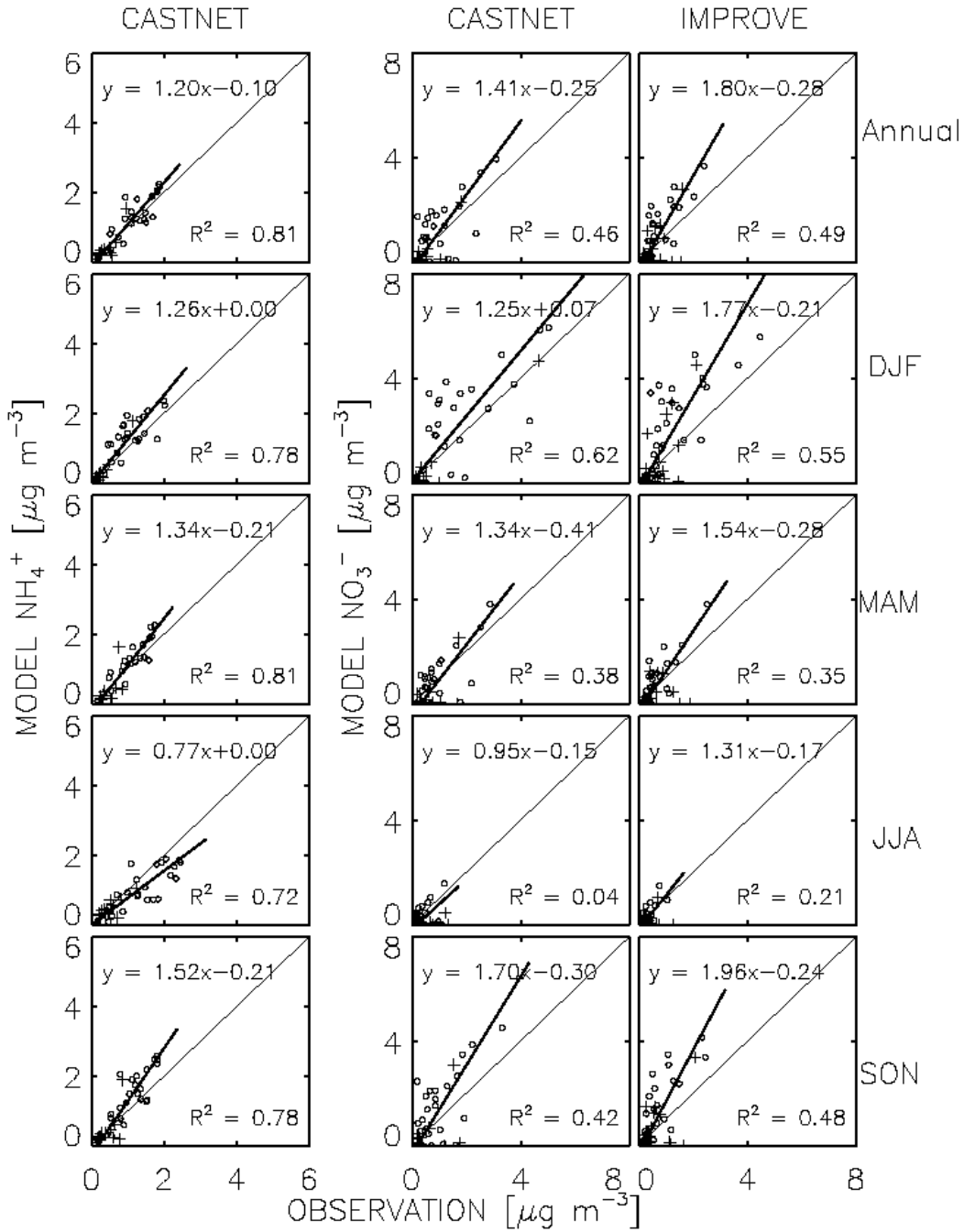


Figure 5. Same as Figure 3 but for nitrate.

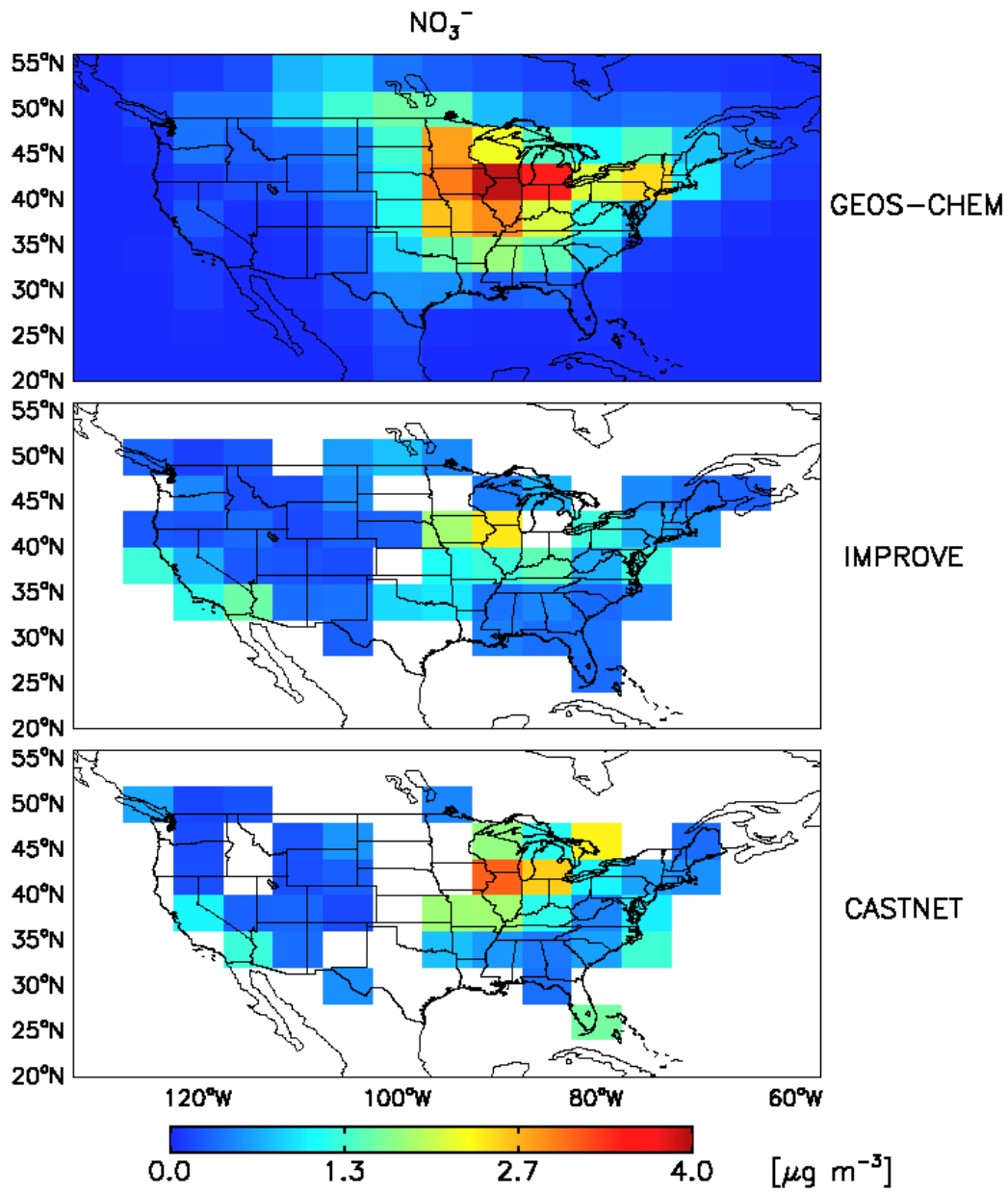


Figure 6. Annual mean concentrations of elemental carbon (EC) aerosol in surface air over the United States in 2002. The top panel shows results from the GEOS-CHEM model. The bottom panel shows the observations from the IMPROVE network.

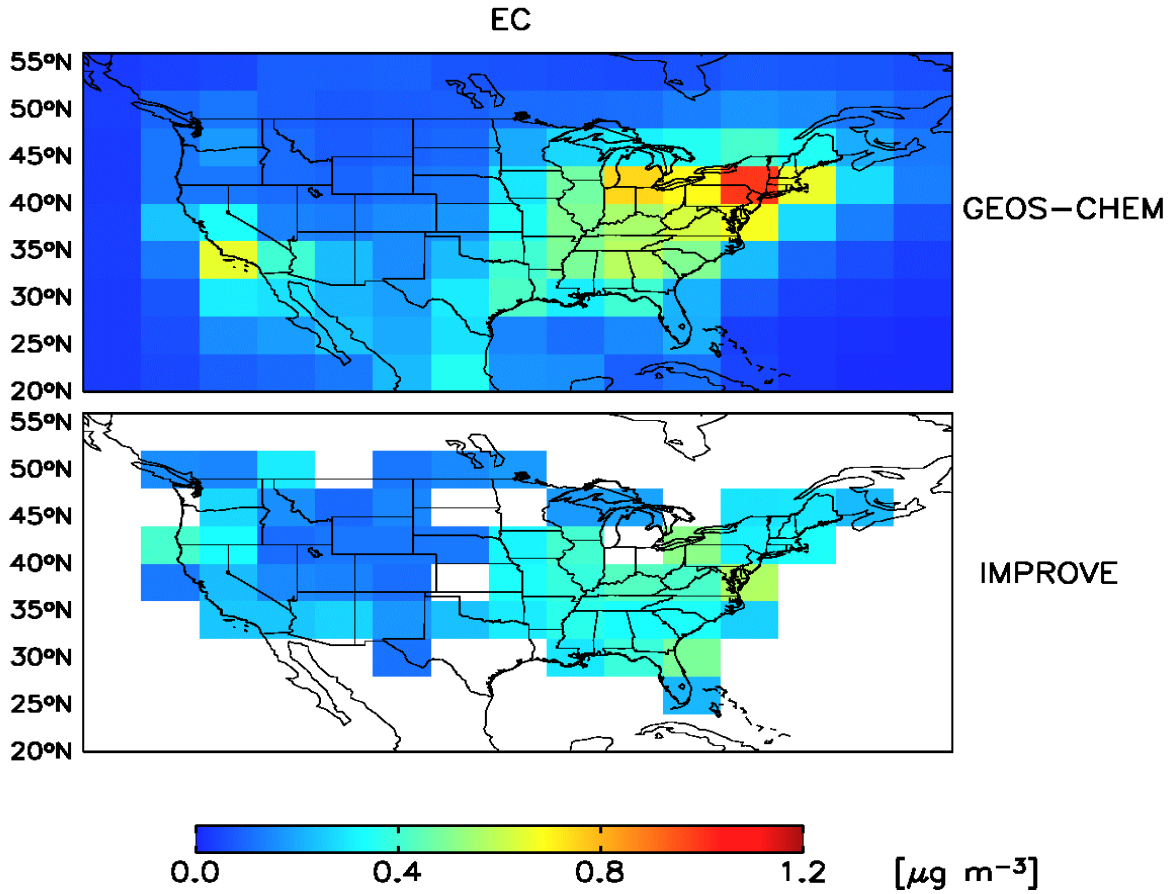


Figure 7. Scatterplot of simulated versus observed EC aerosol concentrations at the IMPROVE sites. Values are seasonal means for 2002. Sites in the western and eastern United States (separated at 95°W) are shown as pluses and open circles, respectively. Thick solid lines are reduced major axis regressions for the ensemble of the data; regression equations and  $R^2$  are shown inset. Thin solid lines show the  $y=x$  relationship. Dotted lines show the  $y=2x$  and  $y=0.5x$  relationships.

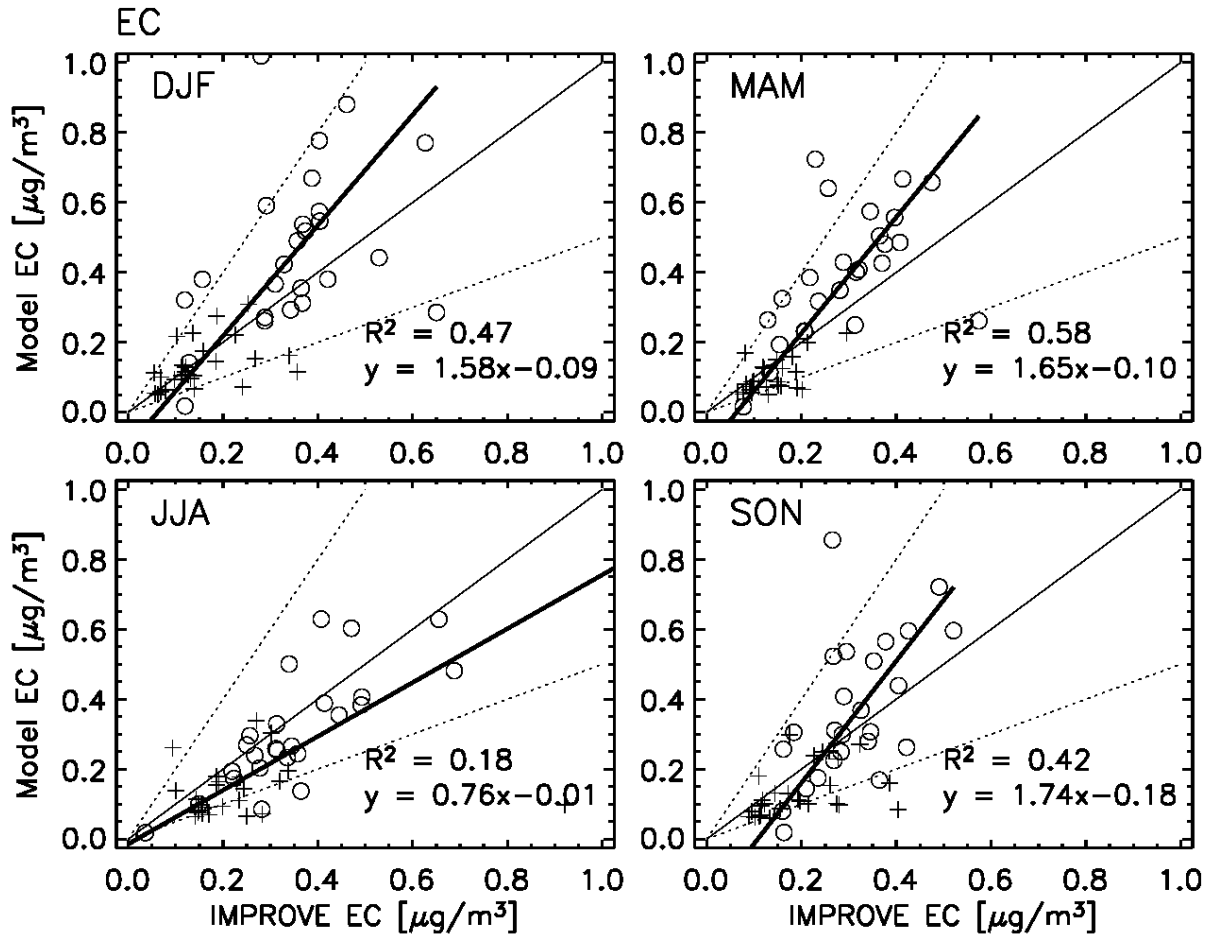


Figure 8. Same as Figure 6 but for organic carbon mass (OMC)

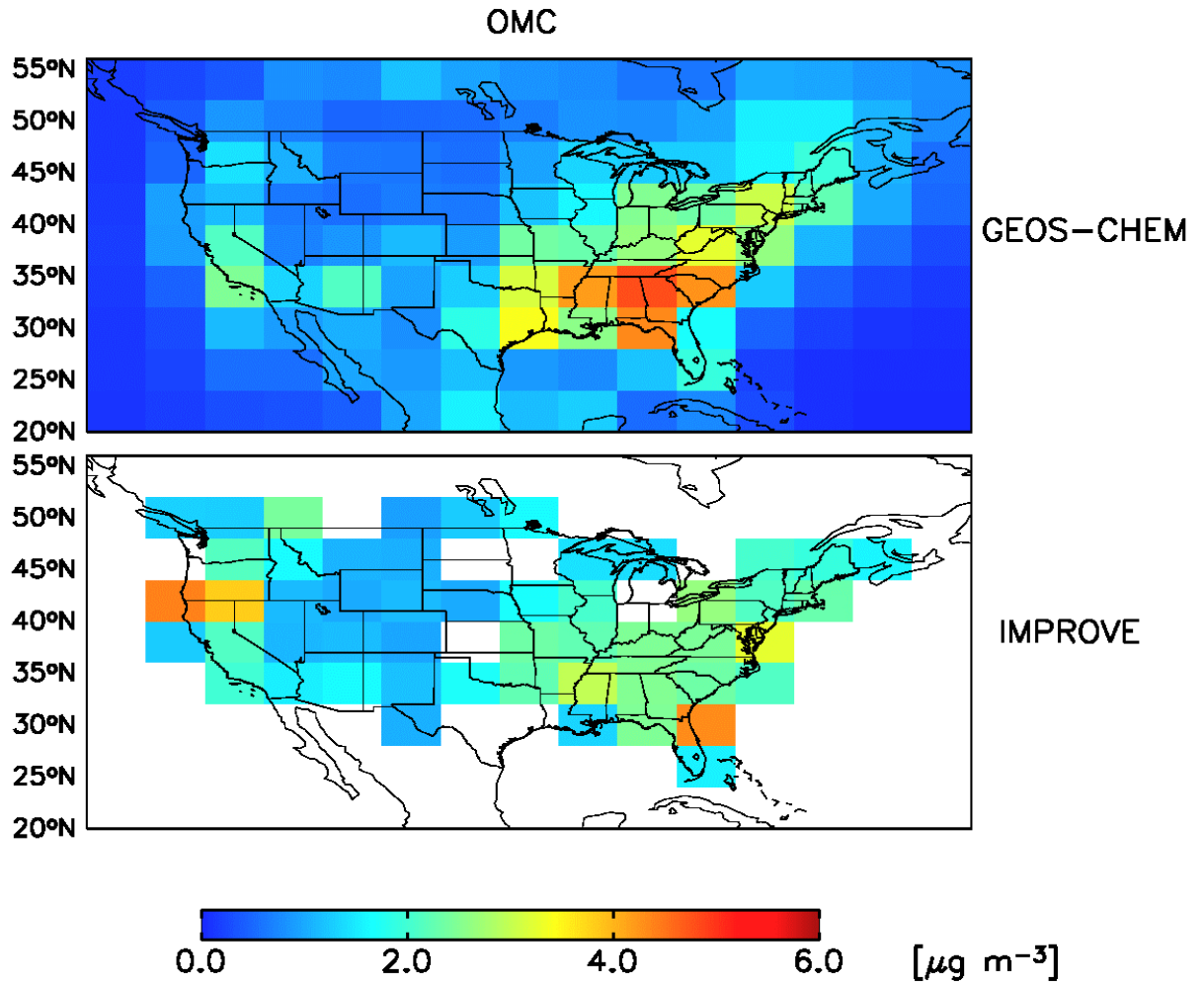
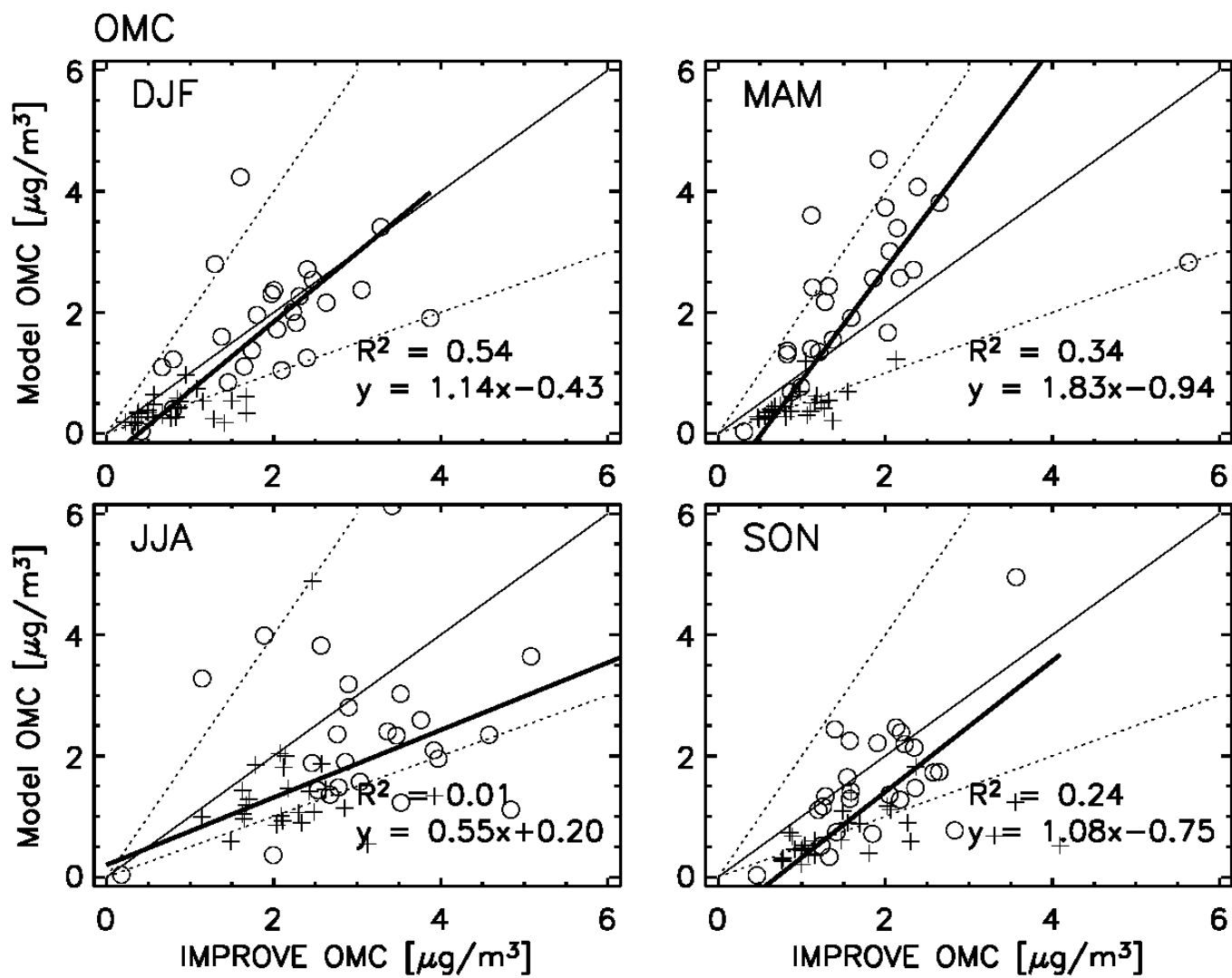


Figure 9. Same as Figure 7 but for organic carbon mass (OMC)



**Appendix A: Rokjin J. Park, Daniel J. Jacob, Mian Chin, and Randall V. Martin (2003), Sources of carbonaceous aerosols over the United States and implications for natural visibility, *J. Geophys. Res.*, 108(D12), 4355, doi:10.1029/2002JD003190.**

**Abstract.** We use a global 3-D model (GEOS-CHEM) to better quantify the sources of elemental carbon (EC) and organic carbon (OC) aerosols in the United States through simulation of year-round observations for 1998 at a network of 45 sites (IMPROVE). Simulation with our best *a priori* understanding of sources, including global satellite data to constrain fire emissions, captures most of the variance in the observations ( $R^2 = 0.84$  for EC, 0.67 for OC) with a low bias of 15% for EC and 26% for OC. Multiple linear regression to fit the IMPROVE data yields best estimates of 1998 U.S. sources of 0.60 Tg yr<sup>-1</sup> EC and 0.52 Tg yr<sup>-1</sup> OC from fossil fuel; 0.07 Tg yr<sup>-1</sup> EC and 0.89 Tg yr<sup>-1</sup> OC from biofuel; 0.08 Tg yr<sup>-1</sup> EC and 0.60 Tg yr<sup>-1</sup> OC from wildfires; and 1.10 Tg yr<sup>-1</sup> OC from vegetation. We find that fires in Mexico and Canada contributed 40-70% of annual mean natural EC in the United States for 1998, and 20-30% of annual mean natural OC. Transpacific transport from Asian pollution sources amounted to less than 10% of the natural EC and less than 2% of the natural OC; in contrast to ozone, we find that intercontinental transport of anthropogenic carbonaceous aerosols does not enhance significantly the natural background. IMPROVE observations and model simulations for the summer of 1995 show that Canadian fire emissions can produce large events of elevated EC and OC in the southeastern United States. Our best estimates of mean natural concentrations of EC and OC in the United States, using a model simulation with climatological monthly mean fire emissions, are 2-3 times higher than the default values recommended by the U.S. Environmental Protection Agency (EPA) for visibility calculations, except for OC in the eastern United States (16% lower).

## **1. Introduction**

Carbonaceous aerosol is one of the least understood components of fine particulate matter (PM). It is usually divided in two fractions, elemental carbon (EC) and organic carbon (OC). OC is the second most abundant component of the aerosol in the United States after sulfate, and the dominant component of the natural continental aerosol [Malm *et al.*, 2000]. EC is the dominant component of the light-absorbing aerosol. Carbonaceous aerosol is presently the subject of intense scrutiny because of its impact on human health, visibility, and climate.

We present here an assessment of the sources of EC and OC in the United States by using a global 3-D model (GEOS-CHEM) simulation of observations from the Interagency Monitoring of Protected Visual Environments (IMPROVE) network. Our focus is on quantifying the anthropogenic and natural sources of these aerosols, the role of transboundary transport, and the implications for visibility. The U.S. Environmental Protection Agency Regional Haze Rule [U.S. EPA, 2001] mandates a schedule of increasing emission controls to achieve “natural visibility conditions” in national parks and other wilderness areas by 2064. The ambiguity in defining “natural visibility conditions” requires better information on natural PM concentrations and the perturbing effects from fires and from sources outside the United States.

Elemental carbon is emitted to the atmosphere by combustion. Major sources in the United States include coal burning and diesel engines. Organic carbon is emitted directly

to the atmosphere (primary OC) and formed *in situ* by condensation of low-volatility products of the photooxidation of hydrocarbons (secondary OC). Primary sources of OC in the United States are wood fuel, coal burning, and wild fires [Seinfeld and Pandis, 1998; Cabada *et al.*, 2002]. Secondary OC includes an anthropogenic component from oxidation of aromatic hydrocarbons, and a biogenic component from oxidation of terpenes [Griffin *et al.*, 1999].

Our approach is to conduct a 3-D model simulation of EC and OC concentrations in the United States for 1998, with best *a priori* sources, compare results with observations from the IMPROVE network, and use the constraints from the comparison to optimize our treatment of sources by multiple linear regression. Our treatment of fire emissions accounts for year-to-year variability through satellite observations; 1998 was a particularly active fire year, thus offering good constraints on emissions from that source. We also present a case study for the summer of 1995 to demonstrate the large-scale enhancements of EC and OC concentrations in the United States that can arise from Canadian fires. We go on to quantify mean natural EC and OC concentrations in the United States for different seasons and regions, using climatological fire emissions and sources from vegetation, and to assess the enhancement of EC and OC background concentrations resulting from transpacific transport of Asian pollution.

## 2. Model Description

### 2.1 General

We use the GEOS-CHEM global 3-D model of tropospheric chemistry [Bey *et al.*, 2001] to simulate EC and OC aerosols for 1998 (1 year) and 1995 (summer). The model (version 4.23, <http://www-as.harvard.edu/chemistry/trop/geos/index.html>) uses assimilated meteorological data from the NASA Goddard Earth Observing System (GEOS) including winds, convective mass fluxes, mixed layer depths, temperature, precipitation, and surface properties. Meteorological data for 1995 and 1998 are available with 6-hour temporal resolution (3-hour for surface variables and mixing depths), 2° latitude by 2.5° longitude horizontal resolution, and 20 (GEOS1 for 1995) or 48 (GEOS3 for 1998) sigma vertical layers. We retain this spatial resolution in the GEOS-CHEM simulation. The lowest model levels are centered at approximately 50, 250, 600, 1100, and 1750 m above the local surface in GEOS1 and 10, 50, 100, 200, 400, 600, 900, 1200, and 1700 m in GEOS3.

The simulation of carbonaceous aerosols in GEOS-CHEM follows that of the Georgia Tech/Goddard Global Ozone Chemistry Aerosol Radiation and Transport (GOCART) model [Chin *et al.*, 2002], with a number of modifications described below. The model resolves EC and OC, with a hydrophobic and a hydrophilic fraction for each (i.e., four aerosol types). Combustion sources emit hydrophobic aerosols that then become hydrophilic with an e-folding time of 1.2 days following Cooke *et al.* [1999] and Chin *et al.* [2002]. We assume that 80% of EC and 50% of OC emitted from all primary sources are hydrophobic [Cooke *et al.*, 1999; Chin *et al.*, 2002; Chung and Seinfeld, 2002]. All secondary OC is assumed to be hydrophilic. The four aerosol types in the model are further resolved into contributions from fossil fuel, biofuel, and biomass burning, plus an OC component of biogenic origin, resulting in a total of 13 tracers transported by the model.

Simulation of aerosol wet and dry deposition follows the schemes used by *Liu et al.* [2001] in previous GEOS-CHEM simulations of  $^{210}\text{Pb}$  and  $^7\text{Be}$  aerosol tracers. Wet deposition includes contributions from scavenging in convective updrafts, rainout from convective anvils, and rainout and washout from large-scale precipitation. Wet deposition is applied only to the hydrophilic component of the aerosol. Dry deposition of aerosols uses a resistance-in-series model [*Walcek et al.*, 1986] dependent on local surface type and meteorological conditions; it is small compared to wet deposition. *Liu et al.* [2001] found no systematic biases in their simulations of  $^{210}\text{Pb}$  and  $^7\text{Be}$  with GEOS-CHEM.

## 2.2 *A priori* sources of EC and OC

We use global anthropogenic emissions of EC ( $6.4 \text{ Tg yr}^{-1}$ ) and OC ( $10.5 \text{ Tg yr}^{-1}$ ) from the gridded *Cooke et al.* [1999] inventory for 1984. This inventory includes contributions from domestic, vehicular, and industrial combustion of various fuel types. In the GOCART simulation of *Chin et al.* [2002], the *Cooke et al.* [1999] inventory was used with no seasonal variation. However, the source from heating fuel should vary with season [*Cabada et al.*, 2002]. *Cooke et al.* [1999] do not resolve the contributions to EC and OC emissions from heating fuel. We assume these contributions to represent 8% (EC) and 35% (OC) of total anthropogenic emissions, based on data for the Pittsburgh area from *Cabada et al.* [2002] and apply local seasonal variations of emissions using the heating degree days approach [*EIA*, 1997; *Cabada et al.*, 2002]. In this manner we find that anthropogenic EC emission in the United States in winter is 15% higher than in summer. For OC the anthropogenic winter emission is twice that in summer.

The *Cooke et al.* [1999] inventory does not include biofuels, which provide however an important source of heating in rural households and are also used in agroindustrial factories. We use a global biofuel use inventory with  $1^\circ \times 1^\circ$  spatial resolution from *Yevich and Logan* [2002] with emission factors of 1.0 g EC and 5 g OC per dry mass burned [*Street et al.*, 2001; *Dickerson et al.*, 2002]. For the United States and Canada, we supersede that inventory with data on wood fuel consumption for residential and industrial sectors available for individual states and provinces [*EIA*, 2001] and which we distribute on a rural population map. Emission factors for this North American wood fuel source are 0.2 g EC and 3.0 g OC per kg dry wood burned [*Cabada et al.*, 2002]. Seasonal variation in biofuel emissions is included for the United States only and is estimated according to the heating degree-days approach.

Biomass burning emissions of EC and OC are calculated using the global biomass burning inventory of *Duncan et al.* [2002]. This inventory uses a fire climatology compiled on a  $1^\circ \times 1^\circ$  grid by *Lobert et al.* [1999], and applies monthly and interannual variability to that climatology from satellite observations. Emission factors are 2g EC and 14 g OC per kg dry mass burned [*Chin et al.*, 2002], higher than for biofuels because combustion is less efficient. For boreal forest fires, which are of particular interest here, emission factors reported in the literature range from 0.38 to 2.55 g EC per kg dry mass burned [*Lavoué et al.*, 2000, and references therein], consistent with the value assumed here. The OC/EC emission ratio of 7 is within the range of 6.9 to 8.2 used by *Lioussé et al.* [1996]. Figure 1 shows the resulting annual OC emissions from biomass burning in North and Central America for 1997-2000 as well as the climatological mean. An ENSO-related drought resulted in catastrophic wildfires in the tropical forests of southern

Mexico and Central America in 1998 [Peppler *et al.*, 2000]. Canadian fire emissions were also unusually large in 1998. Fire emissions in the United States were 38% higher than the climatological mean.

Figure 2 shows the spatial and seasonal distribution of biomass burning OC emission from our model in 1998. Fires in Mexico and Central America were most intense in May [Peppler *et al.*, 2000, Cheng and Lin, 2001]. Canadian fires peaked in July-September. In the United States, most fires occurred in the northwest (Idaho, Montana) in summer; additional fires occurred in spring in Florida, due to the ENSO-induced drought.

Secondary formation of OC from oxidation of large hydrocarbons is an important source but uncertainties are large [Griffin *et al.*, 1999; Kanakidou *et al.*, 2000; Chung and Seinfeld, 2002]. Chung and Seinfeld [2002] find that biogenic terpenes are the main source of secondary OC aerosols. We assume a 10% carbon yield of OC from terpenes [Chin *et al.*, 2002], and apply this yield to a global terpene emission inventory dependent on vegetation type, monthly adjusted leaf area index, and temperature [Guenther *et al.*, 1995].

Table 1 shows a summary of *a priori* EC and OC emissions used in the GEOS-CHEM simulation for 1998. The most important global source for both is biomass burning. In the United States, EC is mostly emitted from the combustion of fossil fuel and OC originates mostly from vegetation (but with large seasonal variation, as discussed below).

### 3. Model evaluation

A global evaluation of the EC and OC aerosol simulation was done by Chin *et al.* [2002] as part of a more general evaluation of aerosol optical depth using ground and satellite observations. Our simulation of aerosol sources and meteorological processes is similar to that of Chin *et al.* [2002] and our global distributions of EC and OC concentrations are comparable. We focus here our model evaluation on the United States, using observations at the IMPROVE sampling sites. The IMPROVE monitoring program was initiated in 1987 in national parks and other protected environments to identify the contribution of different aerosol components to visibility degradation [Malm *et al.*, 1994]. The data for 1995 and 1998 consist of 24-h speciated aerosol concentrations measured twice a week. The EC and OC concentrations are determined using the Thermal Optical Reflectance (TOR) method, which is state of the science but is subject to uncertainties that are difficult to quantify [Chow *et al.*, 1993; Malm *et al.*, 1994]. In the present paper we take the data at face value. There are 45 IMPROVE sites with continuous measurements for 1998 (Figure 3).

Figure 4 compares simulated and observed annual mean EC and OC concentrations at the 45 IMPROVE sites for the year 1998. The IMPROVE measurements are plotted on the  $2^\circ \times 2.5^\circ$  model grid. The bottom panels show the differences (model bias). A general objection to evaluating model results with 24-hr averaged concentrations in continental surface air is the inability of models to resolve nighttime stratification [Jacob *et al.*, 1993]. This is not an issue in our case because of high vertical resolution of the model near the surface and because the IMPROVE sites are not in the vicinity of large sources. We verified that the 24-h average concentrations simulated by the model in layers 1 (0-10m), 2 (10-50m), and 3 (50-100m) are not significantly different.

Observed concentrations of EC and OC are generally higher in the eastern than the western United States, reflecting higher anthropogenic and vegetative (OC) emissions in the east. The OC maximum is shifted south relative to the EC maximum, and shows a secondary maximum along the west coast, reflecting the vegetative source. The model captures well this large-scale spatial distribution of EC and OC. Fires in the model also lead to high concentrations over Central America and western Canada.

Site-to-site comparisons reveal however some major discrepancies between model and observations, as shown in the bottom panel of Figure 4 and in the scatterplot of Figure 5. Some of these discrepancies appear to reflect inadequate spatial resolution in the model. Model overestimates at coastal sites with large local urban or fire sources (BRIG in New Jersey; OKEF in Georgia; REDW, PORE, and PINN in California) are due to the inability of the model to simulate steep subgrid land-to-sea gradients in mixing depth [Fiore *et al.*, 2002]. Model overestimates at SEQU (California) and GLAC (Montana) are due to local fire emissions (Figure 1) for which averaging over the grid scale may induce large errors in the simulation of local observations. We exclude these seven sites in further statistical data analysis.

The model overestimates OC concentrations at THSI (Oregon) and MORA (Washington) sites due to a particularly large vegetative source in the model in summer that is apparently not seen in the observations. The discrepancy is local in nature (it is not found at nearby sites). As discussed further below, our specification of the vegetative OC source appears inadequate to describe OC concentrations at these two sites, and therefore we exclude them from further statistical analysis.

Figure 5 shows that the model generally reproduces the annual mean EC and OC concentrations to within a factor of two and captures the spatial pattern well ( $R^2=0.84$  for EC and  $R^2=0.67$  for OC). However, the slope of the reduced major axis line [Hirsch and Gilroy, 1984] is  $0.85\pm 0.06$  for EC and  $0.74\pm 0.08$  for OC, reflecting a low bias in the model. We will correct for this model bias by adjusting the sources, as discussed below.

Figure 6 and Figure 7 compare seasonal variations of simulated and observed EC and OC concentrations at selected IMPROVE sites. Contributions from individual sources to the model concentrations are shown. Seasonal variations for EC differ considerably from site to site, and the model has significant success in capturing these differences. Fossil fuel is the dominant source for EC at most sites, but seasonal maxima in May-September over the western United States are due to forest fires. The OC concentrations are generally highest in summer and lowest in winter, both in the model and in the observations; this seasonal variation is mostly due to the biogenic source. Peaks in OC in May-September in the western United States are seen both in the model and in the observations and are due to wildfires, as for EC. Wintertime OC is higher in the eastern than the western United States, and includes contributions of comparable importance from biofuels and fossil fuels.

Rogers and Bowman [2001] used satellite measurements and air parcel trajectory calculations to illustrate the transport of the 1998 fire plumes from Central America to the central and southern United States. Our model successfully captures the corresponding peaks of EC and OC observed in May at the IMPROVE sites (e.g., BIBE in Texas, CHIR in Arizona, CANY in Utah, MOZI in Colorado, UPBU in Arkansas, GRSM in Tennessee). The enhancement in concentrations is much stronger for OC than for EC,

both in the model and in the observations, reflecting high OC/EC fire emission ratios and the relatively large fossil fuel source of EC in the United States.

The model has also some success in reproducing the influences from fire emissions within the United States. For example, the high OC in April-June at CHAS in Florida is well captured in the model. Fires in the western United States result in peak EC and OC concentrations in September at several sites (MORA, Washington; THSI, Oregon; LAVO, California; JARB, Nevada).

Figure 8 compares simulated and observed monthly mean concentrations for the ensemble of IMPROVE sites and for separate seasons. The model simulation with *a priori* sources has success in reproducing the variability of observed EC and OC for winter and spring, as measured by the high  $R^2$  (0.67-0.79) correlation between model and observations. The slope of the regression line (0.84-0.98) is close to one for both EC and OC. The  $R^2$  is lower in summer and fall, particularly for OC (0.37-0.40) and the slope of the regression line is off from one (0.72-0.74 for EC and 0.74-1.06 for OC). The slope of the OC regression line in fall is close to one only because high model bias from wildfire sources at western sites offsets the low model bias at eastern sites.

#### 4. Top-down emission estimates

The statistical model biases apparent in Figure 8 could reflect errors in the *a priori* sources. We examine what adjustments in the sources would be needed for least-squares minimization of the bias between simulated and observed monthly mean EC and OC concentrations. We identify for this purpose four source components: fossil fuel, biofuel, biomass burning, and vegetation (the latter for OC only). We use a multiple linear regression to fit the annual mean U.S. source for each component to the monthly mean IMPROVE observations. In order to give equal weight to EC and OC concentrations in the least-squares minimization, we normalize them by their respective annual mean concentrations for the ensemble of IMPROVE sites ( $0.29 \mu\text{g m}^{-3}$  for EC,  $1.23 \mu\text{g m}^{-3}$  for OC).

We find in this manner that fossil fuel and biofuel emissions should be increased by 15% and 65% respectively from *a priori* levels, while biomass burning emissions should be decreased by 17% and the biogenic source for OC should be increased by 11%. We consider these adjustments to be well within the uncertainties on the *a priori* estimates. The *a posteriori* values of our adjusted sources are given in Table 1. The increase in the biofuel source is largely determined by the model underestimate of observed OC for the cold season.

Figure 9 presents annual mean surface air concentrations of EC and OC in the model using *a posteriori* sources. Relative to the simulation with *a priori* sources (Figure 4), there are 15-20% increases in EC and OC concentrations in the eastern United States. Changes in the western United States are smaller because the decrease in the biomass burning source offsets the increase in the biogenic OC source.

The effect of source adjustment on the ability of the model to fit observed EC and OC concentrations is shown by the scatterplots in Figure 8. Compared to the simulation with *a priori* sources, the  $R^2$  correlation coefficients are slightly higher and the slopes of the regression lines are closer to unity. Figures 6 and 7 show the effect of the *a posteriori* sources on the simulation at individual sites. The adjustments are generally too small to

correct site-specific discrepancies, which would require modifying the geographic distributions of the sources.

Figures 10 and 11 show the contributions of individual *a posteriori* sources to EC and OC for winter and summer. Fossil fuel is the most important source of EC everywhere in the United States, except in some areas in the west in summer where wildfires make a more important contribution. For OC, the anthropogenic sources (fossil and biofuel) dominate in winter, while the natural sources (fires and vegetation) are more important in summer. The fossil fuel OC is mostly concentrated in the northeastern corridor, the industrial Midwest and Southern California, whereas the biofuel OC is more widely distributed. Biogenic OC in summer is highest in the southeast and along the west coast. We previously discussed in the context of Figure 7 the large OC enhancements in the southern United States due to fires in Central America, but these enhancements are in spring (cf. Figure 2) and thus not apparent in Figure 11. Figure 11 shows a large enhancement in OC concentrations over the north-central United States due to Canadian fires, but the IMPROVE sites are not well situated to observe this enhancement (Figure 3). We present below a case study for summer 1995 demonstrating Canadian fire influence over the eastern United States.

## 5. Canadian fire influence: a case study for the summer of 1995

Previous studies [Wotawa and Trainer, 2000; Fiore *et al.*, 2002; McKeen *et al.*, 2002] have shown that major Canadian wildfires in June-July 1995 caused large enhancements of CO and smaller enhancements of ozone in the southeastern United States. The Canadian fire plumes were carried by northerly flows associated with high pressure systems on the back side of cold fronts. We use here a GEOS-CHEM simulation for the summer 1995 to demonstrate large aerosol EC and OC enhancements from these fires at IMPROVE sites in Arkansas (UPBU), Tennessee (GRSM) and Kentucky (MACA).

Our simulation of the 1995 Canadian wildfires uses daily, geographically resolved emission data estimated from the area burned in each province. Those data are given by Wotawa and Trainer [2000] for CO, and are scaled here to our climatological biomass burning emission inventory for CO [Lobert *et al.*, 1999] to derive corresponding EC and OC emissions. The resulting EC and OC emissions from the fires are 0.34 and 2.41 Tg, respectively, and are distributed in five areas (Northwest Territories, Alberta, Saskatchewan, Manitoba, and Ontario) for four burning periods from 17 June to 13 July.

Figure 12 shows the time series of simulated and observed EC and OC concentrations at three sites in the southeastern United States: UPBU in Arkansas, MACA in Kentucky, and GRSM in Tennessee. There are two large peaks in the observations, for July 1 and July 8, which are captured by the model and are due to the Canadian fires (compare solid and dashed lines in Figure 12). The timing of those peaks is consistent with those concurrently observed for CO at nearby sites [McKeen *et al.*, 2002]. Our simulation of the magnitude of the July 7-9 event is improved in a sensitivity simulation where we assume initial lifting of the fire emissions up to 4 km altitude (Figure 12, dotted line). Such lifting can be expected from buoyancy, particularly for large crown fires [Lioussé *et al.*, 1996; 1997; Lavoué *et al.*, 2000].

Our model simulation allows us to assess the influence of Canadian fire emissions on seasonal aerosol concentrations in the United States for the summer of 1995. We find that the events associated with Canadian fire plumes persisted typically for 3-5 days. On

a seasonal basis, they caused the mean June-August 1995 natural EC to increase by 80% (east) and 36% (west) and the mean OC to increase by 23% (east) and 16% (west), relative to a sensitivity simulation with no Canadian fires.

## 6. Implications for natural visibility in the United States

We use results from our model to estimate the role of natural carbonaceous aerosols in visibility reduction and compare to the default values recommended by EPA [2001] for application of the Regional Haze Rule. Our 1998 simulation with *a posteriori* sources yields annual average concentrations of natural EC and OC from fires and vegetation of  $0.09 \mu\text{g}/\text{m}^3$  and  $1.09 \mu\text{g}/\text{m}^3$ , respectively, for the western United States (west of  $95^\circ\text{W}$ ) and  $0.06 \mu\text{g}/\text{m}^3$  and  $0.95 \mu\text{g}/\text{m}^3$ , respectively, for the eastern United States. In order to compute the light extinction by OC we need to multiply the OC mass by 1.4 to obtain an Organic Carbon Mass (OMC) that accounts for the non-carbon additional mass attached to OC aerosols [Malm *et al.*, 1994]. The resulting annual average for natural OMC is  $1.52 \mu\text{g}/\text{m}^3$  and  $1.33 \mu\text{g}/\text{m}^3$  for the west and east, respectively. Except for OMC in the eastern United States, our best estimates of natural concentrations for EC and OMC are significantly higher than the default values recommended by EPA [2001] which are  $0.02 \mu\text{g}/\text{m}^3$  for EC, and  $0.47 \mu\text{g}/\text{m}^3$  (west) and  $1.40 \mu\text{g}/\text{m}^3$  (east) for OMC.

Several issues need to be addressed in this comparison to the EPA default values. First, 1998 had unusually high fire emissions, principally from Mexico and Canada, as shown in Figure 1. Second, it is important to quantify the contribution of transboundary transport to natural EC and OC concentrations in the United States. Third, there is ambiguity from a U.S. policy standpoint as to whether intercontinental transport of anthropogenic pollution (as from Asia) should be considered part of the “natural” background. To address these issues we conducted three sensitivity simulations, with sources modified from those in our standard 1998 simulation. The first includes no EC and OC sources in the United States to quantify the contributions from transboundary transport, mostly from Canada and Mexico. The second includes EC and OC sources from Asia only, to quantify the transpacific transport. The third uses climatological biomass burning emissions as shown in Figure 1 in order to derive mean default values of natural EC and OC concentrations in the United States. The results are summarized in Table 2.

We find that the transboundary transport of anthropogenic sources makes only a small contribution (less than 10%) to the total anthropogenic concentrations of EC and OC in the United States. However, the transboundary transport of natural sources, mostly from fires in Canada and Mexico, makes a large contribution to annual mean natural concentrations in the United States for 1998 (44% in the west and 67% in the east for EC; 28% in the west and 37% in the east for OC).

Transpacific transport from Asian sources is found to make little contribution to EC and OC concentrations in the United States, even in the context of the natural background. The concentrations generated in the simulation with anthropogenic and natural Asian sources only (Table 2) amount to less than 2% of the natural OC concentrations from the standard simulation, and less than 10% of the natural EC. The small role of intercontinental transport in contributing to background EC and OC concentrations over the United States reflects the short lifetime of these species against wet deposition, particularly considering that the lifting of air from the continental

boundary layer to the free troposphere involves wet processes [Stohl, 2001]. This can be contrasted to ozone, for which transport from outside North America makes a large contribution to the U.S. background [Fiore *et al.*, 2002].

Our best estimates of mean natural EC and OC concentrations for comparison to the EPA default values are obtained from the simulation using mean climatological fire emissions. We find annual average concentrations of natural EC and OMC of  $0.06 \mu\text{g}/\text{m}^3$  and  $1.25 \mu\text{g}/\text{m}^3$ , respectively, for the western United States and  $0.04 \mu\text{g}/\text{m}^3$  and  $1.17 \mu\text{g}/\text{m}^3$ , respectively, for the eastern United States (Table 2). These are higher by a factor of 2-3 than the EPA default values except for OMC in the eastern United States which is lower by 16%.

The implications of our results for natural visibility estimates are substantial, particularly in the western United States. Our higher natural OMC component relative to EPA's default estimates results in lower natural visibility. For example, EPA [2001] uses its default natural PM concentrations to derive mean light extinctions of  $15.60 \times 10^{-6} \text{m}^{-1}$  and  $15.78 \times 10^{-6} \text{m}^{-1}$  at Bandelier National Monument (BAND, New Mexico) and at Yellowstone National Park (YELL, Wyoming). Applying the EPA [2001] visibility formula with our best estimates of natural EC and OMC (from the simulation with climatological mean fires), and using EPA default values for the other PM components, we find natural light extinctions of  $19.13 \times 10^{-6} \text{m}^{-1}$  and  $19.31 \times 10^{-6} \text{m}^{-1}$  at BAND and YELL, respectively, about 22% higher than EPA values.

## 7. Conclusions

We used the GEOS-CHEM global 3-D model to simulate observed concentrations of elemental carbon (EC) and organic carbon (OC) from a network of 45 sites in relatively remote regions of the United States (IMPROVE network). Our focus was to better quantify the anthropogenic and natural sources of EC and OC in the United States, and the role of transboundary and intercontinental transport, in the context of assessing the effect of these aerosols on visibility.

We conducted a 1-year simulation for 1998 using best *a priori* estimates of EC and OC sources, including global satellite observations of fires, and compared the results to observed concentrations at the IMPROVE sites. Wildfire emissions were from a gridded climatological inventory, scaled to monthly fire emissions for 1998 using satellite fire count data. The model reproduces well the spatial pattern in the observations ( $R^2 = 0.84$  for EC,  $R^2 = 0.67$  for OC) but is biased low by 15% for EC and 26% for OC. From a multiple linear regression fit we concluded that fossil fuel and biofuel emissions for EC and OC in the United States should be increased by 15%, and 65% respectively from *a priori* levels, while biomass burning emissions for both EC and OC should be decreased by 17% and the biogenic source for OC should be increased by 11%. Our best *a posteriori* estimates are given in Table 1.

Canadian fire influence on the United States in 1998 was largely confined to the upper Midwest, where no IMPROVE data are available. We conducted an additional simulation for the summer of 1995, for which large CO enhancements in the southeastern United States from Canadian fires had previously been reported [Wotawa and Trainer, 2000]. We find correspondingly large EC and OC enhancements in the IMPROVE observations for this region, which the model captures and diagnoses as being due to Canadian fire emissions. Model results indicate that Canadian fires in 1995 enhanced the

mean June-August natural EC and OC concentrations in the eastern United States by 80% and 23%, respectively.

Our 1998 and 1995 simulations lead confidence in the representation of fire emissions of EC and OC in the model. We used a simulation with climatological monthly mean fire emissions, together with our best estimate of the biogenic OC source, to estimate natural concentrations of carbonaceous aerosols in the United States for purpose of natural visibility assessments and application of the EPA Regional Haze Rule [EPA, 2001]. Our best estimates of natural annual mean concentrations for EC are  $0.06 \mu\text{g}/\text{m}^3$  in the western United States (west of  $95^\circ\text{W}$ ) and  $0.04 \mu\text{g}/\text{m}^3$  in the east; for organic carbon mass (OMC = 1.4 OC, to account for the non-carbon contribution to OC aerosols), they are  $1.25 \mu\text{g}/\text{m}^3$  in the west and  $1.17 \mu\text{g}/\text{m}^3$  in the east. These values are 2-3 times higher than the default values recommended by EPA [2001] for application of the Regional Haze Rule, except for OMC in the east (16% lower). Our higher estimates of the natural OMC concentrations relative to EPA's default estimates result in higher natural light extinction (and hence lower natural visibility) by 22% in the western United States. We also find a large seasonal variability in natural light extinction from EC and OC, with highest values in summer due to sources from wildfires and vegetation.

We further investigated the contribution from transboundary transport to EC and OC concentrations in the United States. A sensitivity simulation with no EC and OC sources in the United States shows that fires in Mexico and Canada made a large contribution to annual mean natural concentrations of EC (40-70%) and OC (30-40%) in the United States in 1998. A sensitivity simulation with Asian sources only shows that transpacific transport contributes less than 10% of the natural background EC over the United States, and less than 2% of the natural background OC.

**Acknowledgments.** This research was supported by the Electric Power Research Institute (EPRI) and the U.S. Environmental Protection Agency (EPA). The authors are grateful to R. Yevich for providing her annual biofuel emission data.

## References

- Bey I., D. J. Jacob, R. M. Yantosca, J. A. Logan, B. Field, A. M. Fiore, Q. Li, H. Liu, L. J. Mickley, and M. Schultz, Global modeling of tropospheric chemistry with assimilated meteorology: Model description and evaluation, *J. Geophys. Res.*, 106, 23,073-23,096, 2001.
- Cabada, J.C., S.N. Pandis, A.L. Robinson, Sources of atmospheric carbonaceous particulate matter in Pittsburgh, Pennsylvania, *J. Air & Waste Manage. Assoc.*, 52, 732-741, 2002.
- Cheng, M.-D., and C.-J. Lin, Receptor modeling for smoke of 1998 biomass burning in Central America, *J. Geophys. Res.*, 106, 22,871-22,886, 2001.
- Chin, M., P. Ginoux, S. Kinne, O. Torres, B. Holben, B.N. Duncan, R.V. Martin, J.A. Logan, A. Higurashi, and T. Nakajima, Tropospheric aerosol optical thickness from the GOCART model and comparisons with satellite and sunphotometer measurements, *J. Atmos. Sci.*, 59, 461-483, 2002.
- Chow, J. C., J. G. Watson, L. C. Pritchett, W. R. Pierson, C. A. Frazier, and R. G. Purcell, The DRI thermal/optical reflectance carbon analysis system: description, evaluation and applications in U.S. air quality studies, *Atmos. Environ.*, 27A, 1185-1201, 1993.

- Chung, S. H. and J. H. Seinfeld, Global distribution and climate forcing of carbonaceous aerosols, *J. Geophys. Res.*, submitted, 2002.
- Cooke, W.F., C. Liousse, H. Cachier, and J. Feichter, Construction of a 10 x 10 fossil fuel emission data set for carbonaceous aerosol and implementation and radiative impact in the ECHAM-4 model, *J. Geophys. Res.*, 104, 22,137-22,162, 1999.
- Dickerson, R. R., M. O. Andreae, T. Campos, O. L. Mayol-Bracero, C. Neusuess, and D. G. Streets, Analysis of Black Carbon and Carbon Monoxide Observed over the Indian Ocean: Implications for Emissions and Photochemistry, *J. Geophys. Res.*, 10.1029/2001JD000501, 2002.
- Duncan, B. N., R. V. Martin, A. C. Staudt, R. Yevich, J. A. Logan, Interannual and Seasonal Variability of Biomass Burning Emissions Constrained by Satellite Observations, *J. Geophys. Res.*, 4040, doi:10.1029/2002JD002378, 2003.
- Energy Information Administration, State Energy Data Report 1999, 2001.
- EPA, Draft Guidance for Estimating Natural Visibility Conditions under the Regional Haze Rule, U.S. EPA OAQPS report, September 27, 2001.
- Fiore, A.M., D.J. Jacob, I. Bey, R.M. Yantosca, B.D. Field, A.C. Fusco, and J.G. Wilkinson, Background ozone over the United States in summer: Origin, trend, and contribution to pollution episodes, *J. Geophys. Res.*, 107, 10.1029/2001JD000982, 2002.
- Griffin, R. J., D. Dabdub, D. R. C. III, and J. H. Seinfeld, Estimate of global atmospheric organic aerosol from oxidation of biogenic hydrocarbons, *Geophys. Res. Lett.*, 26, 2721-2724, 1999.
- Guenther, A., et al., A global model of natural volatile organic compound emission, *J. Geophys. Res.*, 100, 8873-8892, 1995.
- Hirsch, R. M., and E. J. Gilroy, Methods of fitting a straight line to data: examples in water resources, *Water Res. Bull.*, 20, 705-711, 1984.
- Jacob, D. J., et al., Simulation of Summertime Ozone over North America, *J. Geophys. Res.*, 98, 14,797-14,816, 1993.
- Kanakidou, M., K. Tsigaridis, F. J. Dentener, and P. J. Crutzen, Human-activity-enhanced formation of organic aerosols by biogenic hydrocarbon oxidation, *J. Geophys. Res.*, 105, 9243-9254, 2000.
- Lavoué, D., C. Liousse, and H. Cachier, Modeling of carbonaceous particles emitted by boreal and temperate wildfires at northern latitudes, *J. Geophys. Res.*, 105, 26,871-26,890, 2000.
- Liousse, C., J. E. Penner, C. Chuang, J. J. Walton, H. Eddleman, and H. Cachier, A global three-dimensional model study of carbonaceous aerosols, *J. Geophys. Res.*, 101, 19,411-19,432, 1996.
- Liousse, C., H. Cachier, and W. Guelle, Determining a global climatology for tropical biomass burning aerosols, paper presented at the 6th International Conference on Carbonaceous Particles, Austrian Fed. Minist. of Environ., and Sci. and Technol., Vienna, Sept. 1997.
- Liu, H., D.J. Jacob, I. Bey, and R.M. Yantosca, Constraints from <sup>210</sup>Pb and <sup>7</sup>Be on wet deposition and transport in a global three-dimensional chemical tracer model driven by assimilated meteorological fields, *J. Geophys. Res.*, 106, 12,109-12,128, 2001.
- Lobert, J., W. Keen, J. Logan, and R. Yevich, Global chlorine emissions from biomass burning: Reactive chlorine emissions inventory, *J. Geophys. Res.*, 104, 8373-8389, 1999.
- Malm, W. C., J. F. Sisler, D. Huffman, R. A. Eldred, and T. A. Cahill, Spatial and seasonal trends in particle concentration and optical extinction in the United States, *J. Geophys. Res.*, 99, 1347-1370, 1994.

- Malm, W. C., M. L. Pitchford, M. Scruggs, J. F. Sisler, R. Ames, S. Copeland, K. A. Gebhart, and D. E. Day, Spatial and seasonal Patterns and Temporal Variability of Haze and Its constituents in the United States: Report III, Cooperative Institute for Research, Colorado State University, Fort Collins, Colorado, 2000.
- McKeen, S. A., G. Wotawa, D. D. Parrish, J. S. Holloway, M. P. Buhr, G. Hübler, F. C. Fehsenfeld, J. F. Meagher, Ozone production from Canadian wildfires during June and July of 1995, *J. Geophys. Res.*, 10.1029/2001JD000697, 2002.
- Peppler, R.A., et al., ARM Southern Great Plains site observations of the smoke pall associated with the 1998 Central American Fires, *Bull. Amer. Meteor. Soc.*, 81, 2563-2591, 2000.
- Rogers, C. M. and K. P. Bowman, Transport of smoke from the Central American fires of 1998, *J. Geophys. Res.*, 106, 28,357-28,368, 2001.
- Seinfeld, J. H. and S. N. Pandis, Atmospheric Chemistry and Physics: From Air Pollution to Climate Change, J. Wiley, New York, 1998.
- Stohl, A., A 1-year Lagrangian “Climatology” of airstreams in the Northern Hemisphere troposphere and lowermost stratosphere, *J. Geophys. Res.*, 106, 7263-7279, 2001.
- Streets, D. G., S. Gupta, S.T. Waldhoff, M.Q. Wang, T.C. Bond, B. Yiyun, Black carbon emissions in China, *Atmos. Environ.*, 35., 4281-4296, 2001.
- Walcek, C. J., R. A. Brost, and J. S. Chang, SO<sub>2</sub>, sulfate and HNO<sub>3</sub> deposition velocities computed using regional landuse and meteorological data, *Atmos. Environ.*, 20, 949-964, 1986.
- Wotawa G., and M. Trainer, The influence of Canadian forest fires on pollutant concentrations in the United States, *Science*, 288, 324-328, 2000.
- Yevich, R. and J. A. Logan, An assesment of biofuel use and burning of agricultural waste in the developing world, *Global Biogeochem. Cycles*, submitted, 2002.

## Figures Captions

Figure 1. Yearly biomass burning OC emission in 1997-2000 for North and Central America, and climatological mean value (see text).

Figure 2. Annual biomass burning OC emission over North and Central America in 1998 (top) and seasonal variations for different regions (bottom).

Figure 3. IMPROVE sampling sites with continuous records for 1998.

Figure 4. Annual mean concentrations of EC (left) and OC (right) in surface air over the United States in 1998. The top panel shows results from the GEOS-CHEM model using a priori sources. The middle panel shows the IMPROVE observations plotted on the model  $2^{\circ} \times 2.5^{\circ}$  grid. The bottom panel shows the difference between the two.

Figure 5. Scatterplot of simulated (GEOS-CHEM) vs. observed (IMPROVE) annual mean EC and OC concentrations for the data shown in Figure 4. The pluses and the circles indicate data in the western and eastern United States (separated at  $95^{\circ}$ W), respectively. The asterisks with letter labels indicate sites discarded in the statistical analysis (see text): REDW(A), PORE(B), PINN(C), SEQU(D), GLAC(E), OKEF(F), and BRIG(G). The squares indicate OC data at MORA(H) and THSI(I) sites which were

discarded in statistical analysis for OC. The thin solid and dotted lines represent the  $y = x$  relation and a factor of 2 deviation. The thick solid line represents the reduced major-axis linear regression [Hirsch and Gilroy, 1984], excluding sites A-I. The Pearson correlation coefficients  $R^2$  and regression equations are indicated.

Figure 6. Seasonal variation of monthly mean EC concentrations in 1998 at selected IMPROVE sites. Site locations are shown in Figure 1. Values are monthly means. Closed circles indicate the observations. Dashed and solid lines represent the model simulations with *a priori* and *a posteriori* sources, respectively. The *a priori* model components by source types are indicated as thin solid lines with symbols: asterisks (fossil fuel combustion), diamonds (biomass burning), and squares (biofuel use).

Figure 7. Same as in Figure 6 but for OC. The *a priori* model results by source types are represented as thin solid line with asterisks (fossil fuel), diamonds (biomass burning), squares (biofuel), and triangles (biogenic terpenes).

Figure 8. Scatterplots of monthly mean EC (left two columns) and OC (right two columns) simulated vs. observed concentrations with *a priori* (left) and *a posteriori* (right) sources, for the ensemble of IMPROVE sites and for individual seasons in 1998. Sites in the western and eastern United States (separated at  $95^\circ\text{W}$ ) are shown as pluses and open circles, respectively. Thin solid lines indicate a perfect match of the model results with observations, and dotted lines denote a factor of 2 departure. Thick solid lines represent the reduced major axis regression. The Pearson correlation coefficients  $R^2$  are indicated.

Figure 9. Annual mean concentrations of EC (left) and OC (right) in surface air over the United States in 1998 from the GEOS-CHEM model using *a posteriori* sources.

Figure 10. Contribution from different sources types to EC concentrations ( $\mu\text{g m}^{-3}$ ) in surface air for DJF and JJA. Values are model results for 1998 using a posteriori sources (Table 1).

Figure 11. Same as Figure 10 but for OC.

Figure 12. Concentrations of EC and OC at three southeastern U.S. sites (UPBU, MACA, and GRSM) in June-July 1995. Observations (24-h averages, twice a week) are shown as asterisks. The solid line shows results from the standard model simulation. Results from sensitivity simulations without Canadian fire emissions (dashed line) and with fire emissions initially mixed to 600 hPa (dotted line) are also shown.

## Tables

Table 1. Carbonaceous aerosol sources in the GEOS-CHEM model (1998).

Aerosol	Source type	Global (Tg yr <sup>-1</sup> ) <sup>a</sup>	United States (Tg yr <sup>-1</sup> )	
			<i>A priori</i>	<i>A posteriori</i>
EC		22.0	0.66	0.75
	Fossil fuel	6.6	0.52	0.60
	Biofuel	1.4	0.04	0.07
	Biomass burning	14.0	0.10	0.08
OC		129.8	2.70	3.11
	Fossil fuel	10.6	0.45	0.52
	Biofuel	7.6	0.54	0.89
	Biomass burning	97.9	0.72	0.60
	Biogenic	13.7	0.99	1.10

<sup>a</sup> Including *a posteriori* emissions for the United States.

Table 2. Natural and anthropogenic EC and OC concentrations ( $\mu\text{g m}^{-3}$ ) in the United States<sup>a</sup>.

	Natural concentrations		Anthropogenic concentrations	
	West	East	West	East
EC				
1998 emissions (base)	0.09	0.06	0.21	0.62
No U.S. sources	0.04	0.04	0.02	0.02
Asian sources only	0.003	0.001	0.005	0.003
Climatological fire emissions	0.06	0.04	0.21	0.62
OMC <sup>b</sup>				
1998 emissions (base)	1.52	1.33	0.52	1.90
No U.S. sources	0.43	0.49	0.05	0.05
Asian sources only	0.022	0.013	0.013	0.007
Climatological fire emissions	1.25	1.17	0.52	1.90

<sup>a</sup>Values are annual means from the standard 1998 simulation (base) and from the sensitivity simulations described in section 5. Partition between West and East is at 95°W. The natural concentrations from the simulation with climatological fire emissions can be compared to the default estimates suggested by EPA [2001] for application of the Regional Haze Rule: 0.47  $\mu\text{g m}^{-3}$  (West) and 1.40  $\mu\text{g m}^{-3}$  (East) for OMC, and 0.02  $\mu\text{g m}^{-3}$  for EC.

<sup>b</sup>Organic carbon mass (OMC), defined as 1.4 times the OC mass to account for non-carbon contributions to the organic aerosol.

Figures

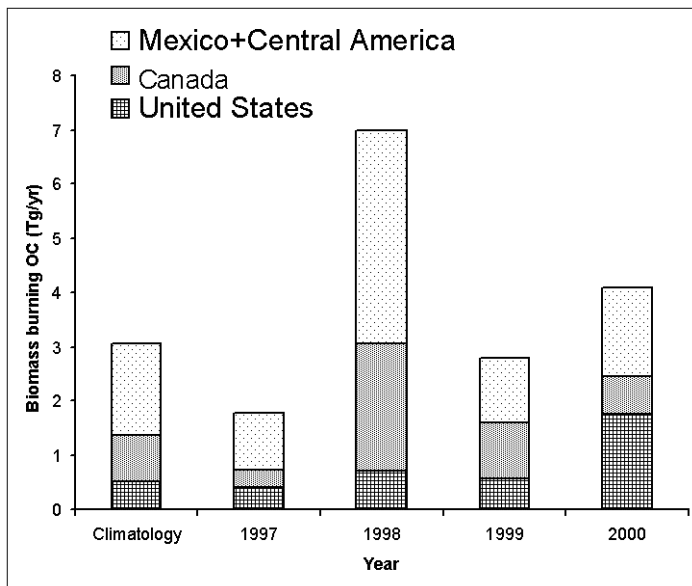


Figure 1. Yearly biomass burning OC emission in 1997-2000 for North and Central America, and climatological mean value (see text).

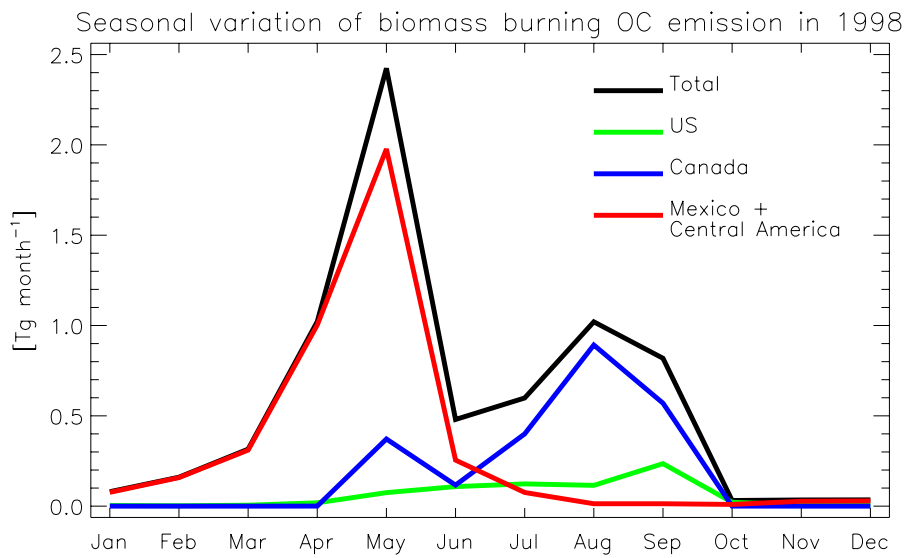
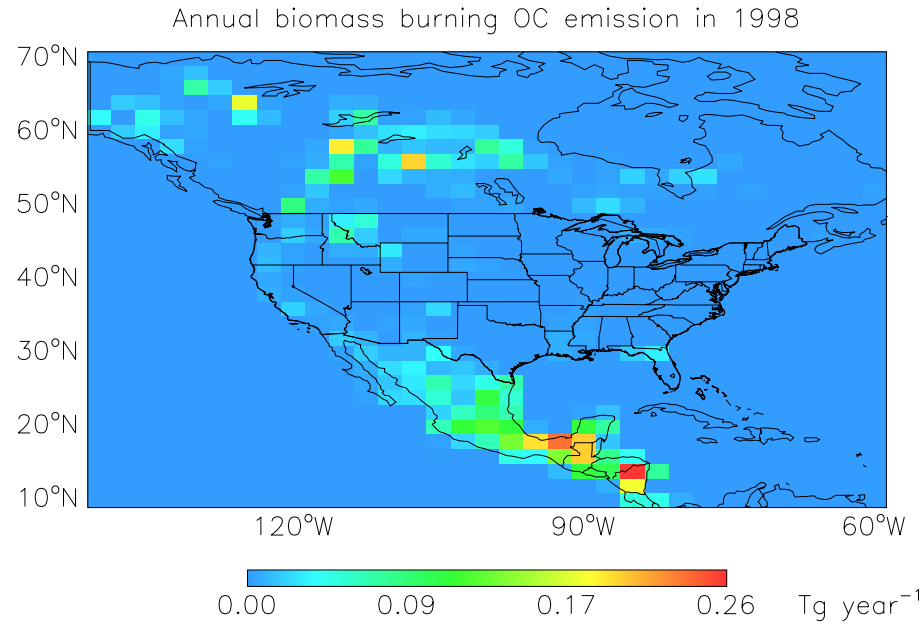


Figure 2. Annual biomass burning OC emission over North and Central America in 1998 (top) and seasonal variations for different regions (bottom).

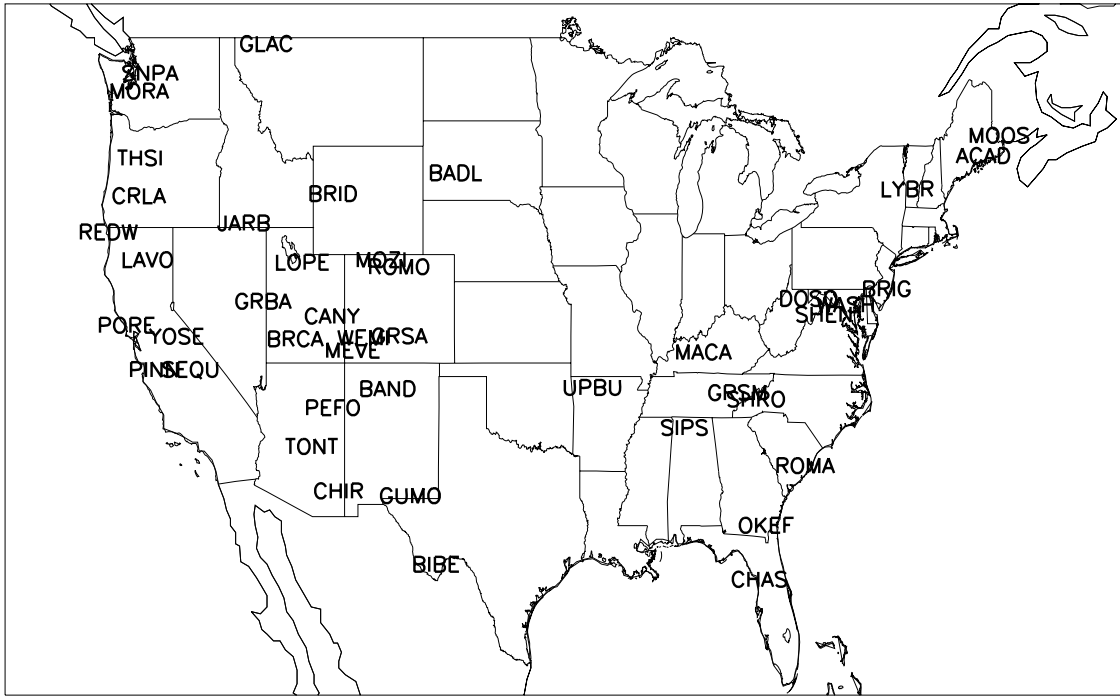


Figure 3. IMPROVE sampling sites with continuous records for 1998.

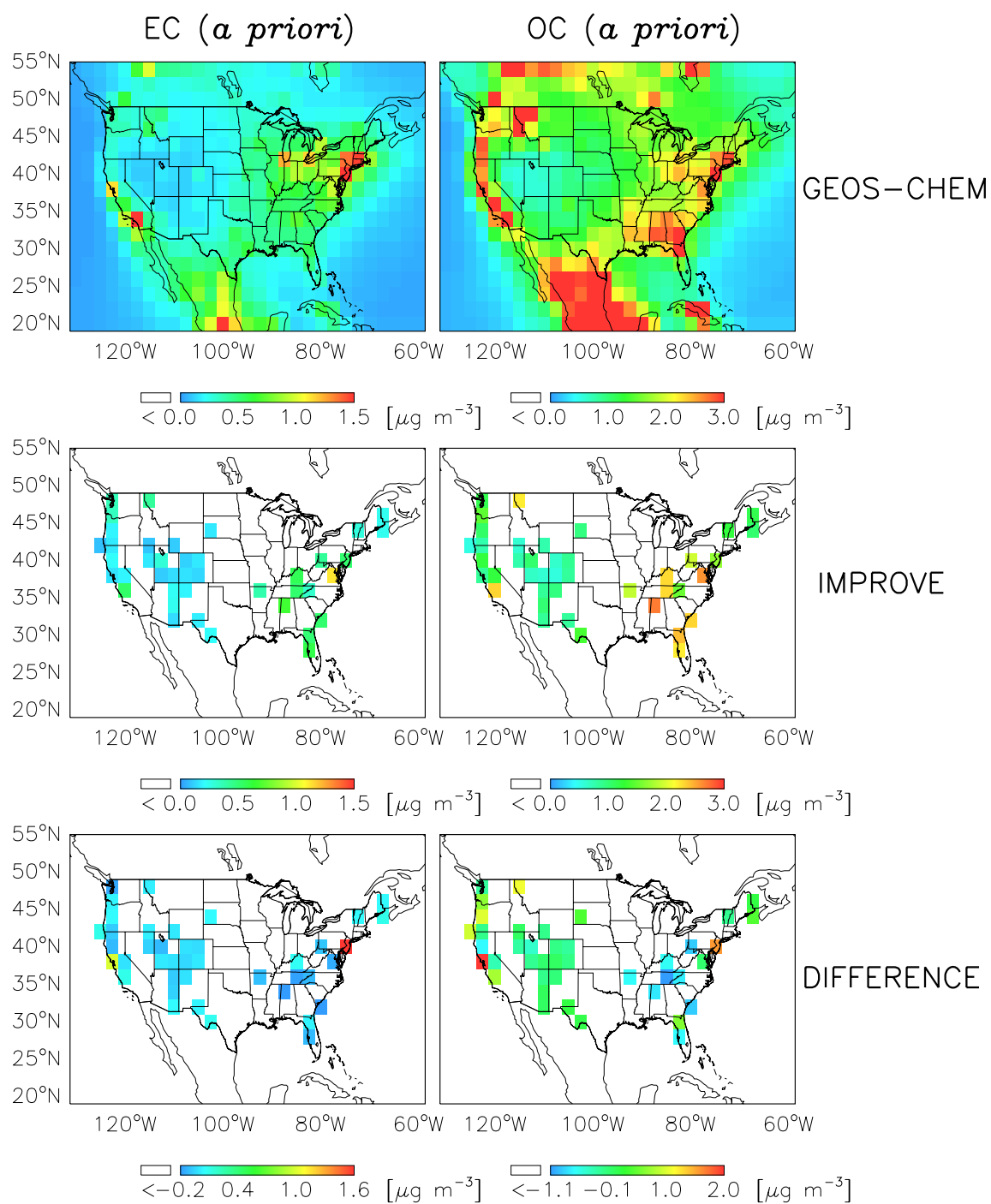


Figure 4. Annual mean concentrations of EC (left) and OC (right) in surface air over the United States in 1998. The top panel shows results from the GEOS-CHEM model using *a priori* sources. The middle panel shows the IMPROVE observations plotted on the model  $2^\circ \times 2.5^\circ$  grid. The bottom panel shows the difference between the two.

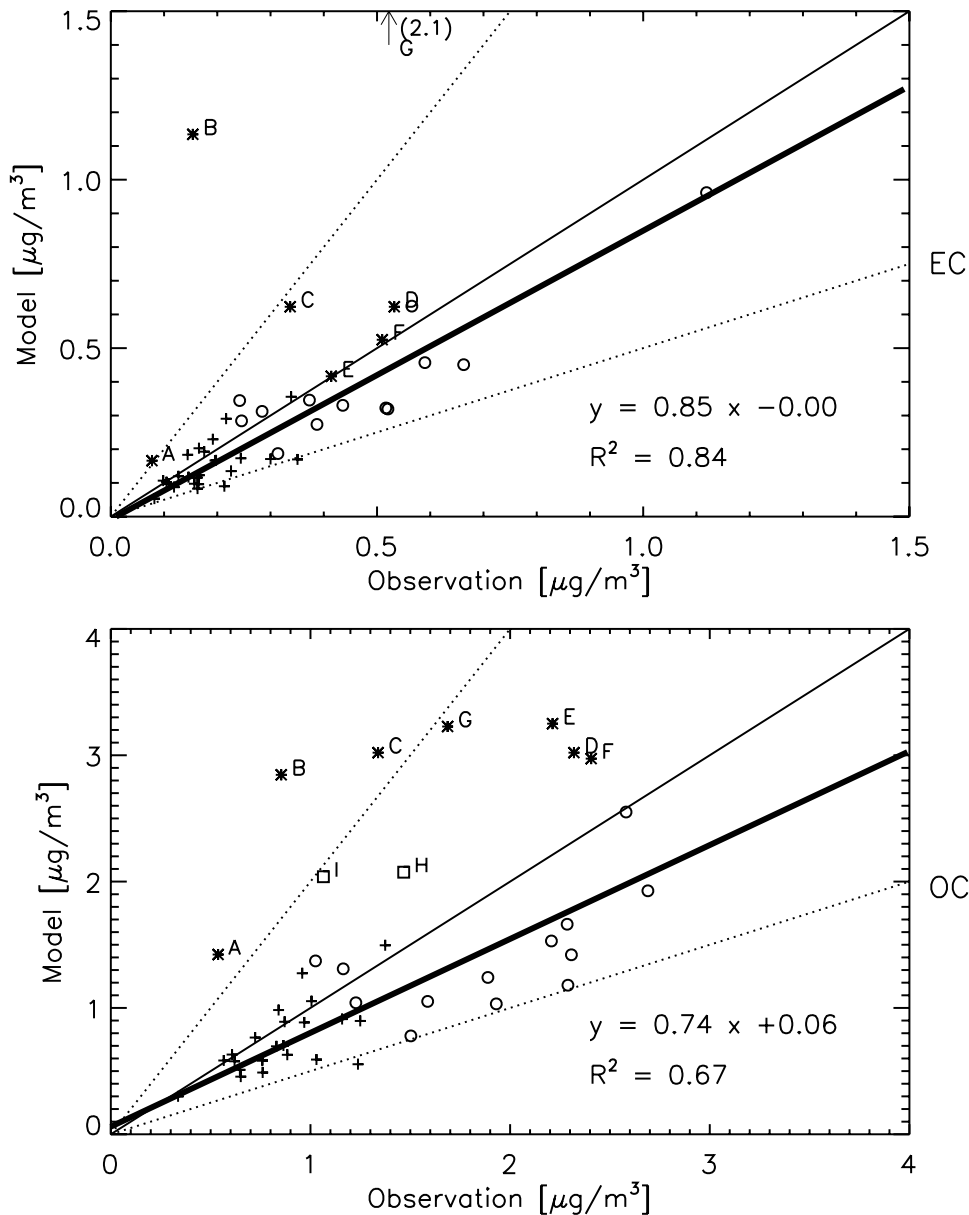


Figure 5. Scatterplot of simulated (GEOS-CHEM) vs. observed (IMPROVE) annual mean EC and OC concentrations for the data shown in Figure 4. The pluses and the circles indicate data in the western and eastern United States (separated at  $95^\circ\text{W}$ ), respectively. The asterisks with letter labels indicate sites discarded in the statistical analysis (see text): REDW(A), PORE(B), PINN(C), SEQU(D), GLAC(E), OKEF(F), and BRIG(G). The squares indicate OC data at MORA(H) and THSI(I) sites which were discarded in statistical analysis for OC. The thin solid and dotted lines represent the  $y = x$  relation and a factor of 2 deviation. The thick solid line represents the reduced major-axis linear regression [Hirsch and Gilroy, 1984], excluding sites A-I. The Pearson correlation coefficients  $R^2$  and regression equations are indicated.

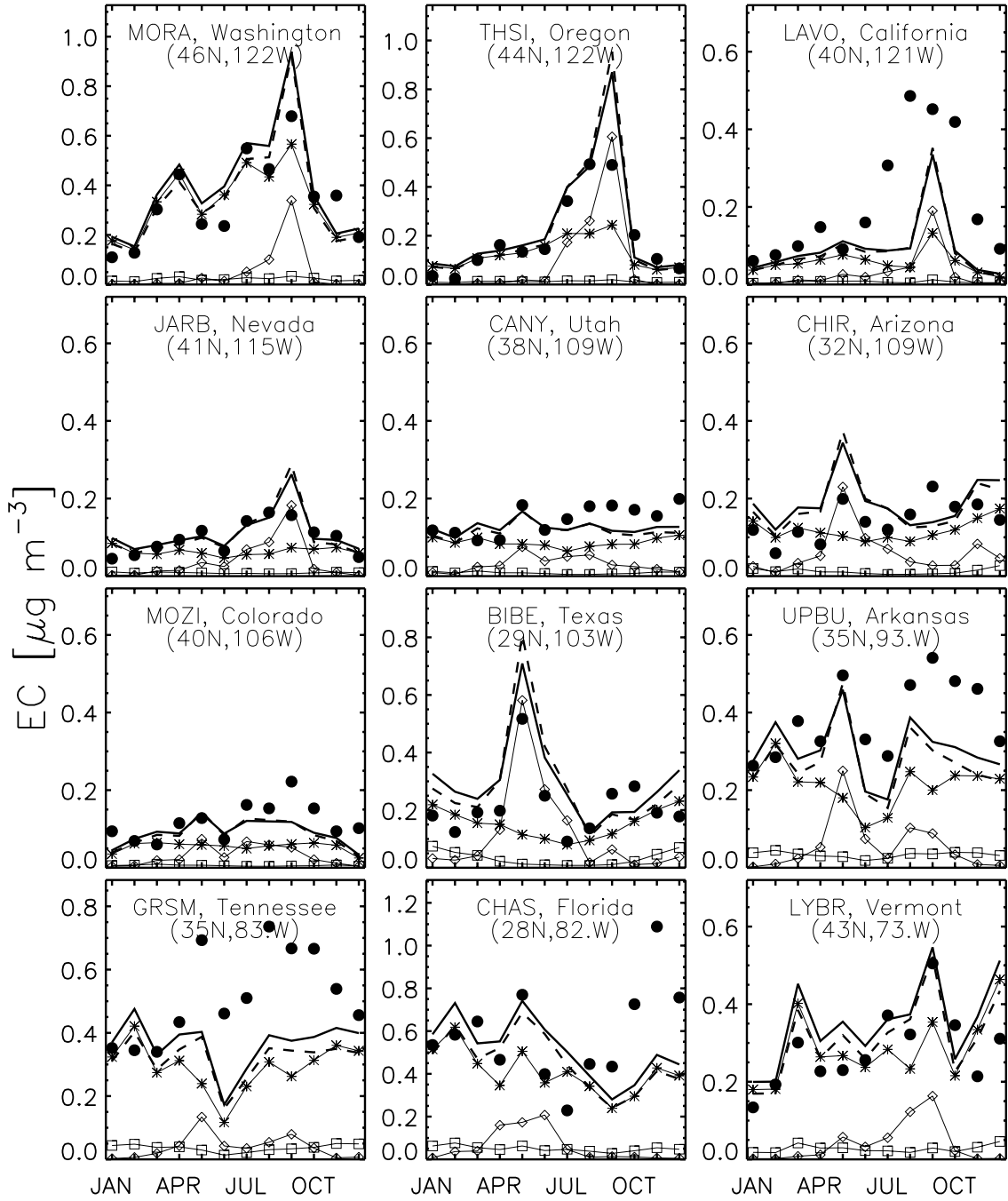


Figure 6. Seasonal variation of monthly mean EC concentrations in 1998 at selected IMPROVE sites. Site locations are shown in Figure 1. Values are monthly means. Closed circles indicate the observations. Dashed and solid lines represent the model simulations with *a priori* and *a posteriori* sources, respectively. The *a priori* model components by source types are indicated as thin solid lines with symbols: asterisks (fossil fuel combustion), diamonds (biomass burning), and squares (biofuel use).

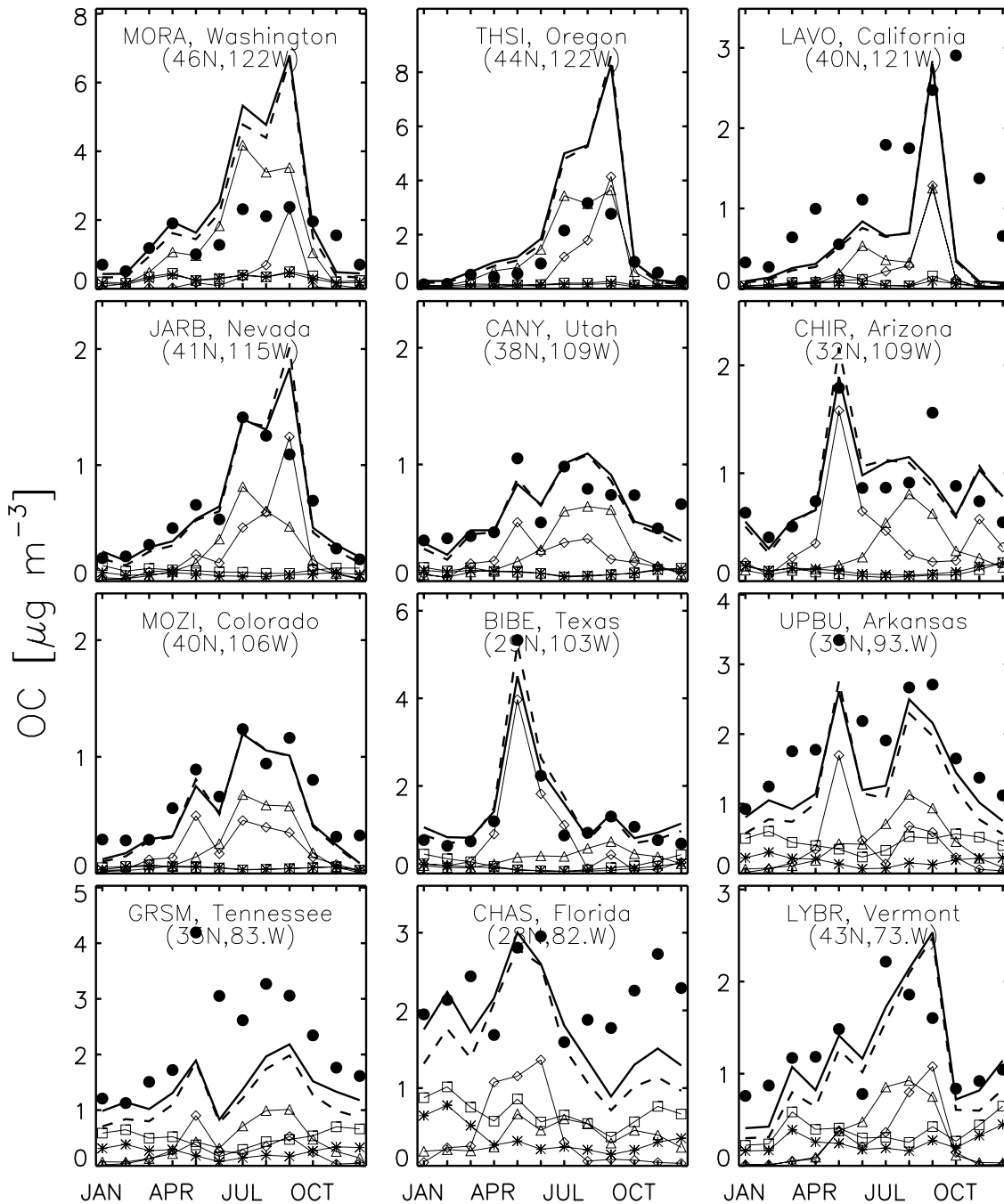


Figure 7. Same as in Figure 6 but for OC. The *a priori* model results by source types are represented as thin solid line with asterisks (fossil fuel), diamonds (biomass burning), squares (biofuel), and triangles (biogenic terpenes).

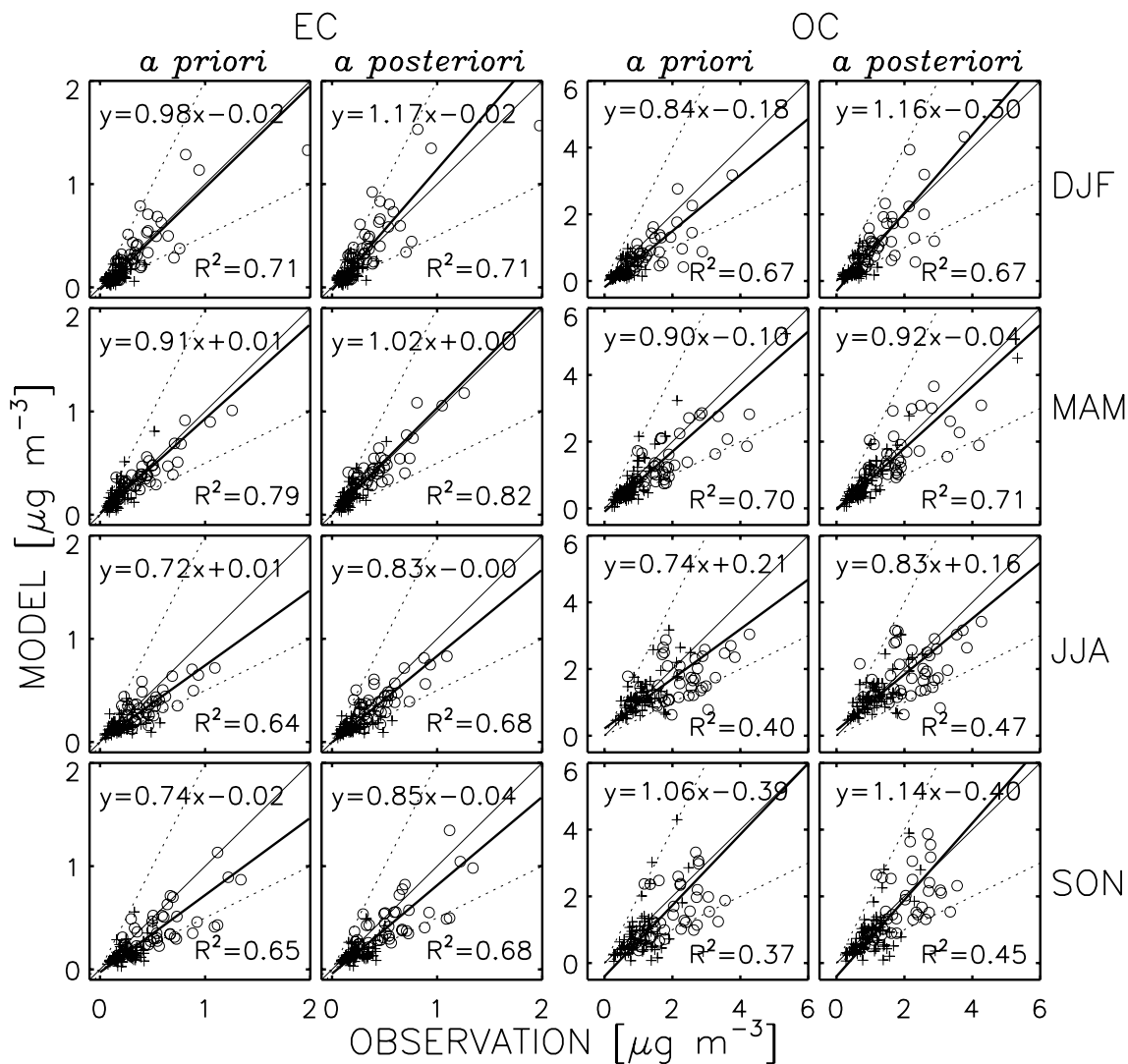


Figure 8. Scatterplots of monthly mean EC (left two columns) and OC (right two columns) simulated vs. observed concentrations with *a priori* (left) and *a posteriori* (right) sources, for the ensemble of IMPROVE sites and for individual seasons in 1998. Sites in the western and eastern United States (separated at 95°W) are shown as pluses and open circles, respectively. Thin solid lines indicate a perfect match of the model results with observations, and dotted lines denote a factor of 2 departure. Thick solid lines represent the reduced major axis regression. The Pearson correlation coefficients  $R^2$  are indicated.

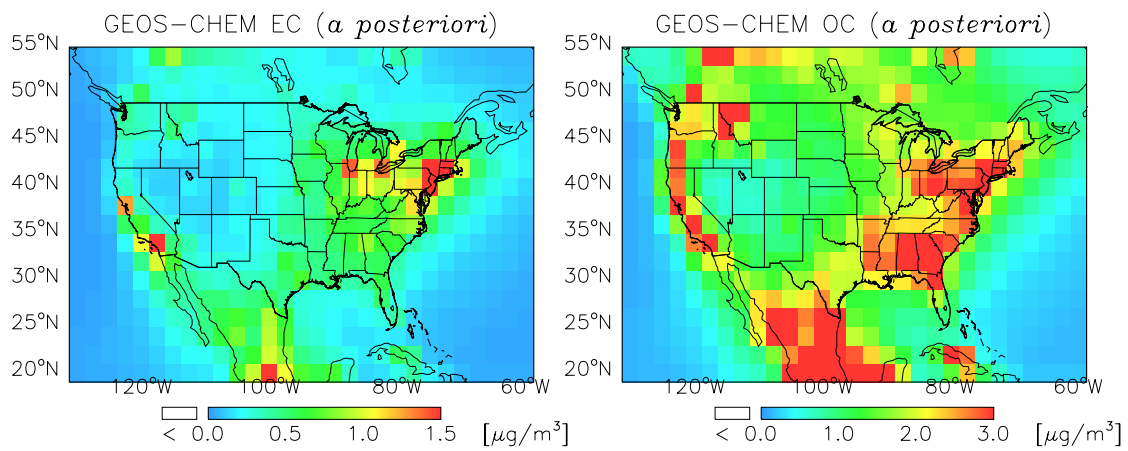


Figure 9. Annual mean concentrations ( $\mu\text{g m}^{-3}$ ) of EC (left) and OC (right) in surface air over the United States in 1998 from the GEOS-CHEM model using *a posteriori* sources.

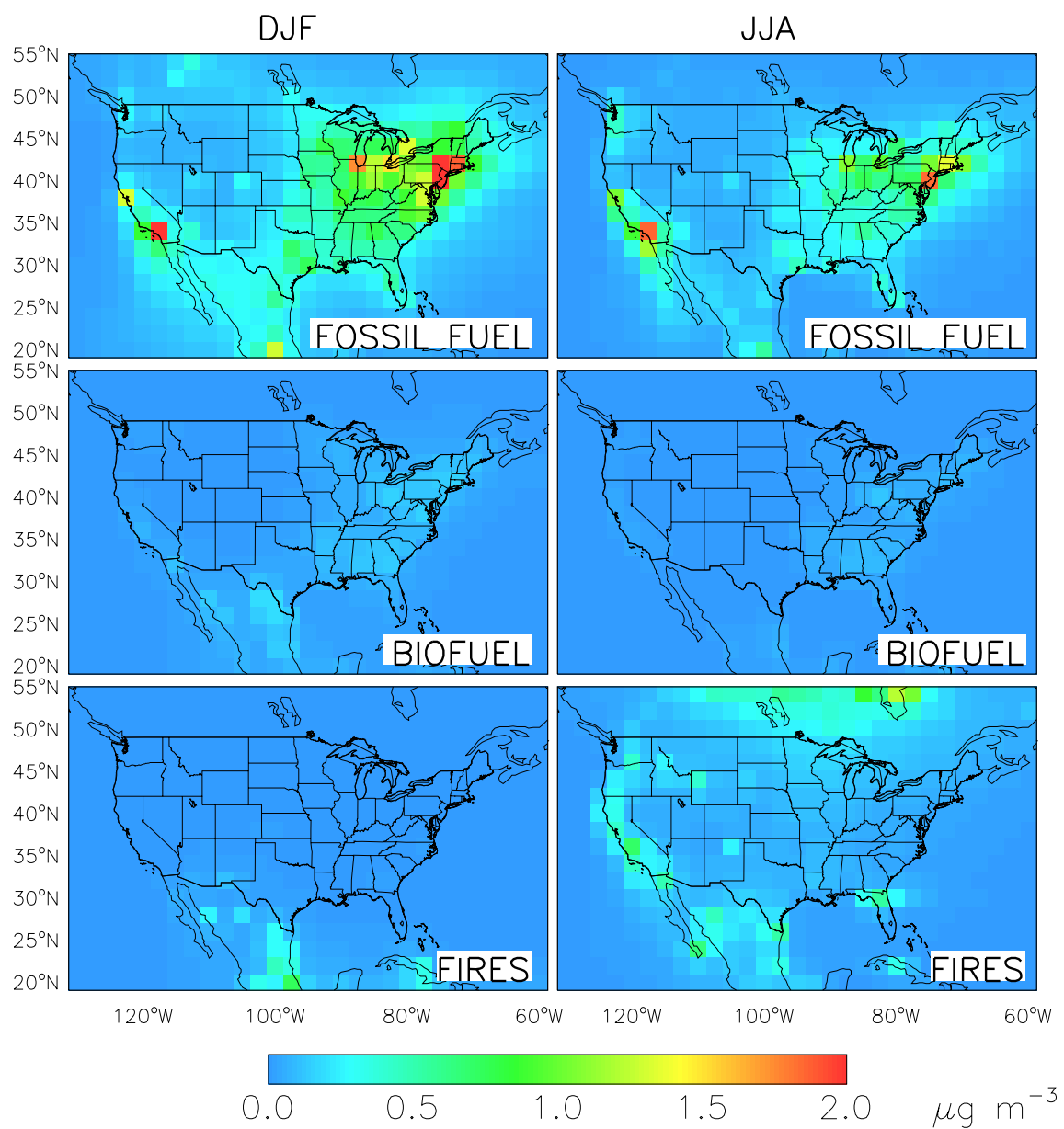


Figure 10. Contribution from different sources types to EC concentrations ( $\mu\text{g m}^{-3}$ ) in surface air for DJF and JJA. Values are model results for 1998 using a posteriori sources (Table 1).

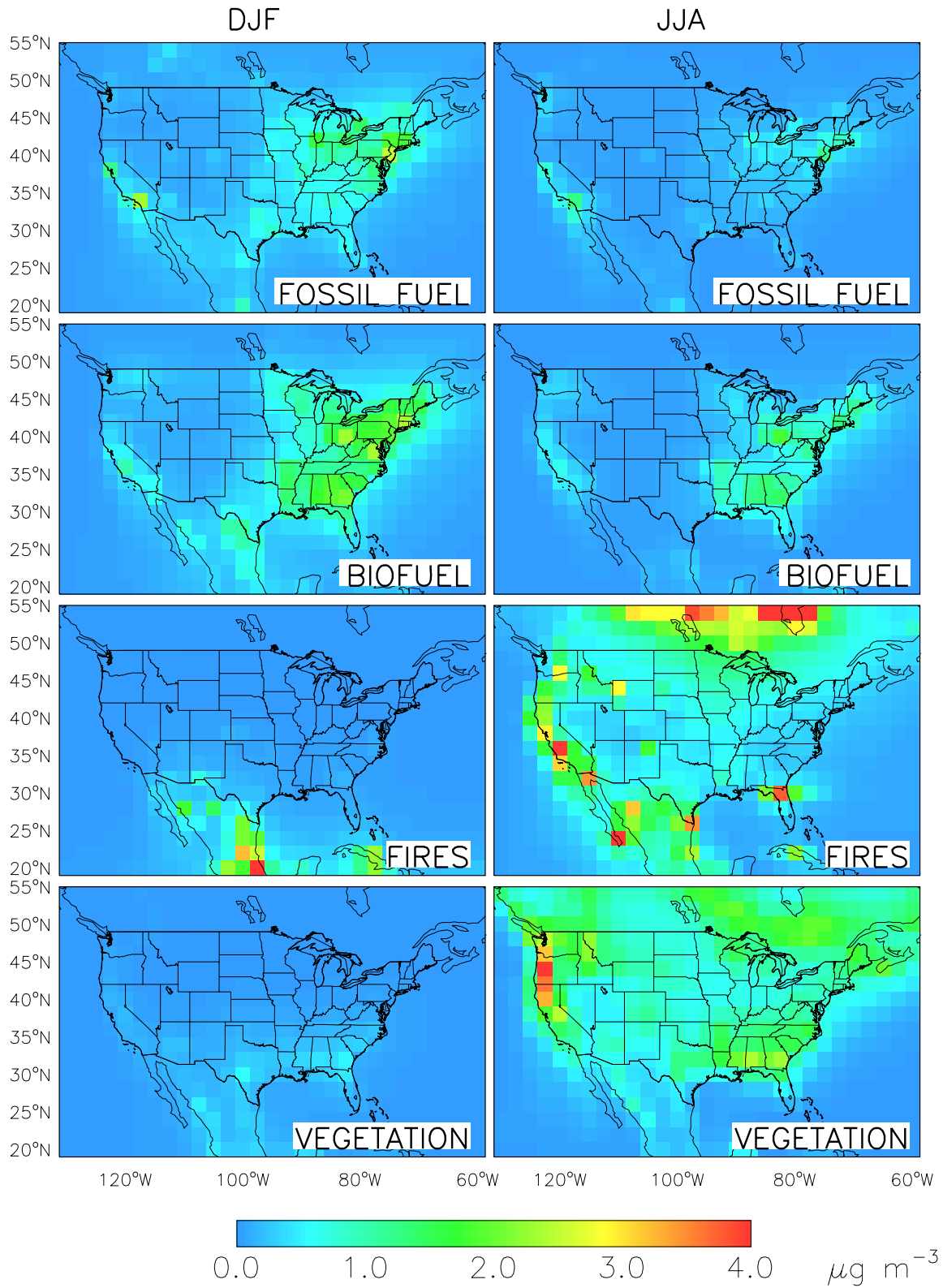


Figure 11. Same as Figure 10 but for OC.

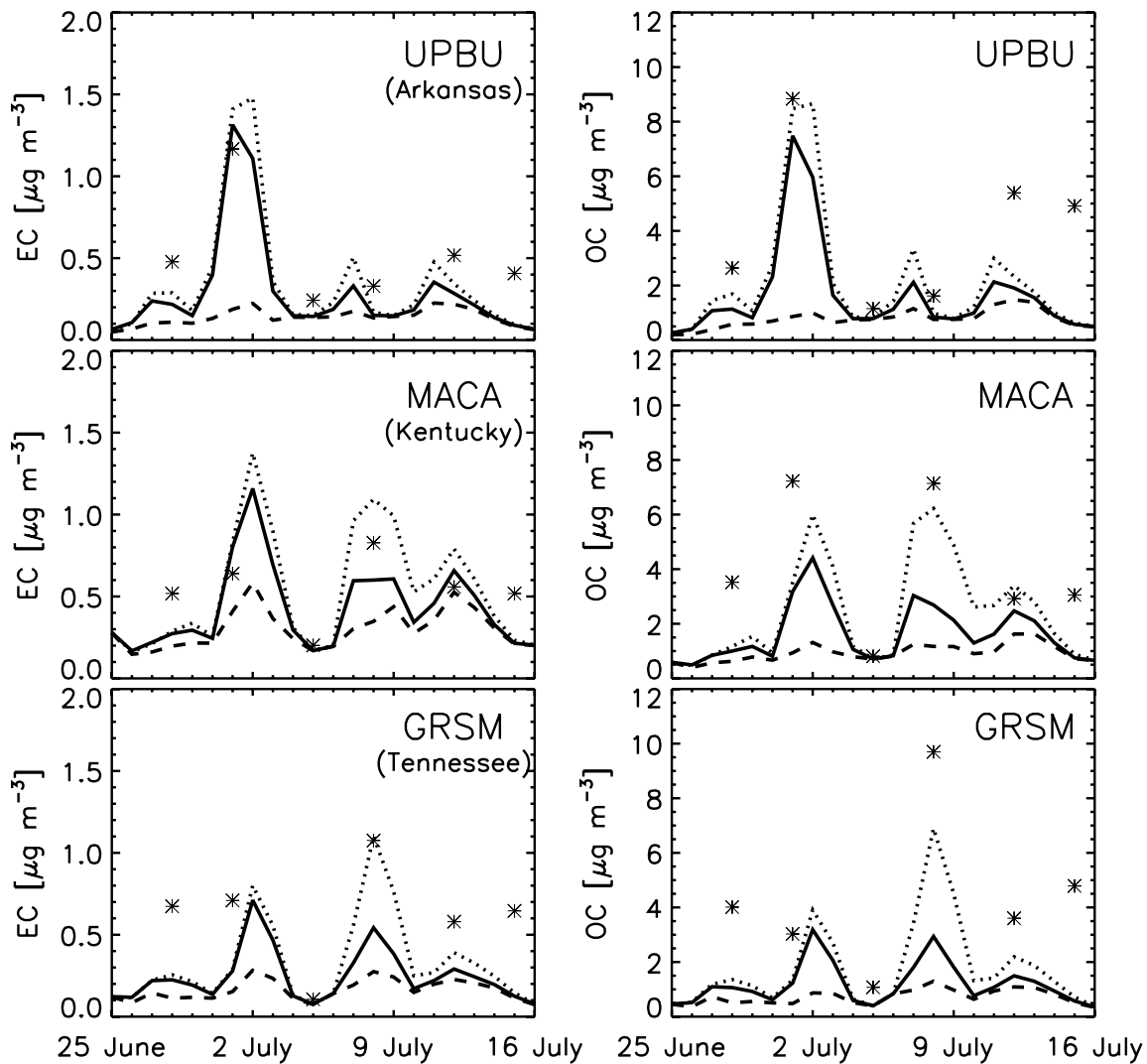


Figure 12. Concentrations of EC and OC at three southeastern U.S. sites (UPBU, MACA, and GRSM) in June-July 1995. Observations (24-h averages, twice a week) are shown as asterisks. The solid line shows results from the standard model simulation. Results from sensitivity simulations without Canadian fire emissions (dashed line) and with fire emissions initially mixed to 600 hPa (dotted line) are also shown.

**Appendix B: Rokjin J. Park, Daniel J. Jacob, Brendan D. Field, Robert M. Yantosca, and Mian Chin (2004), Natural and transboundary pollution influences on sulfate-nitrate-ammonium aerosols in the United States: implications for policy, *J. Geophys. Res.*, 109, D15204, doi:10.1029/2003JD004473.**

**Abstract.**

We use a global 3-D coupled oxidant-aerosol model (GEOS-CHEM) to estimate natural and transboundary pollution influences on sulfate-nitrate-ammonium aerosol concentrations in the United States. This work is motivated in part by the Regional Haze Rule of the U.S. Environmental Protection Agency (EPA), which requires immediate action to improve visibility in U.S. wilderness areas along a linear trajectory towards an endpoint of “natural visibility conditions” by 2064. We present full-year simulations for 1998 and 2001 and evaluate them with nationwide networks of observations in the United States and Europe (IMPROVE, CASTNET, NADP, EMEP) and with Asian outflow observations from the NASA TRACE-P aircraft mission. Shutting off U.S. anthropogenic emissions in the model defines “background” aerosol concentrations representing contributions from both natural and transboundary pollution sources. We find that transboundary transport of pollution from Canada, Mexico, and Asia dominates over natural influences for both sulfate and nitrate. Transpacific transport of Asian pollution accounts for 30% of background sulfate in both the western and eastern United States. Our best estimates of natural concentrations for ammonium sulfate and ammonium nitrate in the United States are either consistent with or lower than the default values recommended by EPA for natural visibility calculations. However, the large transboundary pollution influence in our calculation suggests that a natural visibility objective cannot be approached without international emission controls.

**1. Introduction**

Visibility degradation in the United States is mostly due to fine aerosols [*Malm et al.*, 2000] including carbonaceous (elemental and organic), sulfate, nitrate, and soil dust components. These aerosols originate from both anthropogenic and natural sources. The U.S. Environmental Protection Agency Regional Haze Rule [*U.S. EPA*, 2003a] mandates a schedule of increasing emission controls to achieve “natural visibility conditions” in national parks and other wilderness areas of the United States by 2064. Defining this natural visibility endpoint requires better information on natural aerosol concentrations and on the perturbing effects from transboundary transport of anthropogenic pollution. We previously examined this issue in a global 3-D model simulation of carbonaceous aerosols [*Park et al.*, 2003] and found that quantification of wildfire emissions was of critical importance. Transboundary transport of anthropogenic pollution was relatively unimportant for carbonaceous aerosols because of the large natural sources from wildfires and vegetation. We apply here the same analysis to sulfate and nitrate aerosols, which are other important components of visibility degradation and hence prime targets for regulation. As we will see, transboundary transport of pollution including intercontinental transport from Asia emerges in this case as a critical concern.

The main sources of sulfate and nitrate aerosols are atmospheric oxidation of SO<sub>2</sub> and nitrogen oxides (NO<sub>x</sub> ≡ NO + NO<sub>2</sub>) to H<sub>2</sub>SO<sub>4</sub> and HNO<sub>3</sub>, respectively [*NARSTO*,

2003]. Fossil fuel combustion is the dominant source of SO<sub>2</sub> and NO<sub>x</sub> in the United States. Important natural sources include volcanoes and atmospheric oxidation of oceanic dimethylsulfide (DMS) for SO<sub>2</sub>; and lightning, soils, and wildfires for NO<sub>x</sub> [NARSTO, 2003]. The low vapor pressure of H<sub>2</sub>SO<sub>4</sub> over H<sub>2</sub>SO<sub>4</sub>-H<sub>2</sub>O solutions implies that all of sulfate is in the aerosol phase. The sulfate aerosols can be partly or totally neutralized by ammonia (NH<sub>3</sub>) emitted from livestock, fertilizer use, and other less important sources. If excess ammonia is available beyond that required for sulfate neutralization to ammonium sulfate (NH<sub>4</sub>)<sub>2</sub>SO<sub>4</sub>, then ammonium nitrate (NH<sub>4</sub>NO<sub>3</sub>) aerosol can form; otherwise, and except for cloudy conditions, nitric acid remains in the gas phase. This simple H<sub>2</sub>SO<sub>4</sub>-HNO<sub>3</sub>-NH<sub>3</sub> thermodynamic framework provides a remarkably successful general description of sulfate and nitrate aerosols in the United States [Seinfeld and Pandis, 1998; NARSTO, 2003]. Sulfate and nitrate can also be incorporated in soil dust or sea salt particles, but these contributions appear to be significant only in desert and coastal areas.

Transboundary transport of pollution could compromise the objective of “natural visibility” in the Regional Haze Rule. We define here an aerosol “background” following U.S. EPA [2003b] as the aerosol concentration that would be present over the United States in the absence of domestic anthropogenic emissions. It includes contributions from natural sources but also from transboundary transport of pollution. If the latter are significant, then a “natural visibility” objective can be approached only through international emission controls. Alternatively, one should replace this objective by a “background visibility” objective that allows for uncontrollable emissions outside U.S. borders.

Intercontinental transport of Asian pollution is of particular interest for our study. Previous studies have shown that Asian pollution makes a significant (2-6 ppbv) contribution to background ozone concentrations in surface air in the United States [Berntsen *et al.*, 1999; Jacob *et al.*, 1999; Fiore *et al.*, 2002], principally by enhancing the northern hemispheric ozone background [Fiore *et al.*, 2003b]. Export and transpacific transport of Asian aerosol pollution is expected to be far less efficient than for ozone because the lifting of Asian air to the free troposphere involves wet processes (convection, warm conveyor belts) [Liu *et al.*, 2003] that scavenge aerosols with high efficiency [Koike *et al.*, 2003]. Most previous studies of transpacific transport of aerosols have focused on dust events, where the Asian source is very large and the lifting to the free troposphere takes place by dry processes [Husar *et al.*, 2001; McKendry *et al.*, 2001; Vaughan *et al.*, 2001]. However, Jaffe *et al.* [1999, 2003] and Bertsch *et al.* [2003] also showed significant aerosol enhancements in Asian pollution plumes sampled over the west coast of the United States in spring. As we will see, our model results suggest that transpacific Asian pollution is a major contributor to the sulfate background over the United States on an annual average basis.

## **2. Model description**

### **2.1 General description**

We use the GEOS-CHEM chemical transport model (CTM) [Bey *et al.*, 2001a] to conduct full-year simulations for 1998 and 2001 of the sulfate-nitrate-ammonium inorganic aerosol system coupled to oxidant chemistry. Most of our analysis focuses on the 2001 simulation. The 1998 simulation is used for evaluation with European observations, as 2001 observations were not available in a timely manner. The GEOS-

CHEM model (version 5.03, <http://www-as.harvard.edu/chemistry/trop/geos>) uses assimilated meteorological data from the NASA Goddard Earth Observing System (GEOS) including winds, convective mass fluxes, mixed layer depths, temperature, clouds, precipitation, and surface properties. Meteorological data for 1998 and 2001 are available with 6-hour temporal resolution (3-hour for surface variables and mixing depths),  $1^\circ$  latitude by  $1^\circ$  longitude ( $1^\circ \times 1^\circ$ ) horizontal resolution, and 48 sigma vertical layers. We degrade the horizontal resolution to  $2^\circ \times 2.5^\circ$  for computational expediency. The lowest model levels are centered at approximately 10, 50, 100, 200, 400, 600, 900, 1200, and 1700 m above the local surface.

The GEOS-CHEM simulation of tropospheric oxidant chemistry includes a detailed ozone-NO<sub>x</sub>-hydrocarbon chemical mechanism (~80 species, ~300 reactions). Results from this simulation have been reported in a number of papers [*Bey et al.*, 2001ab; *Li et al.*, 2001, 2002ab; *Liu et al.*, 2002; *Martin et al.*, 2002] including focused studies of surface ozone in North America and North American outflow [*Fiore et al.*, 2002, 2003ab; *Li et al.*, 2004]. GEOS-CHEM simulations of aerosols have been reported previously for radionuclides [*Liu et al.*, 2001] and carbonaceous species [*Park et al.*, 2003]. The H<sub>2</sub>SO<sub>4</sub>-HNO<sub>3</sub>-NH<sub>3</sub> aerosol simulation is a new capability for GEOS-CHEM and is described in more detail below. The aerosol and oxidant simulations are coupled through formation of sulfate and nitrate, HNO<sub>3</sub>(g)/NO<sub>3</sub><sup>-</sup> partitioning of total inorganic nitrate, heterogeneous chemistry [*Jacob*, 2000], and aerosol effects on photolysis rates [*Martin et al.*, 2003]. Partitioning of total ammonia and nitric acid between the gas and aerosol phases is calculated using the MARS-A thermodynamic equilibrium model [*Binkowski and Roselle*, 2003].

The wet deposition scheme for aerosols is described by *Liu et al.* [2001]. It includes contributions from scavenging in convective updrafts, rainout and washout from convective anvils and large-scale precipitation, and it allows for return to the atmosphere following evaporation. We extend it here to soluble gases on the basis of their effective Henry's law partitioning in warm clouds, retention efficiency upon droplet freezing in mixed clouds, and surface coating or co-condensation of ice crystals in cold clouds [*Mari et al.*, 2000]. Scavenging of SO<sub>2</sub> is limited by the local availability of H<sub>2</sub>O<sub>2</sub> as a fast aqueous-phase oxidant converting SO<sub>2</sub> to sulfate [*Chin et al.*, 1996, 2000a]. Dry deposition of aerosols and gases uses a standard resistance-in-series model dependent on local surface type and meteorological conditions [*Wesely*, 1989], and implemented as described by *Wang et al.* [1998].

We conducted five different simulations for 2001 including one standard simulation as described above, and four sensitivity simulations excluding anthropogenic emissions (1) globally, (2) in the United States, (3) in North America, and (4) in Asia. From these we quantify the influences of natural, transboundary, and intercontinental pollution sources on sulfate-nitrate-ammonium aerosol concentrations in the United States.

Each simulation was carried out as follows. We first conducted a fully coupled oxidant-aerosol simulation at  $4^\circ \times 5^\circ$  horizontal resolution for computational expediency. Oxidant concentration fields (OH, O<sub>3</sub>, NO<sub>3</sub>), H<sub>2</sub>O<sub>2</sub> production rates and photolysis frequencies, and total inorganic nitrate concentrations (gas-phase nitric acid plus aerosol nitrate) were archived from this simulation and used to conduct an aerosol-only simulation at finer  $2^\circ \times 2.5^\circ$  horizontal resolution. The aerosol-only simulation includes 9

prognostic chemical species: dimethylsulfide (DMS), SO<sub>2</sub>, sulfate, methane sulfonic acid (MSA), HNO<sub>3</sub>(g), NO<sub>3</sub><sup>-</sup>, NH<sub>3</sub>(g), NH<sub>4</sub><sup>+</sup>, and H<sub>2</sub>O<sub>2</sub>. The 2001 and 1998 simulations were initialized on October 1, 2000 and October 1, 1997, respectively, and conducted for 15 months. The first three months were used to achieve proper initialization, and we focus our attention on the following 12 months.

## 2.2 Sulfur simulation

The sulfur simulation in GEOS-CHEM is based on the Georgia Tech/Goddard Global Ozone Chemistry Aerosol Radiation and Transport (GOCART) model [Chin *et al.*, 2000a], with a number of modifications described below. Our fossil fuel and industrial emission inventory is for 1999-2000 and is obtained by scaling the gridded, seasonally resolved inventory from the Global Emission Inventory Activity (GEIA) for 1985 [Benkovitz *et al.*, 1996] with updated national emission inventories and fuel use data [Bey *et al.*, 2001a]. The emissions for the United States and Canada are from U.S. EPA [2001], and the emissions for European countries are from EMEP [2003]. Asian sulfur emission in the model is 20 Tg S yr<sup>-1</sup>, which can be compared to year 2000 estimates of 17 Tg S yr<sup>-1</sup> by Streets *et al.* [2003] and 25 Tg S yr<sup>-1</sup> by IPCC [2001]. Anthropogenic sulfur is emitted as SO<sub>2</sub> except for a small fraction as sulfate, 5% in Europe and 3% elsewhere [Chin *et al.*, 2000a].

Other anthropogenic sources of SO<sub>2</sub> in the model include gridded monthly aircraft emissions (0.07 Tg S yr<sup>-1</sup>) taken from Chin *et al.* [2000a] and biofuel use. We use a global biofuel CO emission inventory with 1° × 1° spatial resolution from Yevich and Logan [2003] and apply an emission factor of 0.0015 moles SO<sub>2</sub> per mole CO [Andreae and Merlet, 2001]. Seasonal variations in biofuel emissions are specified from the heating degree-days approach [Park *et al.*, 2003].

Natural sources of sulfur in the model include DMS from oceanic phytoplankton and SO<sub>2</sub> from volcanoes and biomass burning. The oceanic emission of DMS is calculated as the product of local seawater DMS concentration and sea-to-air transfer velocity. The seawater DMS concentrations are gridded monthly averages from Kettle *et al.* [1999], and the transfer velocity of DMS is computed using an empirical formula from Liss and Merlivat [1986] as a function of the surface (10m) wind speed. The GEOS surface winds used here assimilate remote sensing data from the Special Sensor Microwave Imager (SSM/I) instrument. Volcanic emissions of SO<sub>2</sub> from continuously active volcanoes are included from the database of Andres and Kasgnoc [1998]. Emissions from sporadically erupting volcanoes show large year-to-year variability and are not included in the model. No major volcanic eruptions occurred in 2001. Biomass burning emissions of SO<sub>2</sub> are calculated using a gridded monthly biomass burning inventory of CO constrained from satellite observations in 2001 by Duncan *et al.* [2003] with an emission factor of 0.0026 moles SO<sub>2</sub> per mole CO [Andreae and Merlet, 2001].

Table 1a summarizes global and contiguous U.S. (excluding Alaska and Hawaii) sulfur emissions for 2001. The United States contribute 10% of the global source (15% of the global anthropogenic source). Natural sources contribute 27% globally and are negligible within the contiguous United States.

The gas-phase sulfur oxidation chemistry in the model includes DMS oxidation by OH to form SO<sub>2</sub> and MSA, by nitrate radicals (NO<sub>3</sub>) to form SO<sub>2</sub>, and SO<sub>2</sub> oxidation by OH to form sulfate. Reaction rates are from DeMore *et al.* [1997] and the yields of

SO<sub>2</sub> and MSA from DMS oxidation are from *Chatfield and Crutzen* [1990]. Aqueous-phase oxidation of SO<sub>2</sub> by O<sub>3</sub> and H<sub>2</sub>O<sub>2</sub> in clouds to form sulfate is included using kinetic data from *Jacob* [1986] and assuming a pH of 4.5 for the oxidation by O<sub>3</sub>. Cloud liquid water content is not available in the GEOS data and we specify it instead in each cloudy grid box by using a temperature-dependent parameterization [*Somerville and Remer*, 1984]. The cloud volume fraction in a given grid box is specified as an empirical function of the relative humidity following *Sundqvist et al.* [1989].

### 2.3 Ammonia simulation

Ammonia emissions in the model are based on annual data for 1990 from the 1° × 1° GEIA inventory of *Bouwman et al.* [1997]. Source categories in that inventory include domesticated animals, fertilizers, human bodies, industry, fossil fuels, oceans, crops, soils, and wild animals. We view the first five as anthropogenic and the last four as natural. Additional emissions from biomass burning and biofuel use are computed using the global inventories of *Duncan et al.* [2003] and *Yevich and Logan* [2003], with an emission factor of 1.3 g NH<sub>3</sub> per kg dry mass burned [*Andreae and Merlet*, 2001]. The resulting total annual source of ammonia for the United States is reduced by 10% to match that derived by *Gilliland et al.* [2003] from an inverse model analysis of monthly precipitation chemistry (NH<sub>4</sub><sup>+</sup>) data.

Table 1b shows a summary of global and contiguous U.S. ammonia emissions for 2001. The United States account for 5% of the global source (6% of the global anthropogenic source). Natural sources amount to 37% of global ammonia emissions and 21% of contiguous U.S. emissions.

Several ammonia sources in Table 1b have strong seasonal variations. For the emissions from domesticated animals and soils we use exponential dependences on temperature reported by *Aneja et al.* [2000] and *Roelle and Aneja* [2002], respectively. Ammonia emissions from crops and fertilizers are assumed to vary seasonally with the number of daylight hours [*Adams et al.*, 1999]. Seasonal variations in biomass burning and biofuel emissions are specified from satellite observations [*Duncan et al.*, 2003] and the heating degree-days approach [*Park et al.*, 2003], respectively. Figure 1 shows the resulting seasonal variation of ammonia emission in the United States. The summer maximum is driven mainly by domesticated animals. Compared to the results of the *Gilliland et al.* [2003] inverse model analysis, also shown in Figure 1, our seasonal cycle lags in phase by 1-2 months and emission in October is a factor of 2 higher.

### 2.4 Nitrate simulation

Production of total inorganic nitrate (gas-phase nitric acid and aerosol nitrate) in the model is computed from the ozone-NO<sub>x</sub>-hydrocarbon chemical mechanism (see section 2.1). Table 1c gives a summary of global and contiguous U.S. NO<sub>x</sub> emissions; details on these sources are in *Bey et al.* [2001a] and *Martin et al.* [2002]. The United States account for 17% of global emissions (25% of global anthropogenic emissions). Natural sources from lightning, soils, and biomass burning account for 38% of global emissions and 9% in the contiguous United States.

### 2.5 Global budgets

Tabulated summaries of the global sulfate, nitrate, and ammonium aerosol budgets in GEOS-CHEM are given by *Martin et al.* [2004], who applied the model to an investigation of phase transition effects on aerosol radiative forcing. The global sulfate, nitrate and ammonium burdens for 2001 are 0.40 Tg S, 0.07 Tg N, and 0.32 Tg N, respectively. The lifetimes against deposition are 3.9, 3.2, and 3.8 days, respectively. Wet deposition accounts for 80 - 90% of total deposition.

Our global sulfate burden is lower than those (0.54-1.03 Tg S) from models that participated in the COmparison of large-scale atmospheric Sulfate Aerosol Models (COSAM) [*Barrie et al.*, 2001]. Our anthropogenic emission (57 Tg S yr<sup>-1</sup>) is lower than that used in COSAM (67 Tg S yr<sup>-1</sup>) because our emission inventory is for 1999-2000 (vs. 1985 in COSAM) and accounts for emission reductions in Europe (by 61% since 1985) and the United States (by 22% since 1985). The major natural sulfur sources in our model from oceans (15 Tg S yr<sup>-1</sup>) and volcanoes (5 Tg S yr<sup>-1</sup>) are also lower than those used in COSAM (29 and 10 Tg S yr<sup>-1</sup>, respectively). These natural sources contribute disproportionately to the global atmospheric sulfate burden because their sulfur can be delivered efficiently to the free troposphere where precipitation is infrequent [*Chin and Jacob*, 1996]. The lifetime of sulfate in our simulation (3.9 days) is at the low end of the 3.6 – 7.5 days found in COSAM.

Our annual average tropospheric ammonium burden (0.32 Tg N) is consistent with values from previous model studies (0.30 – 0.33 Tg N) [*Dentener and Crutzen*, 1994; *Adams et al.*, 1999] and the lifetime of ammonium is also similar (4.2 – 4.5 days). Our annual average tropospheric nitrate burden (0.07 Tg N) is within the range of 0.03 to 0.09 Tg N found in the previous model study by *Adams et al.* [1999, 2001].

### 3. Model evaluation

We focus our model evaluation on surface networks of sulfate-nitrate-ammonium aerosol observations in the United States and Europe. We also use sulfate wet deposition data in the United States as a test of the sulfur budget, and aircraft observations off the Asian Pacific Rim as a test of Asian export. Previous evaluation with sulfate observations at remote sites has been presented by *Chin et al.* [2000b] using the GOCART model which is similar to ours. Previous evaluations of GEOS-CHEM with aerosol radionuclides globally, and with carbonaceous aerosols in the United States, have been presented by *Liu et al.* [2001] and *Park et al.* [2003], respectively. Other GEOS-CHEM studies have evaluated the simulation of ozone and nitrogen oxides in the United States [*Fiore et al.*, 2002, 2003ab; *Li et al.*, 2004] and the transpacific transport of Asian ozone and CO pollution [*Jaeglé et al.*, 2003; *Heald et al.*, 2003].

#### 3.1 United States

We use aerosol observations for the year 2001 at 141 IMPROVE and 79 CASTNET sites, and wet deposition data at 226 NADP sampling sites (Figure 2). The IMPROVE monitoring program was initiated in 1987 in national parks and other protected environments to identify the contributions of different aerosol components to visibility degradation [*Malm et al.*, 1994]. The data for 2001 consist of 24-h sulfate and nitrate concentrations measured every third day by Particle Induced X-ray Emission (PIXE) and ion chromatography (IC), respectively. There are no ammonium data. The CASTNET network of rural sites was initiated in 1990 to monitor regional air pollution

[Lavery *et al.*, 2002]. It provides weekly average concentrations of sulfate, nitrate, and ammonium measured by IC. The NADP network provides weekly chemical precipitation data [NADP, 2002]. Sites are predominantly located in rural areas and away from point sources of pollution. Weekly precipitation samples are analyzed for sulfate using IC.

Figure 3 compares simulated and observed annual mean sulfate concentrations at the 141 IMPROVE and 79 CASTNET sites for the year 2001, plotted on the  $2^{\circ} \times 2.5^{\circ}$  model grid. Values are higher in the eastern than the western United States and are highest in the industrial midwest, reflecting the distribution of anthropogenic emissions. Figure 4 shows scatterplots of simulated vs. observed annual and seasonal sulfate concentrations for the ensemble of IMPROVE (left) and CASTNET sites (center). The right column in Figure 4 compares simulated and observed sulfate precipitation data at NADP sites. The correlation between model and observations is high for the annual mean values ( $R^2 = 0.91-0.94$  for the concentration data, 0.75 for the deposition data) and also for the seasonal means ( $R^2 = 0.79-0.90$  for the concentration data, 0.58-0.74 for the deposition data). Western sites in the scatterplots are represented with “+” symbols and should be in general most representative of background conditions. The  $R^2$  coefficients between model and observations for the subset of western sites alone are 0.35-0.39 for the annual mean concentrations at the IMPROVE and CASTNET sites, lower than for the ensemble of U.S. sites, although this could largely reflect the weaker dynamic range. There is no significant bias in the simulation of concentrations at the cleanest western sites.

Regression lines are computed here and elsewhere with the reduced major axis method, which minimizes the area of the right triangle formed by vertical and horizontal lines running from the observed point to the regression line. It is the most appropriate linear regression to characterize a relationship between two data sets with uncertainties [Hirsch and Gilroy, 1984]. Results in Figure 4 show no significant model bias in the simulation of annual mean concentrations (slope = 0.91-0.95) but a 30% low bias in summer (slope = 0.71-0.74). Loss of SO<sub>2</sub> in convective updrafts accounts for about 50% of sulfate wet deposition in summer in the model, and much less in other seasons. Our algorithm scavenges SO<sub>2</sub> in convective updrafts as a titration reaction limited solely by the supply of H<sub>2</sub>O<sub>2</sub> entrained in the updraft. However, kinetic limitations in the aqueous-phase reaction of SO<sub>2</sub> with H<sub>2</sub>O<sub>2</sub>, as well as scavenging of H<sub>2</sub>O<sub>2</sub>, can greatly reduce the SO<sub>2</sub> scavenging efficiency [Mari *et al.*, 2000; Kreidenweis *et al.*, 2003]. Accounting for these limitations might correct the model bias but was not attempted here.

Figure 5 compares simulated and observed annual mean concentrations of ammonium at CASTNET sites. Observed concentrations are higher in the east than in the west and are highest in the midwest, reflecting agricultural operations. The model reproduces this spatial distribution but is too high in the midwest. Scatterplots of simulated vs. observed annual and seasonal ammonium concentrations are shown in Figure 6 (left column) for the ensemble of sites. The model reproduces the variability of observed ammonium concentrations, both in an annual mean sense ( $R^2 = 0.90$ ) and in different seasons ( $R^2 = 0.82-0.85$ ). It shows a 30% high bias in annual mean concentrations which is mainly driven by the fall (slope = 2.0). Comparison with results from the Gilliland *et al.* [2003] inverse model analysis suggests that our ammonia emissions are excessive in the fall (Figure 1). It appears that a simple exponential temperature dependence of emissions from livestock, as assumed here, does not

adequately describe the seasonal variation of this dominant source. For the subset of western sites alone the model has a lower  $R^2$  coefficient (0.53) between the simulated and observed annual mean concentration than that for the ensemble of U.S. sites but no apparent high bias (slope = 1.02).

Figure 7 compares simulated and observed annual mean nitrate concentrations at the 141 IMPROVE and 79 CASTNET sites for 2001. The spatial distribution is similar to that of ammonium concentrations in both the observations and the model, reflecting the limitation of ammonium nitrate formation by the availability of ammonia as discussed further below. The model tends to be too high, by a factor of 2 on an annual basis as shown by the scatterplots of Figure 6. Most of the bias is driven by summer and fall. Nitrate formation is determined by the availability of ammonia beyond that required for sulfate neutralization; we find in a sensitivity analysis that the summer high bias for nitrate can be explained in large part by the low bias of sulfate. High nitrate in fall is likely caused by excessive ammonia emissions. However, the factor of 2 high bias for the simulated annual mean nitrate concentration relative to the observation is not apparent for the subset of western sites alone (slope = 1.09 - 1.34).

Figure 8 shows the simulated Gas Ratio (GR) defined as

$$GR = \frac{[NH_3^T] - 2[SO_4^{2-}]}{[HNO_3^T]}, \quad (1)$$

where concentrations are in molar units,  $[NH_3^T]$  is the sum of gas-phase ammonia and aerosol-phase ammonium concentrations,  $[HNO_3^T]$  is the total inorganic nitrate concentration (sum of gas-phase nitric acid and aerosol nitrate), and  $[SO_4^{2-}]$  is the sulfate concentration. The value of GR diagnoses the limiting reactant (ammonia or nitric acid) for the formation of ammonium nitrate [Ansari and Pandis, 1998]. We find that ammonium nitrate formation in most of North America is generally limited by the supply of ammonia ( $GR < 1$ ). Exceptions are the upper Midwest and Mexico, where  $GR > 1$  indicates that nitrate formation is limited by the supply of nitric acid. Negative GR values, indicating an acidic sulfate aerosol, are mainly confined to the oceans. This neutralization of the aerosol is further illustrated in Figure 9, which compares the simulated (top) vs. observed (bottom) acidity of aerosols at CASTNET sites for different seasons as the regression slopes of the  $[NH_4^+]$  vs.  $(2[SO_4^{2-}] + [NO_3^-])$  scatterplots. The observations show an annual mean slope of 0.84, i.e., within 16% of neutralization, and varying from 0.79 in summer to 0.93 in winter. The higher acidity in summer reflects the faster sulfate formation. The model is slightly less acidic than the observations on an annual mean basis (slope 0.90) but has the same seasonal trend (0.84 in summer, 0.98 in winter). The weaker apparent model acidity reflects at least in part the association of sulfate and nitrate in the observations with other alkaline cations (e.g.,  $Ca^{2+}$ ) not included in the model.

### 3.2 Europe

Figure 10 compares model results to annual and seasonal mean observations of sulfate, nitrate, and ammonium at 93 European EMEP sites in 1998. Sulfate in the model reproduces the variability in the observations ( $R^2 = 0.60 - 0.78$ ) with no systematic bias (the regression slope for the annual mean data is 0.98). There is a slight underestimate in winter (slope = 0.84), possibly caused by seasalt sulfate included in the EMEP observations but not in the model [Chin *et al.*, 2000b; Gong *et al.*, 2002]. Simulated

nitrate and ammonium compare less well with observations, with 40-60% overestimates of ammonium in summer and fall, likely due to excessive ammonia emission.

### 3.3 Asia

We evaluate our simulation of Asian outflow by using sulfate observations from the TRACE-P aircraft mission conducted off the Asian Pacific Rim from bases in Hong Kong and Japan during February-April 2001 [Jacob *et al.*, 2003]. Previous applications of GEOS-CHEM to simulation of TRACE-P observations for ozone, CO, CO<sub>2</sub>, CH<sub>4</sub>, and nitriles indicate a good simulation of Asian outflow pathways [Liu *et al.*, 2004; Heald *et al.*, 2003; Palmer *et al.*, 2003; Kiley *et al.*, 2003; Suntharalingam *et al.*, 2003; Xiao *et al.*, 2003; Li *et al.*, 2003]. Bulk aerosol measurements from the DC-8 aircraft indicate that 40% of non-seasalt sulfate (nss-SO<sub>4</sub><sup>2-</sup>) on average was incorporated in dust particles [Jordan *et al.*, 2003]. Figure 11 compares mean vertical profiles of simulated and observed nss-SO<sub>4</sub><sup>2-</sup> concentrations for the ensemble of DC-8 flights over the NW Pacific west of 177°E and at 30°-45°N latitude [Liu *et al.*, 2003]. Monthly mean concentrations in the model were sampled along the flight tracks. The observations shows strong outflow in the 0-5 km column. The model also shows an enhancement in that column but is lower than observations, by up to a factor of two. Targeted sampling of Asian outflow in the observations [Jacob *et al.*, 2003] could account for part of this discrepancy. In any case, the comparison argues that the model does not overestimate the outflow of sulfate from Asia. This is an important point for our later discussion of transpacific pollution influence.

## 4. Background aerosol in the United States: transboundary pollution influence

We now apply our model simulations to quantify background sulfate-nitrate-ammonium aerosol concentrations in the United States, and to separate the contributions to this background from natural sources and from transboundary pollution. We use for this purpose a sequence of four sensitivity simulations excluding anthropogenic emissions of both oxidant and aerosol precursors (1) globally, (2) in the United States, (3) in North America, and (4) in Asia. The results are summarized in Table 2 as annual averages for the western (west of 95°W) and eastern United States. The EPA Regional Haze Rule document [EPA, 2003a] recommends “default average natural concentrations of ammonium sulfate and ammonium nitrate” in these two regions to serve as 2064 endpoints for application of the Rule. For purpose of comparison we present our model results for sulfate and nitrate in Table 2 as those of the corresponding ammonium salts; in the model, almost all of the sulfate and nitrate are indeed associated with ammonium (Figure 9). Model results for the sum of natural and transboundary pollution contributions do not exactly add up to the independently calculated background concentrations because of chemical nonlinearities [Chin and Jacob, 1996; West *et al.*, 1999].

Our 2001 base simulation yields annual average concentrations of ammonium sulfate and ammonium nitrate of 1.52 and 1.53  $\mu\text{g m}^{-3}$ , respectively, for the western United States and 4.11 and 3.26  $\mu\text{g m}^{-3}$ , respectively, for the eastern United States. We use the sensitivity simulation with anthropogenic emissions shut off globally to estimate natural concentrations. They are 0.11  $\mu\text{g m}^{-3}$  ammonium sulfate and 0.03  $\mu\text{g m}^{-3}$  ammonium nitrate for both the western and eastern United States. Our estimate of natural concentrations for ammonium sulfate is consistent with the EPA default value (0.12  $\mu\text{g}$

$\text{m}^{-3}$ ) in the west but is factor of 2 lower than that ( $0.23 \mu\text{g m}^{-3}$ ) in the east. Oxidation of DMS is the major natural source of sulfate in the United States in the model. Our estimate of natural ammonium nitrate is three times lower than the EPA default value ( $0.1 \mu\text{g m}^{-3}$ ); it is not clear how that default value was obtained.

Let us now examine the background concentrations from the sensitivity simulation including anthropogenic emissions only outside of the United States. The mean annual concentrations of background ammonium sulfate and nitrate in surface air over the United States are  $0.43$  and  $0.27 \mu\text{g m}^{-3}$  for the west and  $0.38$  and  $0.37 \mu\text{g m}^{-3}$  for the east. These values are several-fold higher than the natural concentrations because of the influence from transboundary pollution. Background sulfate is slightly higher in the west than the east, because of Asian pollution influence as discussed further below, while background nitrate is higher in the east because of Canadian pollution influence.

We thus find that transboundary pollution influence dominates over natural sources in contributing to sulfate and nitrate background concentrations in the United States. Transboundary transport of anthropogenic emissions from Canada and Mexico is most important for nitrate, but for sulfate transpacific transport of Asian pollution is of comparable importance (Table 2). Remarkably, we find that this transpacific pollution source accounts for 30% of the sulfate aerosol background in the United States.

Figure 12a shows the global distribution of Asian pollution influence on sulfate-nitrate-ammonium aerosol concentrations in surface air, as determined by difference between the standard simulation and the sensitivity simulation with anthropogenic Asian emissions shut off. Transpacific transport from Asia to the United States mostly involves lifting of Asian air to the free troposphere by wet processes (convection, warm conveyor belts), followed by rapid advection in the westerlies and subsidence over the United States, generally behind cold fronts. Ammonium aerosol as well as gas-phase ammonia are scavenged in this wet lifting and we see therefore that transpacific transport of ammonium is negligible. In contrast, significant transpacific transport of sulfate can occur as  $\text{SO}_2$  partly escapes scavenging during lifting [Mari *et al.*, 2000; Koike *et al.*, 2003; Tu *et al.*, 2003]. Subsidence over the United States takes place mainly in the downwelling regions of the west and east, less in the upwelling region in the center of the country. Ammonium nitrate as we have seen is largely determined by difference between the total ammonium [ $\text{NH}_3^T$ ] and the sulfate concentration, and the preferential export of sulfate relative to ammonium from Asia leads to a slight negative effect of Asian pollution on nitrate concentrations in the United States.

It is of interest to compare the transpacific influence of Asian pollution on North America to the transatlantic influence of North American pollution on Europe. Figure 12b shows the latter as the difference between the standard simulation and the sensitivity simulation with anthropogenic emissions in North America shut off. We find a sulfate enhancement  $> 0.1 \mu\text{g m}^{-3}$  in surface air in Western Europe and northern Africa, comparable in magnitude to Asian pollution influence over North America. As in the case of Asian pollution, we find that export of ammonium from North American pollution is far less efficient than for sulfate, resulting in small negative influences on nitrate aerosol concentrations over Europe and Asia.

We show also in Table 2 the natural and background concentrations of elemental carbon (EC) and organic carbon mass (OMC) from our previous work [Park *et al.*, 2003]. In that work we derived optimized estimates of individual EC and OMC sources by

fitting model results to observations from the IMPROVE sites. We concluded that the EPA default natural estimates were a factor of 3 too low in the west due to underestimate of wildfire influences. Our values for the east were more consistent with EPA. In contrast to sulfate and nitrate, transboundary transport of anthropogenic carbonaceous aerosols is insignificant relative to the large natural influences from wildfires and vegetation. We further find that transpacific transport of carbonaceous aerosols from Asian pollution is less efficient than for sulfate because of scavenging in the wet lifting processes involved in Asian outflow. The excess of SO<sub>2</sub> over H<sub>2</sub>O<sub>2</sub> in the Asian outflow allows part of the sulfur to escape scavenging [Koike *et al.*, 2003; Tu *et al.*, 2003]. This result is consistent with Jaffe *et al.* [2003] who found a larger increase in sulfate concentrations relative to carbonaceous aerosol at three IMPROVE sites in the western United States during a transpacific transport event of Asian pollution.

### 5. Policy implications: the Regional Haze Rule

The U.S. EPA Regional Haze Rule [U.S. EPA, 2003a] requires states to develop plans for achieving natural visibility conditions in national parks and other wilderness areas by 2064. Visibility degradation is measured by the deciview index

$$dv = 10 \ln (b_{ext}/10), \quad (2)$$

where  $b_{ext}$  is atmospheric light extinction in units of inverse megameters ( $\text{Mm}^{-1} = 10^{-6} \text{m}^{-1}$ ). In the phase 1 implementation of the Regional Haze Rule, states have to show how they will decrease anthropogenic emissions over the 2004-2018 period in order to achieve a linear trajectory of decreasing deciviews towards the natural visibility endpoint of 2064. A linear decrease in deciviews implies an exponential decrease in aerosol extinction; as a result, and as we will see, the definition of the 2064 endpoint has important implications for determining the level of emission controls required during the 2004-2018 phase 1 implementation.

The EPA Regional Haze Rule document [U.S. EPA, 2003a] recommends a simple formula to estimate aerosol extinction by using dry mass concentrations of individual aerosol components (ammonium sulfate, ammonium nitrate, OMC, EC, soil dust, and coarse mass (CM)), as follows:

$$b_{ext} = 3f(RH)[(NH_4)_2SO_4] + 3f(RH)[NH_4NO_3] + 4[OMC] + 10[EC] + [soil] + 0.6[CM] + 10, \quad (3)$$

where  $b_{ext}$  is in units of  $\text{Mm}^{-1}$ , aerosol concentrations are in units of  $\mu\text{g m}^{-3}$ , and  $f(RH)$  is a correction factor for hygroscopic growth as a function of relative humidity (RH). The constant of 10  $\text{Mm}^{-1}$  describes the scattering by air molecules and is such that an aerosol-free atmosphere would have a deciview index of zero. “Soil” in equation (3) is the fine component of soil dust (diameter < 2.5  $\mu\text{m}$ ) and “coarse mass” is the total mass of particles with diameter > 2.5  $\mu\text{m}$ , mostly contributed by dust and sea salt. Recommended values of  $f(RH)$  for individual wilderness areas are given in the Regional Haze Rule document [U.S. EPA, 2003a]. In what follows we use typical  $f(RH)$  values of 2 and 3 for the west and east, respectively.

Applying equation (3) to aerosol concentrations given in Table 2, and assuming EPA natural default values for fine soil dust (0.5  $\mu\text{g m}^{-3}$ ) and coarse mass (3.0  $\mu\text{g m}^{-3}$ ), we compute deciview index values for baseline (present-day) conditions and for different definitions of the 2064 natural or background visibility endpoint. We use the results (Table 3) to estimate the implications of our results for phase 1 (2004-2018)

implementation of the Regional Haze Rule. Under the EPA Regional Haze Rule, the linear improvement in visibility is to be applied to the 20% most impaired visibility days and at specific locations. Here we use visibility calculated from annual mean aerosol extinctions averaged over the western and eastern United States. Nevertheless, the results serve to illustrate the sensitivity of the required 2004-2018 emission controls to the choice of 2064 endpoint.

Table 3 gives a baseline (current) visibility degradation of 14 and 23 deciviews for the western and the eastern United States, respectively. The natural visibility degradation is 6.3 and 6.2 deciviews, respectively. Organic aerosols are the dominant contributors to natural visibility degradation. Our estimate for natural visibility degradation as expressed in deciviews is 37% higher in the west and 17% lower in the east than the values computed using the natural default aerosol concentrations recommended by EPA (4.6 and 7.5 deciviews). We have previously argued in *Park et al.* [2003] that the EPA natural default concentrations underestimate the influence of wildfires in the west.

Figure 13 shows the trajectories of linear visibility improvement towards a 2064 endpoint of natural visibility defined either from our results (dashed line) or from the EPA defaults (dotted line). Following these trajectories, we find that visibility degradation during the 2004-2018 phase 1 implementation of the Regional Haze Rule should be reduced by 1.8 deciviews (west) and 3.9 deciviews (east) if our estimate of the 2064 natural visibility endpoint is used, and by 2.2 deciviews (west) and 3.6 deciviews (east) if the EPA default endpoint is used. The corresponding reductions in light extinction are  $6.7 \text{ Mm}^{-1}$  (west) and  $32.2 \text{ Mm}^{-1}$  (east) if our estimate of the 2064 natural visibility endpoint is used, and  $8.1 \text{ Mm}^{-1}$  (west) and  $30.1 \text{ Mm}^{-1}$  (east) if the EPA default endpoint is used.

Let us now estimate the required percentage reductions in U.S. anthropogenic emissions needed to achieve such improvements in light extinction. We assume a linear correspondence between aerosol extinction, aerosol concentrations, and emissions. The current aerosol extinction from U.S. anthropogenic emissions can be calculated from the data in Table 2 by subtracting the background from the baseline aerosol concentrations, and applying equation (3). We obtain values of  $18.1 \text{ Mm}^{-1}$  in the west and  $73 \text{ Mm}^{-1}$  in the east. The resulting percentage decreases of U.S. anthropogenic emissions over 2004-2018 are shown in Figure 13. They are 37% and 44% for the western and eastern United States, respectively, using our natural visibility endpoint, and 44% and 41%, respectively, using the EPA natural visibility endpoint.

These differences are significant, but looking beyond the 2018 horizon exposes a more fundamental problem with the Regional Haze Rule. Continued linear decrease towards a 2064 natural visibility endpoint would require total shutdown of U.S. anthropogenic emissions by 2041-2049 (west) or 2053-2058 (east), as shown in Figure 13. Because of transboundary pollution (assumed here to be unchanged in the future), natural visibility cannot be achieved even with total suppression of U.S. anthropogenic emissions. It will be therefore necessary to either impose emission controls on an international level or to amend the 2064 endpoint to allow for uncontrollable transboundary pollution influences. Such an amendment should define the 2064 endpoint as a background rather than natural visibility. One would then have to make estimates of future trends in foreign emissions.

However, amendment of the Regional Haze Rule to target a background visibility endpoint has major implications for phase 1 (2004-2018) emission controls in the west. Using the background deciview values in Table 3 as 2064 endpoint, the required 2004-2018 decrease in visibility degradation is 1.4 deciviews (west) and 3.3 deciviews (east). The corresponding percentage decrease of U.S. anthropogenic emissions in the west is 29%, much lower than 37% if a natural visibility endpoint from our results is used or 44% if the natural visibility endpoint from the EPA defaults is used.

## 6. Conclusions

We used a global 3-D coupled oxidant-aerosol model (GEOS-CHEM) to quantify natural and transboundary pollution influences on sulfate-nitrate-ammonium aerosol concentrations in the United States. The U.S. EPA Regional Haze Rule requires immediate action to improve visibility in U.S. national parks and other wilderness areas along a linear trajectory towards an endpoint of “natural visibility conditions” by 2064. We need to better quantify the natural aerosol concentrations defining this natural visibility, and to determine if transboundary transport of pollution not amenable to domestic emission controls elevates background aerosol concentrations in the United States significantly above the natural values. If they do, then the Regional Haze Rule must either involve international emission controls or be amended to an endpoint of “background” as opposed to “natural” visibility. “Background” is defined here following EPA [2003b] as the aerosol concentrations that would be present in the absence of U.S. anthropogenic emissions, but allowing for contributions from transboundary pollution.

We conducted full-year simulations for 1998 and 2001. Results were evaluated with observations from surface networks in the United States and Europe (IMPROVE, CASTNET, NADP, EMEP) and with Asian outflow observations from the NASA TRACE-P aircraft mission over the northwest Pacific. The model reproduces well the spatial pattern and variability of sulfate observations in the United States and Europe across all seasons, with no systematic biases. Comparison with the TRACE-P observations indicates that Asian outflow of sulfate is if anything underestimated. Nitrate and ammonium aerosol concentrations in the model are highly correlated with observations but are too high in summer and fall, a problem that we attribute to seasonal overestimate of ammonia emissions [Gilliland *et al.*, 2003]. We find that the availability of ammonia limits the formation of ammonium nitrate in most of North America. The aerosol is typically 80-100% neutralized, both in the model and in the observations, with maximum acidity in summer.

We used a sequence of sensitivity simulations to quantify background sulfate-nitrate-ammonium aerosol concentrations in the United States, and to separate the contributions to this background from natural sources and from transboundary pollution. Our 2001 base simulation yields annual average concentrations of ammonium sulfate and ammonium nitrate of 1.52 and 1.53  $\mu\text{g m}^{-3}$ , respectively, for the western United States and 4.11 and 3.26  $\mu\text{g m}^{-3}$ , respectively, for the eastern United States. Our best estimates of mean annual natural concentrations are 0.11  $\mu\text{g m}^{-3}$  ammonium sulfate and 0.03  $\mu\text{g m}^{-3}$  ammonium nitrate for both the western and eastern United States. Our values are consistent with or lower than the default values recommended by EPA for natural visibility calculations in the context of the Regional Haze Rule.

Our best estimates of background concentrations for ammonium sulfate and ammonium nitrate are 0.43 and 0.27  $\mu\text{g m}^{-3}$  for the west and 0.38 and 0.37  $\mu\text{g m}^{-3}$  for the east. These values are considerably higher than the natural concentrations, pointing to the dominance of transboundary pollution in defining the background. Transpacific transport of Asian pollution is of comparable importance to transport from Canada and Mexico in contributing to the background sulfate enhancement over the United States. A significant enhancement of sulfate relative to other aerosols in the Asian outflow can occur as  $\text{SO}_2$  partly escapes scavenging during wet lifting processes. In the case of ammonium nitrate, the transboundary pollution enhancement is mostly from Canada, and transpacific Asian pollution actually causes a slight depression (less than 0.1  $\mu\text{g m}^{-3}$ ) due to the added sulfate.

We assessed the implications of our results for implementation of the Regional Haze Rule. For this purpose we used our model to define the linear trend of visibility from present (2004) to natural or background (2064) conditions. We found that transboundary pollution prevents natural visibility from being achieved even with total suppression of U.S. anthropogenic emissions, implying the need for either international emission controls or for amendment of the 2064 endpoint to allow for uncontrollable transboundary pollution influences. The latter would require some estimates of future trends in transboundary pollution influences but these have large uncertainties. Projections by *IPCC* [2001] for 2060 anthropogenic sulfur emissions from Asia range from 30% to 160% of present-day levels depending on the socioeconomic scenario. Consideration of a background rather than natural visibility 2064 endpoint would have immediate implications for phase 1 implementation (2004-2018) of the Regional Haze Rule. It would imply, at least in the west, a significantly slower schedule of U.S. anthropogenic emission reductions.

Our results are only a first attempt to quantify natural and transboundary pollution influences in the United States using a global 3-D model analysis. In future work we plan to examine in more detail the observational constraints on aerosol background concentrations in the United States, including site-by-site analysis and frequency distributions of aerosol concentrations. Specification of natural and background aerosol concentrations for regulatory purposes will require formal uncertainty bounds to be placed on model estimates, and again this will require more extensive evaluation with observations as well as higher-resolution simulations with a nested regional model.

**Acknowledgments.** This work was supported by the Electric Power Research Institute (EPRI) and by the EPA Intercontinental transport and Climatic effects of Air Pollutants (ICAP) program. Development of the GEOS-CHEM model is supported by the Atmospheric Chemistry Modeling and Analysis Program (ACMAP) of the National Aeronautics and Space Administration (NASA).

## References

Adams, P. J., J. H. Seinfeld, and D. M. Koch, Global concentrations of tropospheric sulfate, nitrate, and ammonium aerosol simulated in a general circulation model, *J. Geophys. Res.*, 104(D11), 13,791-13,823, 1999.

- Adams, P., J. Seinfeld, D. Koch, L. Mickley, D. Jacob, General circulation model assessment of direct radiative forcing by the sulfate-nitrate-ammonium-water inorganic aerosol system, *J. Geophys. Res.*, *106*(D1), 1097-1112, 2001.
- Andreae, M. O. and P. Merlet, Emission of trace gases and aerosols from biomass burning, *Global Biogeochem. Cycles*, *15*(4), 955-966, 2001.
- Andres, R. J., and A. D. Kasgnoc, A time-averaged inventory of subaerial volcanic sulfur emissions, *J. Geophys. Res.*, *103*, 25,251-25,261, 1998.
- Aneja, V. P., J. P. Chauhan, and J. T. Walker, Characterization of atmospheric ammonia emissions from swine waste storage and treatment lagoons, *J. Geophys. Res.*, *105*(D9), 11,535-11,545, 2000.
- Ansari, A. S., and S. N. Pandis, Response of inorganic PM to precursor concentrations, *Environ. Sci. Technol.*, *32*, 2706-2714, 1998.
- Barrie, L. A., Y. Yi, W. R. Leitch, U. Lohmann, P. Kasibhatla, G. J. Roelofs, J. Wilson, F. McGovern, C. Benkovitz, M. A. Melieres, K. Law, J. Prospero, M. Kritz, D. Bergmann, C. Bridgeman, M. Chin, J. Christensen, R. Easter, J. Feichter, C. Land, A. Jeuken, E. Kjellstrom, D. Koch, and P. Rasch, A comparison of large-scale atmospheric sulphate aerosol models (COSAM): overview and highlights, *Tellus Ser. B-Chem. Phys. Meteorol.*, *53*(5), 615-645, 2001.
- Benkovitz, C. M., M. T. Scholtz, J. Pacyna, L. Tarrason, J. Dignon, E. C. Voldner, P. A. Spiro, J. A. Logan, and T. E. Graedel, Global gridded inventories of anthropogenic emissions of sulfur and nitrogen, *J. Geophys. Res.*, *101*(D22), 29,239-29,253, 1996.
- Berntsen, T. K., S. Karlsdóttir, and D. A. Jaffe, Influence of Asian emissions on the composition of air reaching the North Western United States, *Geophys. Res. Lett.*, *26*(14), 2171-2174, 1999.
- Bertschi, I. T., D. A. Jaffe, L. Jaeglé, H. U. Price, and J. B. Dennison, PHOBEA/ITCT 2002 Airborne Observations of trans-Pacific Transport of Ozone, CO, VOCs, and Aerosols to the Northeast Pacific: Impacts of Asian Anthropogenic and Siberian Boreal Fire Emissions, *J. Geophys. Res.*, submitted, 2003.
- Bey I., D. J. Jacob, R. M. Yantosca, J. A. Logan, B. Field, A. M. Fiore, Q. Li, H. Liu, L. J. Mickley, and M. Schultz, Global modeling of tropospheric chemistry with assimilated meteorology: Model description and evaluation, *J. Geophys. Res.*, *106* (D19), 23,073-23,096, 2001a.
- Bey, I., D. J. Jacob, J. A. Logan, and R. M. Yantosca, Asian chemical outflow to the Pacific in spring: Origins, pathways, and budgets, *J. Geophys. Res.*, *106* (D19), 23097-23113, 2001b.
- Binkowski, F. S., and S. J. Roselle, Models-3 Community Multiscale Air Quality (CMAQ) model aerosol component, 1, Model description, *J. Geophys. Res.*, *108* (D6), 4183, doi:10.1029/2001JD001409, 2003.
- Bouwman, A. F., D. S. Lee, W. A. H. Asman, F. J. Dentener, K. W. VanderHoek, and J. G. J. Olivier, A global high-resolution emission inventory for ammonia, *Glob. Biogeochem. Cycle*, *11*(4), 561-587, 1997.
- Chatfield, R. B., and P. J. Crutzen, Are there interactions of iodine and sulfur species in marine air photochemistry? *J. Geophys. Res.*, *95*, 22,319-22,341, 1990.
- Chin, M., D. J. Jacob, G. M. Gardner, M. S. Foreman-Fowler, and P. A. Spiro, and D. L. Savoie, A global three-dimensional model of tropospheric sulfate, *J. Geophys. Res.*, *101*(D13), 18,667-18,690, 1996.
- Chin, M., and D. J. Jacob, Anthropogenic and natural contributions to tropospheric sulfate: A global model analysis, *J. Geophys. Res.*, *101*(D13), 18,691-18,699, 1996.
- Chin, M., R. B. Rood, S.-J. Lin, J.-F. Müller, and A. M. Thompson, Atmospheric sulfur cycle simulated in the global model GOCART: Model description and global properties, *J. Geophys. Res.*, *105*(D20), 24,671-24,687, 2000a.

- Chin, M., D. L. Savoie, B. J. Huebert, A. R. Bandy, D. C. Thornton, T. S. Bates, P. K. Quinn, E. S. Saltzman, and W. J. De Bruyn, Atmospheric sulfur cycle simulated in the global model GOCART: Comparison with field observations and regional budgets, *J. Geophys. Res.*, *105*(D20), 24,689-24,712, 2000b.
- DeMore, W. B., S. P. Sander, D. M. Golden, R. F. Hampson, M. J. Kurylo, C. J. Howard, A. R. Ravishankara, C. E. Kolb, and M. J. Molina, Chemical kinetics and photochemical data for use in stratospheric modeling, Evaluation number 12, *JPL Publ.* 97-4, 1997.
- Dentener, F. J., and P. J. Crutzen, A 3-Dimensional Model of the Global Ammonia Cycle, *J. Atmos. Chem.*, *19*(4), 331-369, 1994.
- Duncan, B. N., R. V. Martin, A. C. Staudt, R. Yevich, J. A. Logan, Interannual and Seasonal Variability of Biomass Burning Emissions Constrained by Satellite Observations, *J. Geophys. Res.*, *108*, 4040, doi:10.1029/2002JD002378, 2003.
- EMEP/UNECE, Present state of emission data, EB. AIR/GE., 2003.
- Fiore, A. M., D. J. Jacob, I. Bey, R. M. Yantosca, B. D. Field, A. C. Fusco, and J. G. Wilkinson, Background ozone over the United States in summer: Origin, trend, and contribution to pollution episodes, *J. Geophys. Res.*, *107*, doi:10.1029/2001JD000982, 2002.
- Fiore, A. M., D. J. Jacob, R. Mathur, and R. V. Martin, Application of empirical orthogonal functions to evaluate ozone simulations with regional and global models, *J. Geophys. Res.*, *108*, 4431, doi: 10.1029/2002JD003151, 2003a.
- Fiore, A. M., D. J. Jacob, H. Liu, R. M. Yantosca, T. D. Fairlie, and Q. B. Li, Variability in surface ozone background over the United States: Implications for air quality policy, *J. Geophys. Res.*, *108*, 4787, doi:10.1029/2003JD003855, 2003b.
- Gilliland, A. B., R. L. Dennis, S. J. Roselle, and T. E. Pierce, Seasonal NH<sub>3</sub> emission estimates for the eastern United States based on ammonium wet concentrations and an inverse modeling method, *J. Geophys. Res.*, *108*(D15), 4477, doi:10.1029/2002JD003063, 2003.
- Gong, S. L., L. A. Barrie, and M. Lazare, Canadian Aerosol Module (CAM): A size-segregated simulation of atmospheric aerosol processes for climate and air quality models, 2, Global sea-salt aerosol and its budgets, *J. Geophys. Res.*, *107*(D24), 4779, doi:10.1029/2001JD002004, 2002.
- Heald, C.L., D.J. Jacob, A.M. Fiore, L.K. Emmons, J.C. Gille, M.N. Deeter, J. Warner, D.P. Edwards, J.H. Crawford, A.J. Hamlin, G.W. Sachse, E.V. Browell, M.A. Avery, S.A. Vay, D.J. Westberg, D. R. Blake, H.B. Singh, S.T. Sandholm, R.W. Talbot, H.E. Fuelberg Asian outflow and transpacific transport of carbon monoxide and ozone pollution: An integrated satellite, aircraft and model perspective, *J. Geophys. Res.*, *108*(D24), 4804, doi:10.1029/2003JD003507, 2003.
- Hirsch, R. M., and E. J. Gilroy, Methods of fitting a straight line to data: examples in water resources, *Water Res. Bull.*, *20*, 705-711, 1984.
- Husar, et al., Asian dust events of April 1998, *J. Geophys. Res.*, *106*(D16), 18,317-18,330, 2001.
- Intergovernmental Panel on Climate Change (IPCC), *Special Report on Emissions Scenarios*, edited by Nebojsa Nakicenovic, Cambridge Univ. Press, New York, 2001.
- Jacob, D. J., Chemistry of OH in Remote Clouds and Its Role in the Production of Formic-Acid and Peroxymonosulfate, *J. Geophys. Res.*, *91*(D9), 9807-9826, 1986.
- Jacob, D. J., J. A. Logan, and P. P. Murti, Effect of rising Asian emissions on surface ozone in the United States, *Geophys. Res. Lett.*, *26*(14), 2175-2178, 1999.
- Jacob, D. J., Heterogeneous chemistry and tropospheric ozone, *Atmos. Environ.*, *34*, 2131-2159, 2000.

- Jacob, D. J., J. H. Crawford, M. M. Kleb, V. S. Connors, R. J. Bendura, J. L. Raper, G. W. Sachse, J. C. Gille, L. Emmons, and C. L. Heald, Transport and Chemical Evolution over the Pacific (TRACE-P) aircraft mission: Design, execution, and first results, *J. Geophys. Res.*, *108*(D20), 9000, doi:10.1029/2002JD003276, 2003.
- Jaeglé, L., D. Jaffe, H.U. Price, P. Weiss, P.I. Palmer, M.J. Evans, D.J. Jacob, and I. Bey, Sources and budgets for CO and ozone in the northeastern Pacific during the spring of 2001: results from the PHOBEA -II experiment, *J. Geophys. Res.*, *108*, 8803, 10.1020/2002JD003121, 2003.
- Jaffe, D., T. Anderson, D. Covert, R. Kotchenruther, B. Trost, J. Danielson, W. Simpson, T. Berntsen, S. Karlsdottir, D. Blake, J. Harris, G. Carmichael, and I. Uno, Transport of Asian air pollution to North America, *Geophys. Res. Lett.*, *26*(6), 711-714, 1999.
- Jaffe, D., I. McKendry, T. Anderson, and H. Price, Six 'new' episodes of trans-Pacific transport of air pollutants, *Atmos. Environ.*, *37*(3), 391-404, 2003.
- Jordan, C. E., J. E. Dibb, B. E. Anderson, and H. E. Fuelberg, Uptake of nitrate and sulfate on dust aerosols during TRACE-P, *J. Geophys. Res.*, *108*(D21), 8817, doi:10.1029/2002JD003101, 2003.
- Kettle, A. J., et al., A global database of sea surface dimethylsulfide (DMS) measurements and a procedure to predict sea surface DMS as a function of latitude, longitude, and month, *Glob. Biogeochem. Cycle*, *13*(2), 399-444, 1999.
- Koike, M., et al., Export of anthropogenic reactive nitrogen and sulfur compounds from the East Asia region in spring, *J. Geophys. Res.*, *108*(D20), 8789, doi:10.1029/2002JD003284, 2003.
- Kreidenweis S. M., C. J. Walcek, G. Feingold, W. Gong, M. Z. Jacobson, C.-H. Kim, X. Liu, J. E. Penner, A. Nenes, and J. H. Seinfeld, Modification of aerosol mass and size distribution due to aqueous-phase SO<sub>2</sub> oxidation in clouds: Comparisons of several models, *J. Geophys. Res.*, *108*(D7), 4213, doi:10.1029/2002JD002697, 2003.
- Kiley, C. M., et al., An intercomparison and evaluation of aircraft-derived and simulated CO from seven chemical transport models during the TRACE-P experiment, *J. Geophys. Res.*, *108*(D21), 8819, doi:10.1029/2002JD003089, 2003.
- Lavery, T. F., C. M. Rogers, H. Kemp Howell, M. C. Burnett, C. A. Wanta, M. O. Stewart, Clean Air Status and Trends Network (CASTNet) 2001 Annual Report, 2002.
- Li, Q., D. J. Jacob, J. A. Logan, I. Bey, R. M. Yantosca, H. Liu, R. V. Martin, A. M. Fiore, B. D. Field, B. N. Duncan, and V. Thouret, A tropospheric ozone maximum over the Middle East, *Geophys. Res. Lett.*, *28*, 3235-3238, 2001.
- Li, Q., D. J. Jacob, I. Bey, P. I. Palmer, B. N. Duncan, B. D. Field, R. V. Martin, A. M. Fiore, R. M. Yantosca, D. D. Parrish, P. G. Simmonds, and S. J. Oltmans, Transatlantic transport of pollution and its effects on surface ozone in Europe and North America, *J. Geophys. Res.*, *107*(D13), doi:10.1029/2001JD001422, 2002a.
- Li, Q., D. J. Jacob, T. D. Fairlie, H. Liu, R. V. Martin, and R. M. Yantosca, Stratospheric versus pollution influences on ozone at Bermuda: Reconciling past analyses, *J. Geophys. Res.*, *107*(D22), 4611, doi:10.1029/2002JD00213, 2002b.
- Li Q., D. J. Jacob, R. Yantosca, C. Heald, H. Singh, M. Koike, Y. Zhao, G. W. Sachse, and D. Streets, A global three-dimensional model analysis of the atmospheric budgets of HCN and CH<sub>3</sub>CN: constraints from aircraft and ground measurements, *J. Geophys. Res.*, *108*(D21), 8827, doi:10.1029/2002JD003075, 2003.
- Li, Q. B., D. J. Jacob, R. M. Yantosca, J. W. Munger, and D. D. Parrish, Export of NO<sub>y</sub> from the North American Boundary Layer: Reconciling Aircraft Observations and Global Model Budgets, *J. Geophys. Res.*, *109*(D2), D02109, 10.1029/2003JD003912, 2004.

- Liss, P. S., and L. Merlivat, Air-sea gas exchange rates: Introduction and synthesis, in *The Role of Air-Sea Exchange in Geochemical Cycling*, edited by P. Buat-Ménard, D. Riedel, pp. 113-127, Norwell, Mass., 1986.
- Liu, H., D. J. Jacob, I. Bey, and R. M. Yantosca, Constraints from  $^{210}\text{Pb}$  and  $^7\text{Be}$  on wet deposition and transport in a global three-dimensional chemical tracer model driven by assimilated meteorological fields, *J. Geophys. Res.*, *106*, 12,109-12,128, 2001.
- Liu, H., D. J. Jacob, L. Y. Chan, S. J. Oltmans, I. Bey, R. M. Yantosca, J. M. Harris, B. N. Duncan, and R. V. Martin, Sources of tropospheric ozone along the Asian Pacific Rim: An analysis of ozonesonde observations, *J. Geophys. Res.*, *106*, 10.1029/2001JD002005, 2002.
- Liu, H., D. J. Jacob, I. Bey, R. M. Yantosca, B. N. Duncan, and G. W. Sachse, Transport pathways for Asian pollution outflow over the Pacific: Interannual and seasonal variations, *J. Geophys. Res.*, *108*(D20), 8786, doi:10.1029/2002JD003102, 2003.
- Liu, H., D. J. Jacob, J. E. Dibb, A. M. Fiore, and R. M. Yantosca, Constraints on the sources of tropospheric ozone from  $^{210}\text{Pb}$ - $^7\text{Be}$ -O<sub>3</sub> correlations, *J. Geophys. Res.*, in press, 2004.
- Malm, W. C., J. F. Sisler, D. Huffman, R. A. Eldred, and T. A. Cahill, Spatial and seasonal trends in particle concentration and optical extinction in the United States, *J. Geophys. Res.*, *99*, 1347-1370, 1994.
- Malm, W. C., M. L. Pitchford, M. Scruggs, J. F. Sisler, R. Ames, S. Copeland, K. A. Gebhart, and D. E. Day, Spatial and seasonal Patterns and Temporal Variability of Haze and Its constituents in the United States: Report III, Cooperative Institute for Research, Colorado State University, Fort Collins, Colorado, 2000.
- Mari, C., D. J. Jacob, and P. Bechtold, Transport and scavenging of soluble gases in a deep convective cloud, *J. Geophys. Res.*, *105*(D17), 22255-22267, 2000.
- Martin, R. V., D. J. Jacob, J. A. Logan, I. Bey, R. M. Yantosca, A. C. Staudt, Q. Li, A. M. Fiore, B. N. Duncan, H. Liu, P. Ginoux, and V. Thouret, Interpretation of TOMS observations of tropical tropospheric ozone with a global model and in-situ observations, *J. Geophys. Res.*, *107*(D18), 4351, 10.1029/2001JD001480, 2002.
- Martin, R. V., D. J. Jacob, R. M. Yantosca, M. Chin, and P. Ginoux, Global and Regional Decreases in Tropospheric Oxidants from Photochemical Effects of Aerosols, *J. Geophys. Res.*, *108*(D3), 4097, doi:10.1029/2002JD002622, 2003.
- Martin, S. T., H. M. Hung, R. J. Park, D. J. Jacob, R. J. D. Spurr, K. V. Chance, and M. Chin, Effects of the Physical State of Tropospheric Ammonium-Sulfate Nitrate Particles on Global Aerosol Direct Radiative Forcing, *Atmos. Chem. Phys.*, *4*, 183-214, 2004
- McKendry, I. G., J. P. Hacker, R. Stull, S. Sakiyama, D. Mignacca, and K. Reid, Long-range transport of Asian dust to the Lower Fraser Valley, British Columbia, Canada, *J. Geophys. Res.*, *106*(D16), 18,361-18,370, 2001.
- National Atmospheric Deposition Program (NADP), National Atmospheric Deposition Program 2001 Annual Summary, *NADP Data Report 2002-01*, Illinois State Water Survey, Champaign, IL, 2002.
- NARSTO, Particulate matter science for policy makers, NARSTO Management office (Envair), Pasco, Washington, <http://www.cgenv.com/Narston/>, 2003.
- Palmer P. I., D. J. Jacob, D. B. A. Jones, C. L. Heald, R. M. Yantosca, J. A. Logan, G. W. Sachse, D. G. Streets, Inverting for emissions of carbon monoxide from Asia using aircraft observations over the western Pacific, *J. Geophys. Res.*, *108*(D21), 8828, doi:10.1029/2003JD003397, 2003.
- Park, R. J., D. J. Jacob, M. Chin and R. V. Martin, Sources of carbonaceous aerosols over the United States and implications for natural visibility, *J. Geophys. Res.*, *108*(D12), 4355, doi:10.1029/2002JD003190, 2003.

- Roelle, P. A., and V. P. Aneja, Characterization of ammonia emissions from soils in the upper coastal plain, North Carolina, *Atmos. Environ.*, *36*, 1087-1097, 2002.
- Seinfeld, J. H., and S. N. Pandis, Atmospheric Chemistry and Physics: From Air Pollution to Climate Change, J. Wiley, New York, 1998.
- Somerville, R. C. J., and L. A. Remer, Cloud optical thickness feedbacks in the CO<sub>2</sub> climate problem, *J. Geophys. Res.*, *89*, 9668-9672, 1984.
- Sundqvist, H., E. Berge, and J. E. Kristiansson, Condensation and cloud parameterization studies with a mesoscale numerical weather prediction model, *Mon. Weather Rev.*, *117*, 1641-1657, 1989.
- Suntharalingam, P., D. J. Jacob, P. I. Palmer, J. A. Logan, R. M. Yantosca, Y. Xiao, M. J. Evans, D. G. Streets, S. L. Vay, and G. W. Sachse, Improved quantification of Chinese carbon fluxes using CO<sub>2</sub>/CO correlations in Asian outflow, *J. Geophys. Res.*, submitted, 2003.
- Streets, D. G., et al., An inventory of gaseous and primary aerosol emissions in Asia in the year 2000, *J. Geophys. Res.*, *108*(D21), 8809, doi:10.1029/2002JD003093, 2003.
- Tu, F. H., D. C. Thornton, A. R. Bandy, M.-S. Kim, G. Carmichael, Y. Tang, L. Thornhill, and G. Sachse, Dynamics and transport of sulfur dioxide over the Yellow Sea during TRACE-P, *J. Geophys. Res.*, *108*(D20), 8790, doi:10.1029/2002JD003227, 2003.
- U.S. EPA, National Air Quality and Emissions Trends Report, 1999, U. S. EPA OAQPS report, Research Triangle Park, EPA 454/R-01-004, 2001.
- U.S. EPA, Guidance for Estimating Natural Visibility Conditions Under the Regional Haze Rule, U. S. EPA OAQPS report, Research Triangle Park, EPA 454/B-03-005, 2003a.
- U.S. EPA, Air Quality Criteria for Ozone and Related Photochemical Oxidants, Research Triangle Park, NC, manuscript in preparation, 2003b.
- Vaughan, J. K., C. Claiborn, and D. Finn, April 1998 Asian dust event over the Columbia Plateau, *J. Geophys. Res.*, *106*(D16), 18,381-18,402, 2001.
- Wang, Y., D. J. Jacob, and J. A. Logan, Global simulation of tropospheric O<sub>3</sub>-NO<sub>x</sub>-hydrocarbon chemistry, 1. Model formulation, *J. Geophys. Res.*, *103*(D9), 10,713-10,726, 1998.
- Wesely, M. L., Parameterization of surface resistance to gaseous dry deposition in regional-scale numerical models, *Atmos. Environ.*, *23*, 1293-1304, 1989.
- West J., A. Ansari, and S. N. Pandis, Marginal PM<sub>2.5</sub> – Nonlinear aerosol mass response to sulfate reductions, *J. Air Waste Man. Assoc.*, *49*, 1415-1424, 1999.
- Xiao Y., D. J. Jacob, J. S. Wang, J. A. Logan, P. I. Palmer, P. Suntharalingam, R. M. Yantosca, G. W. Sachse, D. R. Blake, D. G. Streets, Constraints on Asian and European sources of methane from CH<sub>4</sub> - C<sub>2</sub>H<sub>6</sub>-CO correlations in Asian outflow, *J. Geophys. Res.*, submitted, 2003.
- Yevich, R. and J. A. Logan, An assesment of biofuel use and burning of agricultural waste in the developing world, *Global Biogeochem. Cycles*, *17*(4), 1095, doi:10.1029/2002GB001952, 2003.

## Figures Captions

Figure 1. Monthly ammonia emissions in the contiguous United States. The values used in this work, broken down by source type (left bars), are compared to the values reported by Gilliland *et al.* [2003] (right bars) from inverse modeling of eight months of precipitation NH<sub>4</sub><sup>+</sup> data.

Figure 2. Sampling sites from the I[M]PROVE, [C]ASTNET, and NA[D]P networks in 2001.

Figure 3. Annual mean concentrations of sulfate in surface air over the United States in 2001. The top panel shows results from the GEOS-CHEM model. The middle and bottom panels show the observations from the IMPROVE and CASTNET networks, respectively, averaged over the model  $2^\circ \times 2.5^\circ$  grid.

Figure 4. Scatterplot of simulated versus observed sulfate concentrations at the IMPROVE and CASTNET sites, and sulfate deposition fluxes at NADP sites (Figure 2). Values are annual means (top panels) and seasonal means for 2001. Sites in the western and eastern United States (separated at  $95^\circ\text{W}$ ) are shown as pluses and open circles, respectively. Thick solid lines are reduced major axis regressions for the ensemble of the data; regression equations and  $R^2$  are shown inset. Thin solid lines show the  $y=x$  relationship.

Figure 5. Annual mean concentrations of ammonium in surface air over the United States in 2001. The top panel shows results from the GEOS-CHEM model. The bottom panel shows the observations from the CASTNET networks averaged over the model  $2^\circ \times 2.5^\circ$  grid (ammonium is not measured at the IMPROVE sites).

Figure 6. Scatterplot of simulated versus observed ammonium concentrations at the CASTNET sites (left column), and nitrate concentrations at the CASTNET and IMPROVE sites (right two columns). Values are annual means (top panels) and seasonal means for 2001. Sites in the western and eastern United States (separated at  $95^\circ\text{W}$ ) are shown as pluses and open circles, respectively. Thick solid lines are reduced major axis regressions for the ensemble of the data; regression equations and  $R^2$  are shown inset. Thin solid lines show the  $y=x$  relationship.

Figure 7. Same as in Figure 3 but for nitrate.

Figure 8. Simulated gas ratio (GR; equation (1)) defined as the available ammonia concentration beyond that required for sulfate neutralization, divided by the total inorganic nitrate concentration (gas + aerosol) [Ansari and Pandis, 1998]. Values are computed from annual mean concentrations in surface air. Formation of ammonium nitrate aerosol is limited by the availability of nitric acid if  $\text{GR} > 1$ , by the availability of ammonia if  $0 < \text{GR} < 1$ , and is totally suppressed if  $\text{GR} < 0$ .

Figure 9. Scatterplot of seasonal mean  $[\text{NH}_4^+]$  vs.  $(2[\text{SO}_4^{2-}] + [\text{NO}_3^-])$  at CASTNET sites in 2001, in the GEOS-CHEM model (top) and in observations (bottom). The reduced-major-axis regression slopes (given on the Figure) indicate the degree of acid neutralization.

Figure 10. Scatterplot of simulated versus observed sulfate (left), nitrate (middle) and ammonium (right) concentrations at 93 European EMEP sites. Values are annual means (top panels) and seasonal means for 1998. Thick solid lines are reduced major axis

regressions for the ensemble of the data; regression equations and  $R^2$  are shown inset. Thin solid lines show the  $y=x$  relationship.

Figure 11. Simulated vs. observed mean vertical profiles of non-sea-salt sulfate ( $\text{nss-SO}_4^{2-}$ ) concentrations over the NW Pacific from the TRACE-P aircraft mission in February-April 2001. The observations are binned vertically in 1-km intervals. The solid line shows mean observed values from *Jordan et al.* [2003] for the ensemble of DC-8 flights north of  $30^\circ\text{N}$  ( $30\text{-}45^\circ\text{N}$ ,  $124\text{-}177^\circ\text{E}$ ), with standard deviations represented by horizontal bars. The dashed line shows the corresponding monthly mean model values along the flight tracks.

Figure 12a. Enhancements of sulfate-nitrate-ammonium aerosol concentrations in surface air due to anthropogenic emissions from Asia. Values are annual means for 2001 and were obtained by difference between the standard model simulation and a sensitivity simulation with Asian anthropogenic sources shut off.

Figure 12b. Same as in Figure 12a but for anthropogenic emissions from North America.

Figure 13. Illustrative example of required visibility improvements (top) and domestic emission reductions (bottom) over the 2004-2064 period for the western and the eastern United States (separated at  $95^\circ\text{W}$ ) under the EPA Regional Haze Rule [*U.S. EPA*, 2003a]. The visibility endpoints are as given in Table 3. The required percentage decrease in U.S. anthropogenic emissions corresponding to a given visibility improvement is computed by assuming a linear correspondence between aerosol extinction and emissions. Results are shown for different choices for the 2064 endpoint: (1) EPA natural default visibility (dotted lines), (2) our estimate of natural visibility (dashed lines), and (3) our estimate of background visibility (solid lines). Background includes contributions from both natural and transboundary pollution sources. Year 2018 (thin vertical line) is the target date for phase 1 implementation of the Regional Haze Rule.

## Tables

Table 1a. Sulfur emissions for 2001 (Tg S yr<sup>-1</sup>).

Source type	Globe	Contiguous United States
Total	78	8.3
<b>Anthropogenic source total</b>	<b>57</b>	<b>8.3</b>
Industrial activity	56	8.3
Biofuel use	0.27	< 0.01
Aircraft	0.07	0.02
<b>Natural source total</b>	<b>21</b>	<b>0.01</b>
Ocean (DMS)	15	0
Volcanoes	4.8	0
Biomass burning	1.3	0.01

Table 1b. Ammonia emissions for 2001 (Tg N yr<sup>-1</sup>).

Source type	Globe	Contiguous United States
Total	55	2.8
<b>Anthropogenic source total</b>	<b>35</b>	<b>2.2</b>
Domesticated animals	21	1.3
Fertilizers	9.0	0.49
Human bodies	2.6	0.13
Biofuel use	1.6	0.18
Industry	0.2	0.03
Fossil fuel use	0.1	0.06
<b>Natural source total</b>	<b>20</b>	<b>0.59</b>
Ocean	8.2	0
Biomass burning	5.9	0.04
Crop	3.5	0.44
Soil	2.4	0.1
Wild animals	0.1	0.01

Table 1c. NO<sub>x</sub> emissions for 2001 (Tg N yr<sup>-1</sup>).

Source type	Globe	Contiguous United States
Total	43	7.4
<b>Anthropogenic source total</b>	<b>27</b>	<b>6.8</b>
Fossil fuel use	24	6.7
Biofuel use	2.2	0.02
Fertilizer	0.47	0.07
<b>Natural source total</b>	<b>17</b>	<b>0.66</b>
Biomass burning	6.5	0.05
Natural soil	5.3	0.36
Lightning	4.7	0.25

Table 2. Background aerosol concentrations ( $\mu\text{g m}^{-3}$ ) in the United States<sup>a</sup>.

	Ammonium sulfate		Ammonium nitrate		Elemental carbon		Organic carbon mass	
	West	East	West	East	West	East	West	East
Baseline (2001)	1.52	4.11	1.53	3.26	0.27	0.66	1.77	3.07
Background	0.43	0.38	0.27	0.37	0.08	0.06	1.30	1.22
Natural	0.11	0.11	0.03	0.03	0.06	0.04	1.25	1.17
Transboundary pollution	0.28	0.26	0.18	0.23	0.02	0.02	0.05	0.05
Canada and Mexico	0.15	0.14	0.2	0.25	0.02	0.02	0.04	0.04
Asia	0.13	0.12	-0.02	-0.02	<0.01	<0.01	0.01	<0.01
EPA natural defaults <sup>b</sup>	0.12	0.23	0.1	0.1	0.02	0.02	0.47	1.40

<sup>a</sup>Values are annual and spatial means from the standard 2001 simulation (baseline) and from the sensitivity simulations described in section 2.1. Partitioning between west and east is at 95°W. Background and natural concentrations are obtained from the sensitivity simulations without U.S. and global anthropogenic emissions, respectively.

Transboundary pollution influences from Canada and Mexico are determined by difference between two sensitivity simulations with anthropogenic emissions shut off in the United States versus in all of North America. Transpacific pollution influences from Asia are determined by difference between the standard simulation and the sensitivity simulation with anthropogenic sources shut off in Asia. Results for elemental carbon (EC) and organic carbon mass (OMC) are from our previous work [Park *et al.*, 2003] in a simulation using climatological emissions from wildfires.

<sup>b</sup>“Default average natural concentrations” recommended by U.S. EPA [2003a] for estimating natural visibility conditions as 2064 endpoint in the application of the EPA Regional Haze Rule.

Table 3. Visibility degradation (deciviews) in the United States<sup>a</sup>.

	West	East
Baseline (2001)	14	23
Background <sup>b</sup>	8.1	9.0
Natural		
This work	6.3	6.2
EPA default	4.6	7.5

<sup>a</sup>Visibility degradation in deciviews (equation (2)) calculated from mean annual aerosol extinction as given by equation (3). Aerosol concentrations for use in equation (3) are from Table 2, with in addition EPA default natural values for soil ( $0.5 \mu\text{g m}^{-3}$ ) and coarse mass (CM) ( $3.0 \mu\text{g m}^{-3}$ ). Values of  $f(RH)$  in equation (3) are 2 in the west and 3 in the east.

<sup>b</sup>Including contributions to visibility degradation from both natural and transboundary pollution sources.

Figures

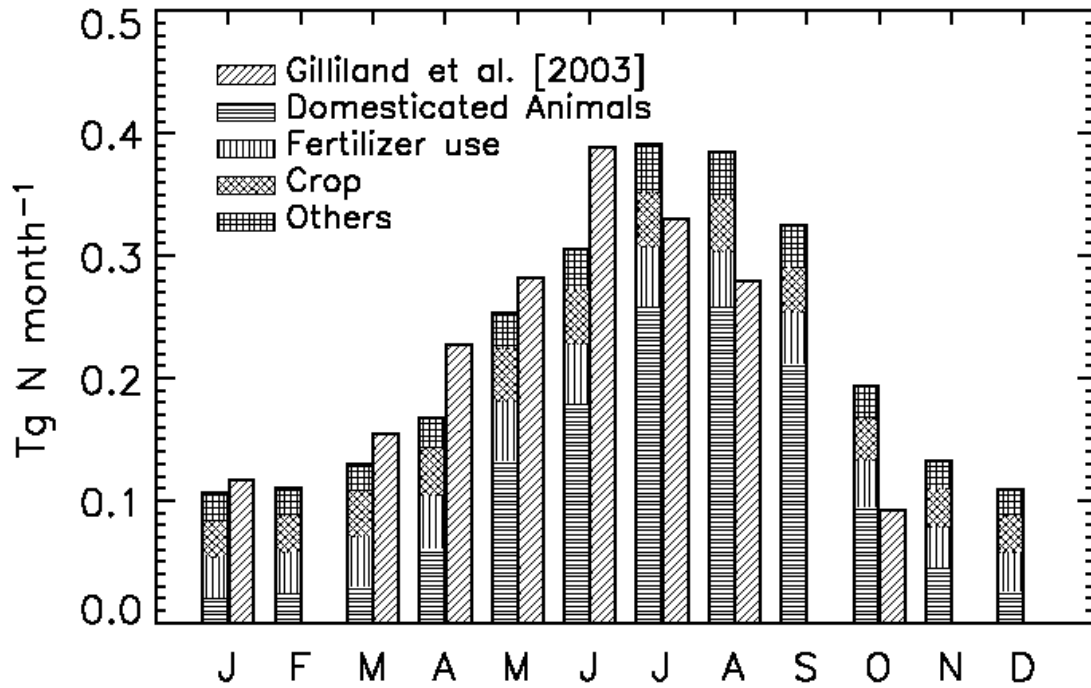


Figure 1. Monthly ammonia emissions in the contiguous United States. The values used in this work, broken down by source type (left bars), are compared to the values reported by Gilliland *et al.* [2003] (right bars) from inverse modeling of eight months of precipitation  $\text{NH}_4^+$  data.

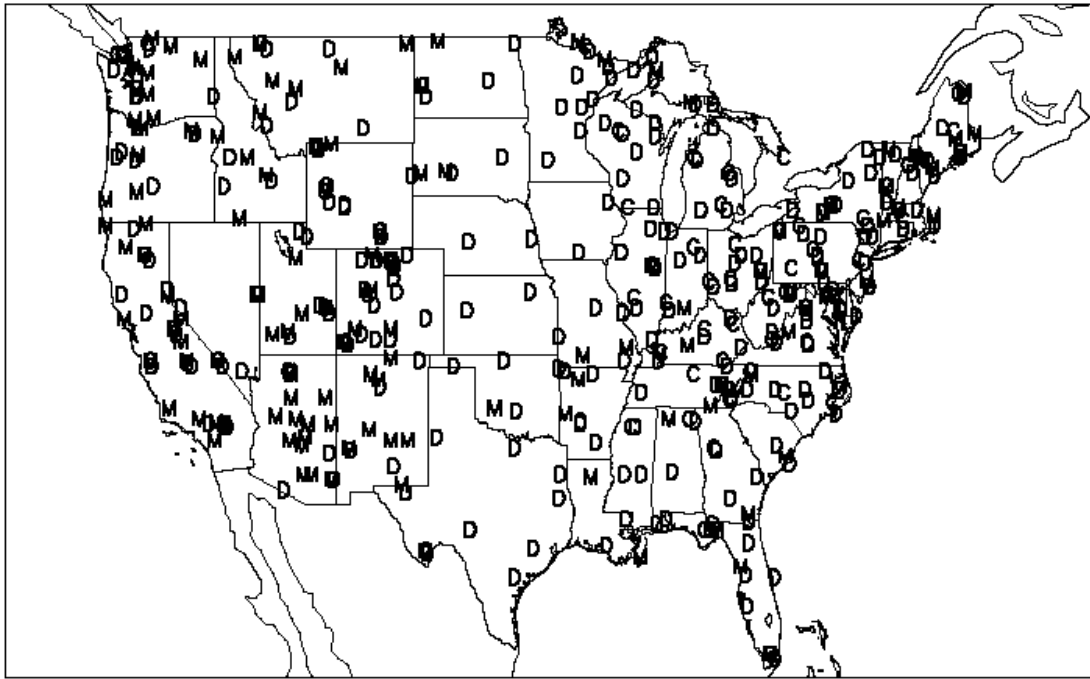


Figure 2. Sampling sites from the I[M]PROVE, [C]ASTNET, and NA[D]P networks in 2001.

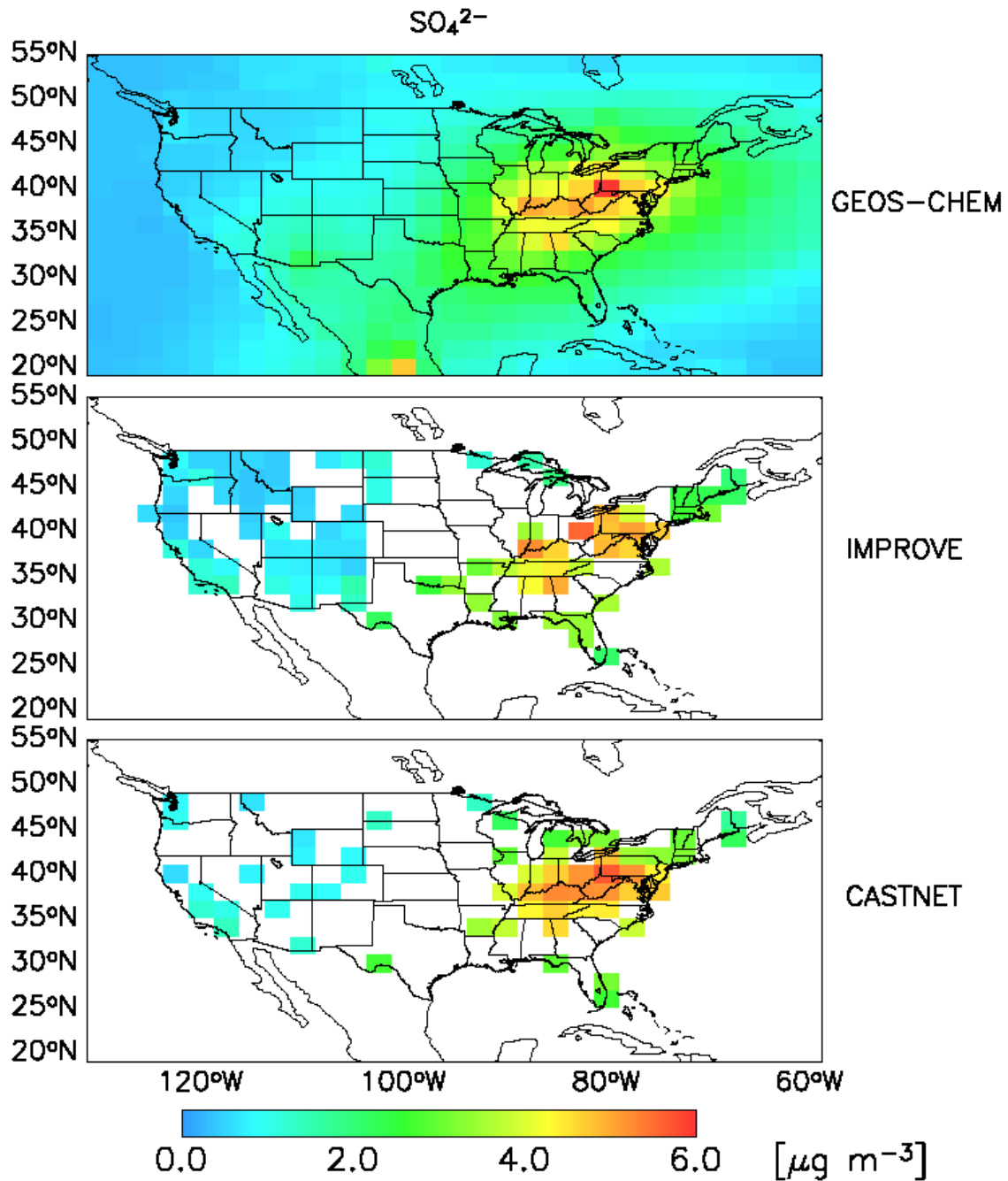


Figure 3. Annual mean concentrations of sulfate in surface air over the United States in 2001. The top panel shows results from the GEOS-CHEM model. The middle and bottom panels show the observations from the IMPROVE and CASTNET networks, respectively, averaged over the model  $2^\circ \times 2.5^\circ$  grid.

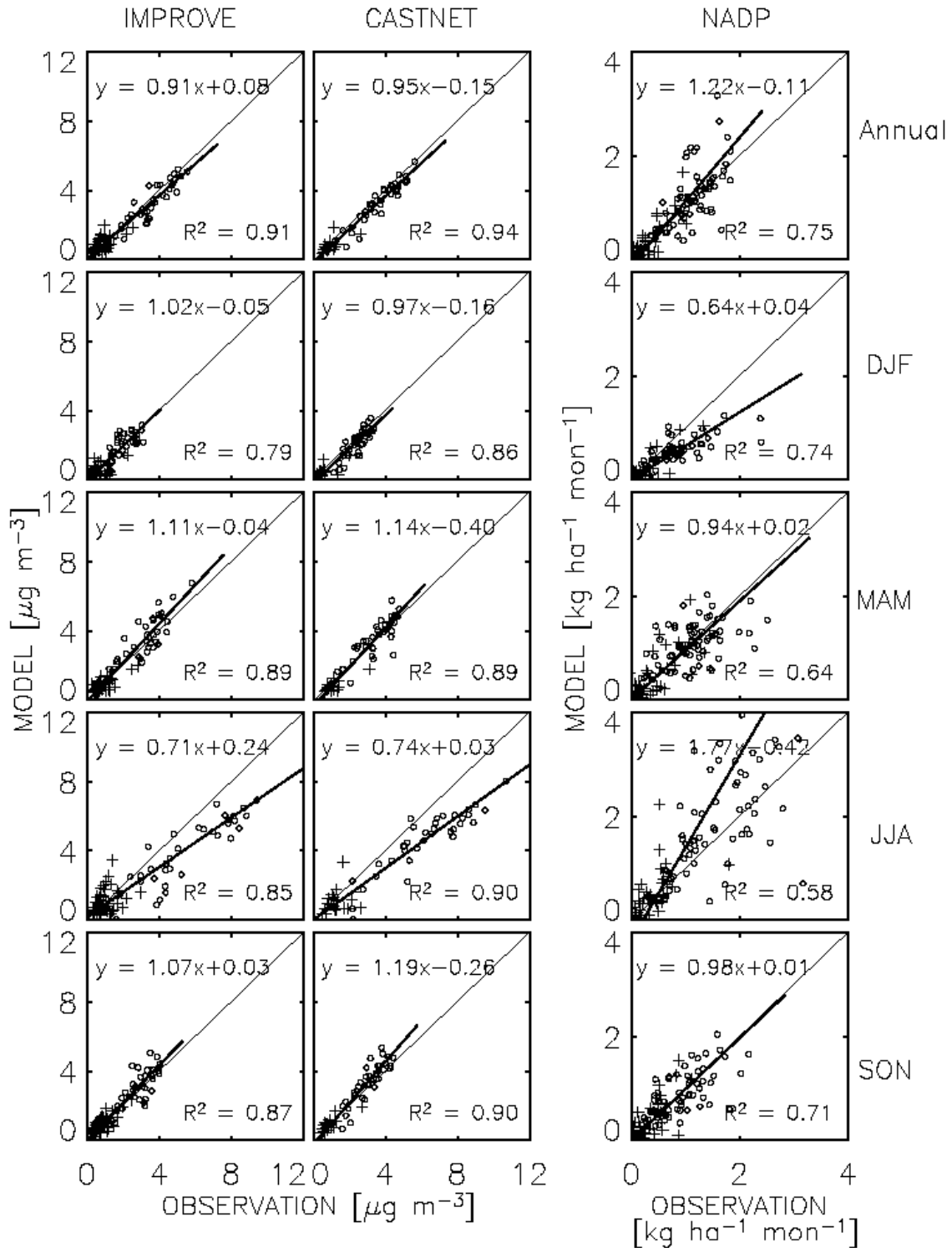


Figure 4. Scatterplot of simulated versus observed sulfate concentrations at the IMPROVE and CASTNET sites, and sulfate deposition fluxes at NADP sites (Figure 2). Values are annual means (top panels) and seasonal means for 2001. Sites in the western and eastern United States (separated at 95°W) are shown as pluses and open circles, respectively. Thick solid lines are reduced major axis regressions for the ensemble of the

data; regression equations and  $R^2$  are shown inset. Thin solid lines show the  $y=x$  relationship.

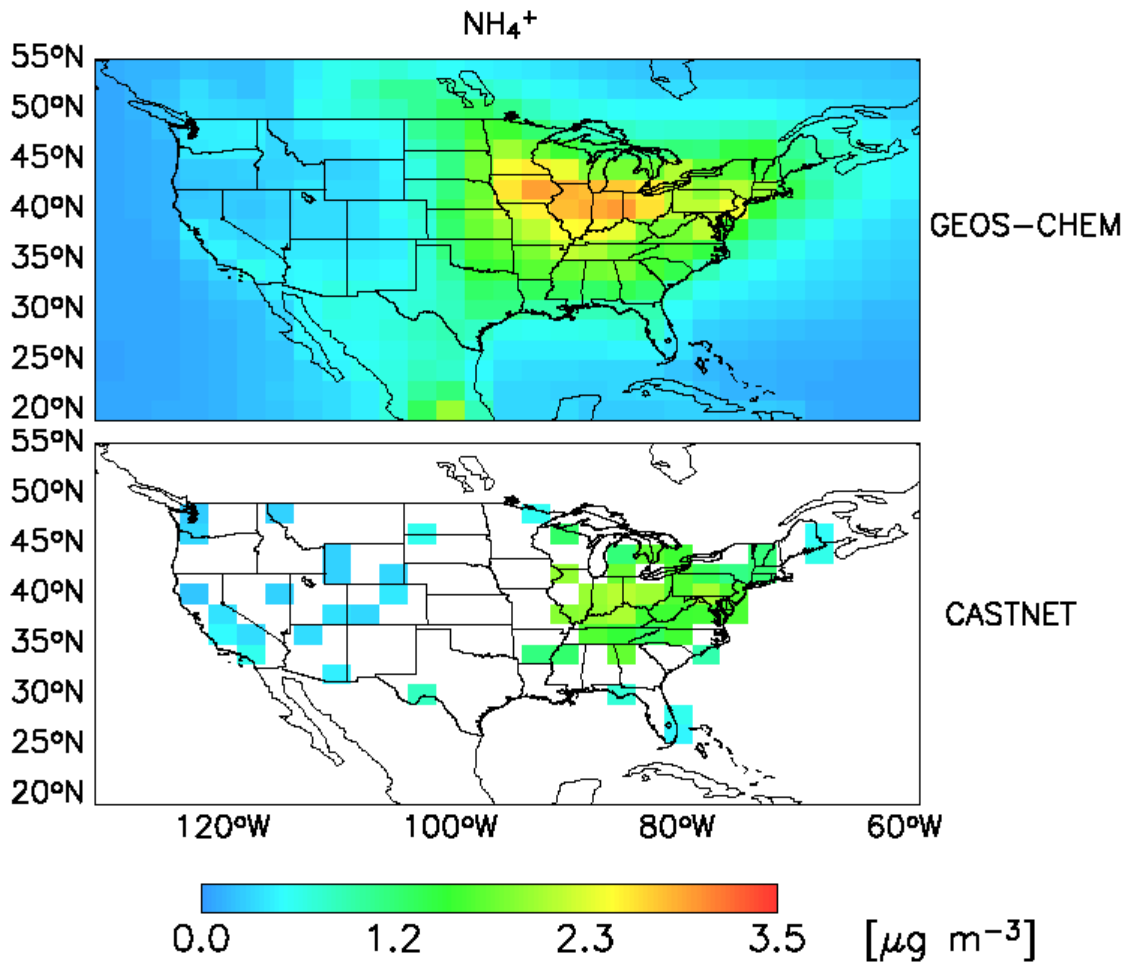


Figure 5. Annual mean concentrations of ammonium in surface air over the United States in 2001. The top panel shows results from the GEOS-CHEM model. The bottom panel shows the observations from the CASTNET networks averaged over the model  $2^\circ \times 2.5^\circ$  grid (ammonium is not measured at the IMPROVE sites).

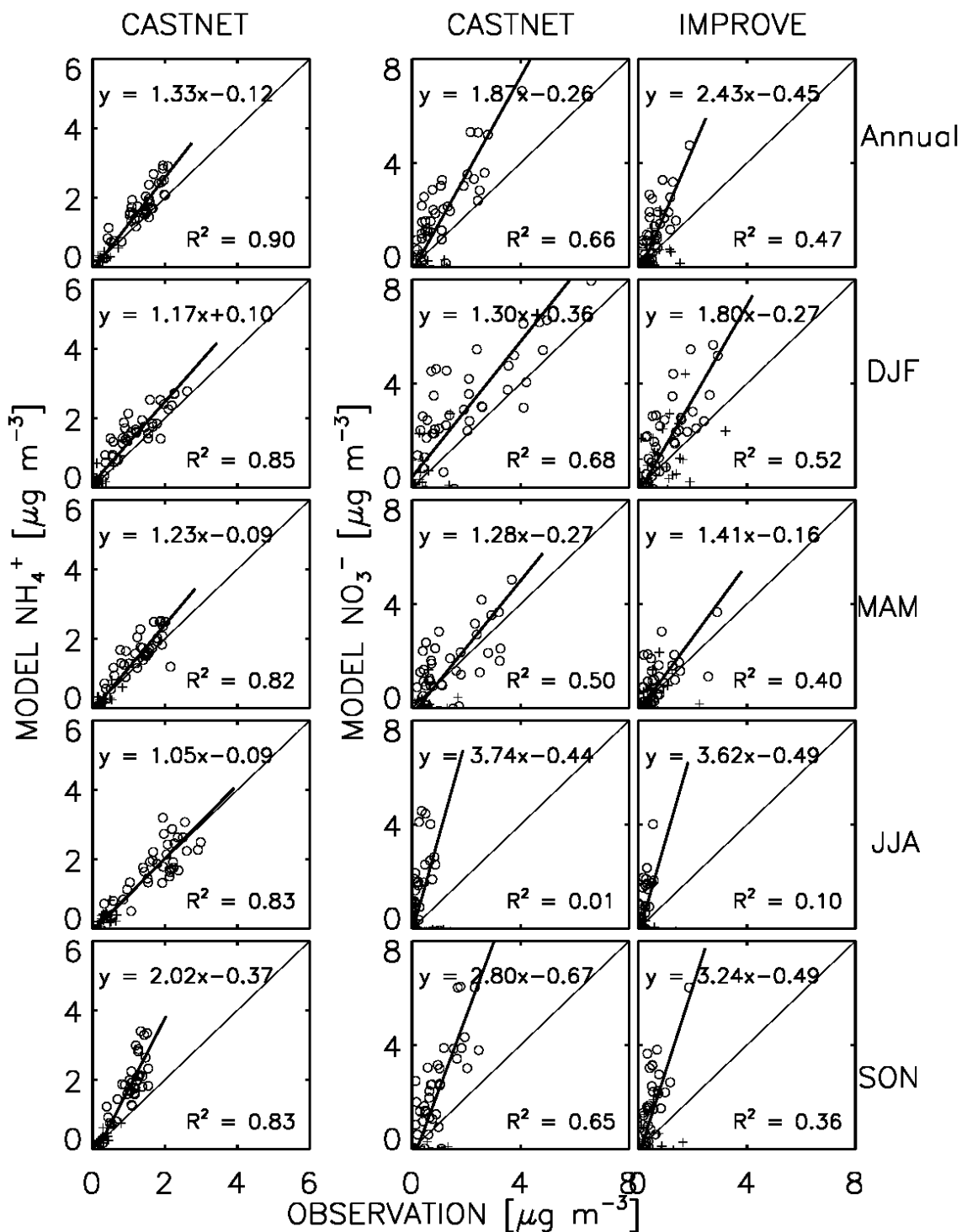


Figure 6. Scatterplot of simulated versus observed ammonium concentrations at the CASTNET sites (left column), and nitrate concentrations at the CASTNET and IMPROVE sites (right two columns). Values are annual means (top panels) and seasonal means for 2001. Sites in the western and eastern United States (separated at 95°W) are shown as pluses and open circles, respectively. Thick solid lines are reduced major axis

regressions for the ensemble of the data; regression equations and  $R^2$  are shown inset. Thin solid lines show the  $y=x$  relationship.

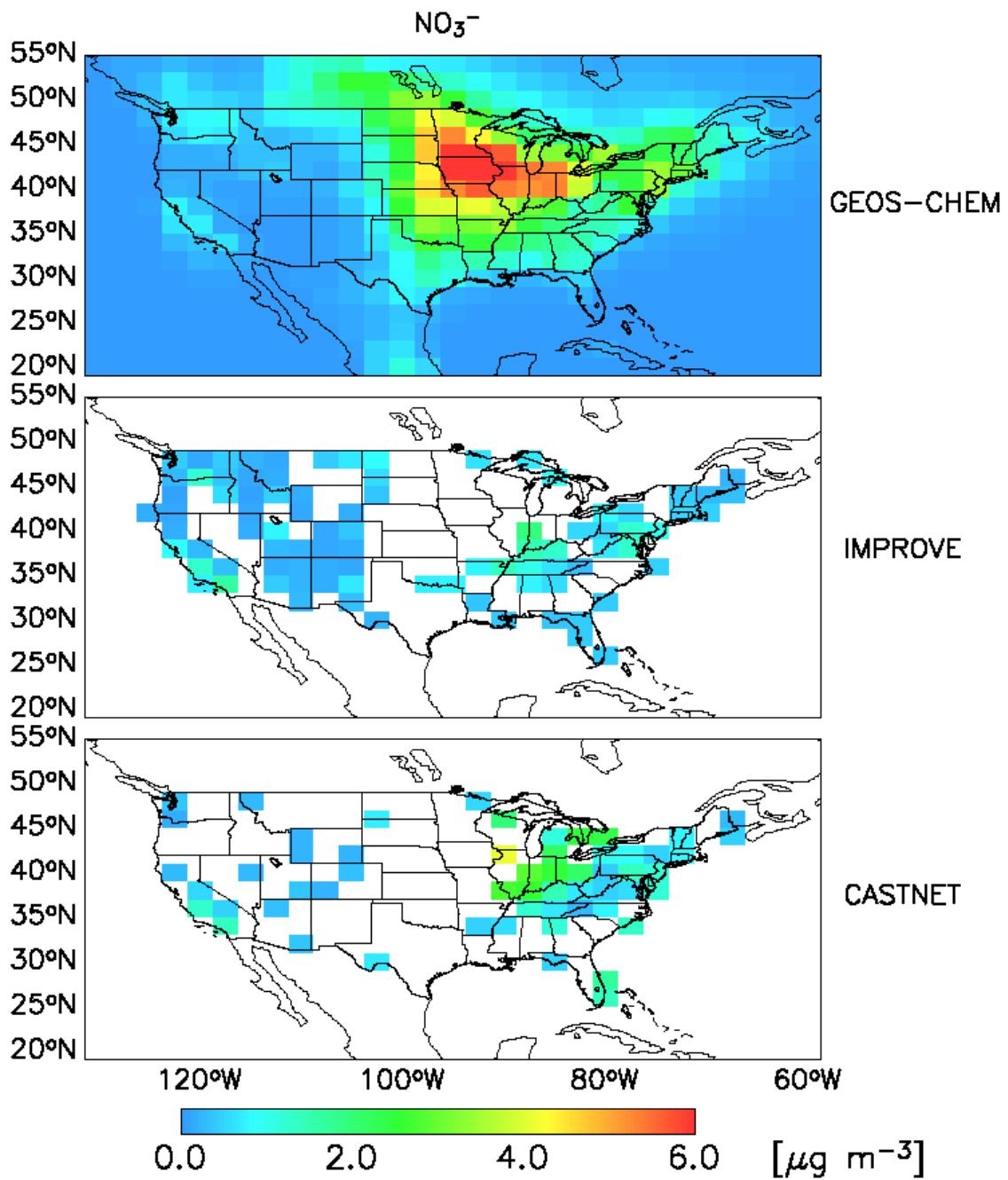


Figure 7. Same as in Figure 3 but for nitrate.

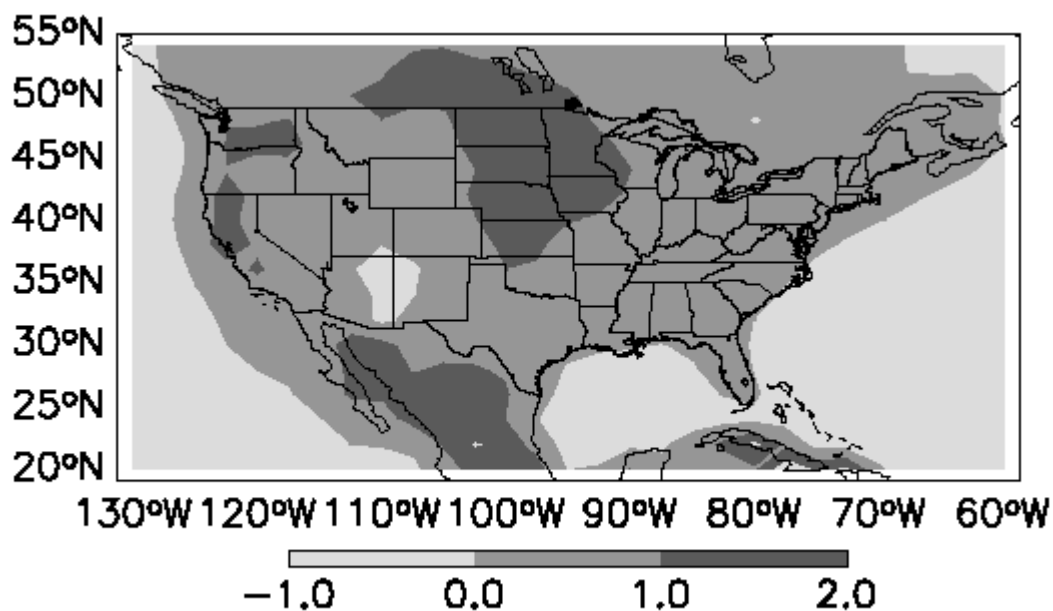


Figure 8. Simulated gas ratio (GR; equation (1)) defined as the available ammonia concentration beyond that required for sulfate neutralization, divided by the total inorganic nitrate concentration (gas + aerosol) [Ansari and Pandis, 1998]. Values are computed from annual mean concentrations in surface air. Formation of ammonium nitrate aerosol is limited by the availability of nitric acid if  $GR > 1$ , by the availability of ammonia if  $0 < GR < 1$ , and is totally suppressed if  $GR < 0$ .

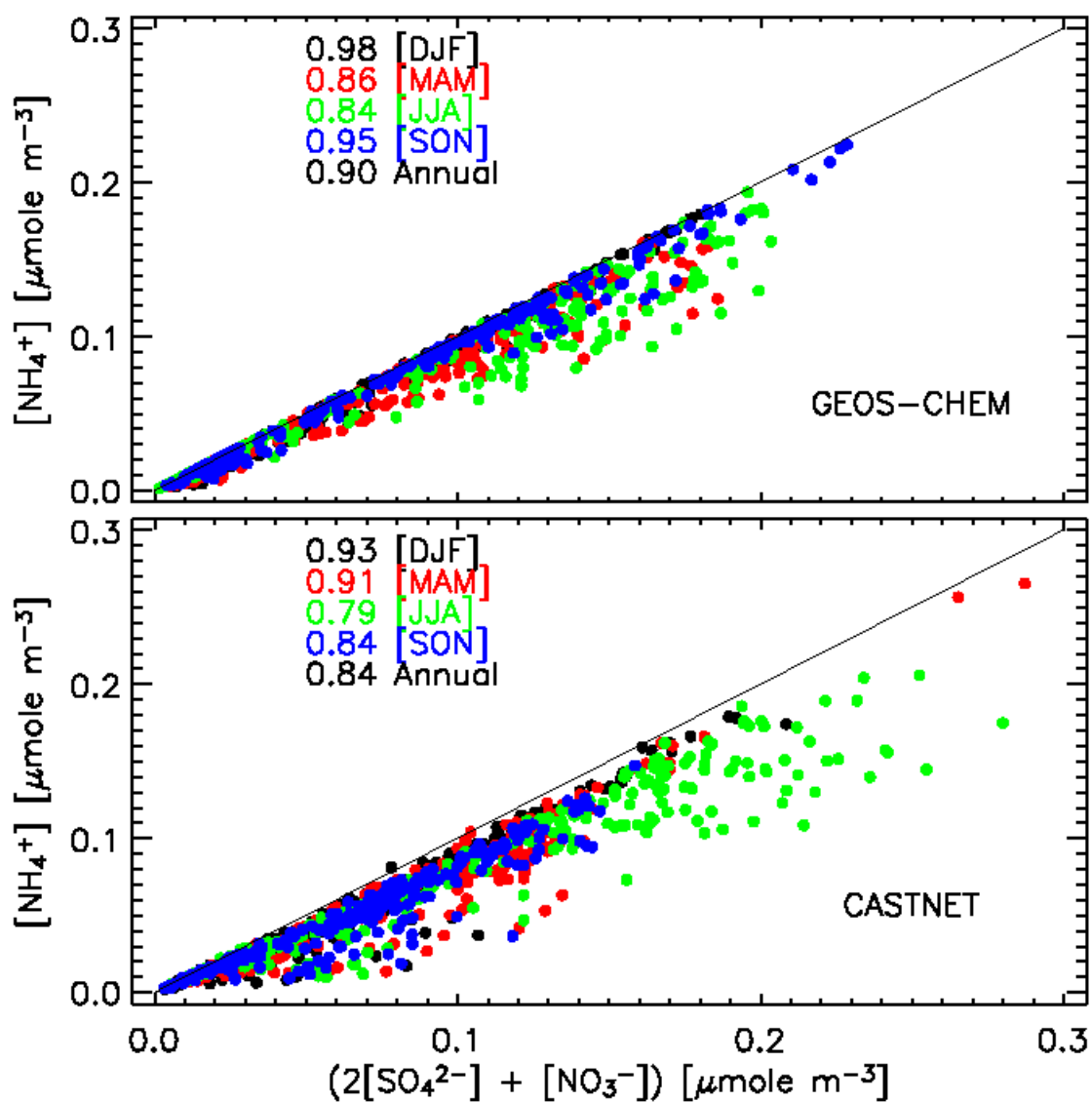


Figure 9. Scatterplot of seasonal mean  $[\text{NH}_4^+]$  vs.  $(2[\text{SO}_4^{2-}] + [\text{NO}_3^-])$  at CASTNET sites in 2001, in the GEOS-CHEM model (top) and in observations (bottom). The reduced-major-axis regression slopes (given on the Figure) indicate the degree of acid neutralization.

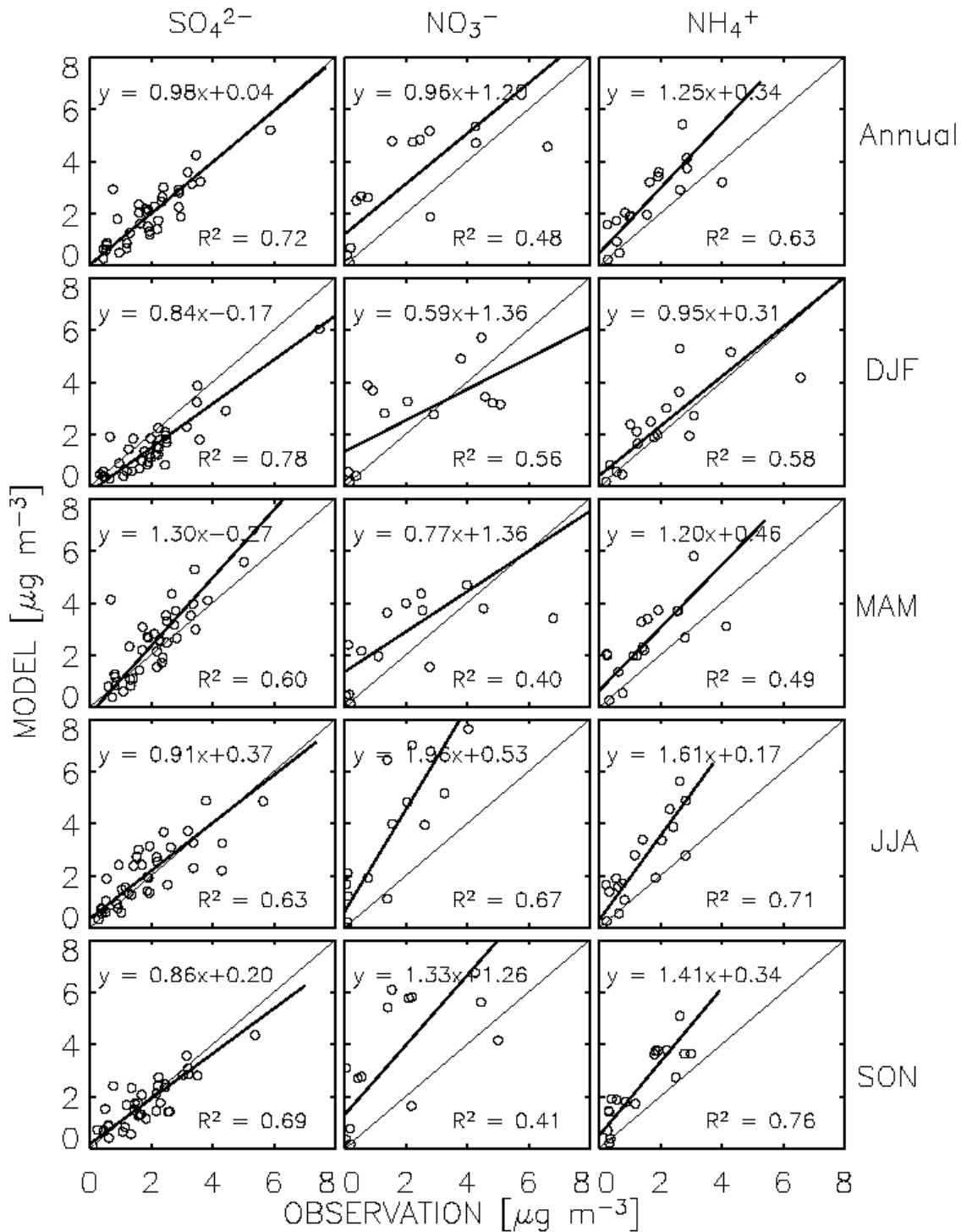


Figure 10. Scatterplot of simulated versus observed sulfate (left), nitrate (middle) and ammonium (right) concentrations at 93 European EMEP sites. Values are annual means (top panels) and seasonal means for 1998. Thick solid lines are reduced major axis regressions for the ensemble of the data; regression equations and  $R^2$  are shown inset. Thin solid lines show the  $y=x$  relationship.

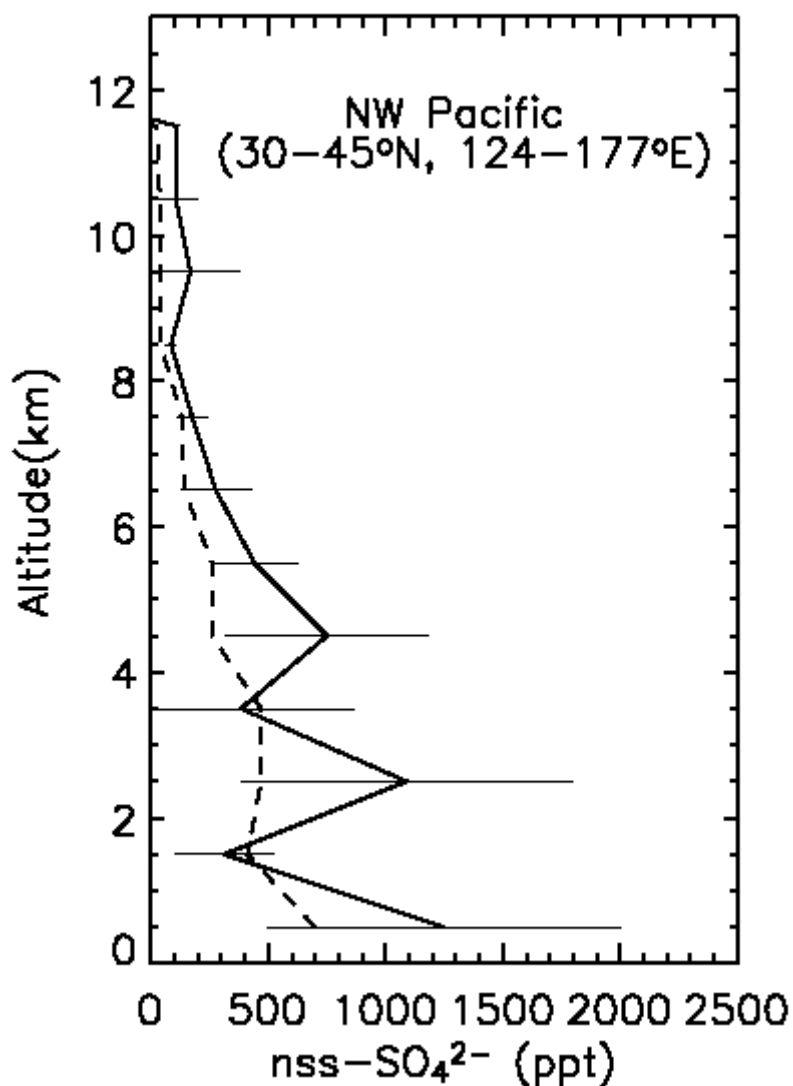


Figure 11. Simulated vs. observed mean vertical profiles of non-sea-salt sulfate ( $\text{nss-SO}_4^{2-}$ ) concentrations over the NW Pacific from the TRACE-P aircraft mission in February-April 2001. The observations are binned vertically in 1-km intervals. The solid line shows mean observed values from *Jordan et al.* [2003] for the ensemble of DC-8 flights north of 30°N (30–45°N, 124–177°E), with standard deviations represented by horizontal bars. The dashed line shows the corresponding monthly mean model values along the flight tracks.

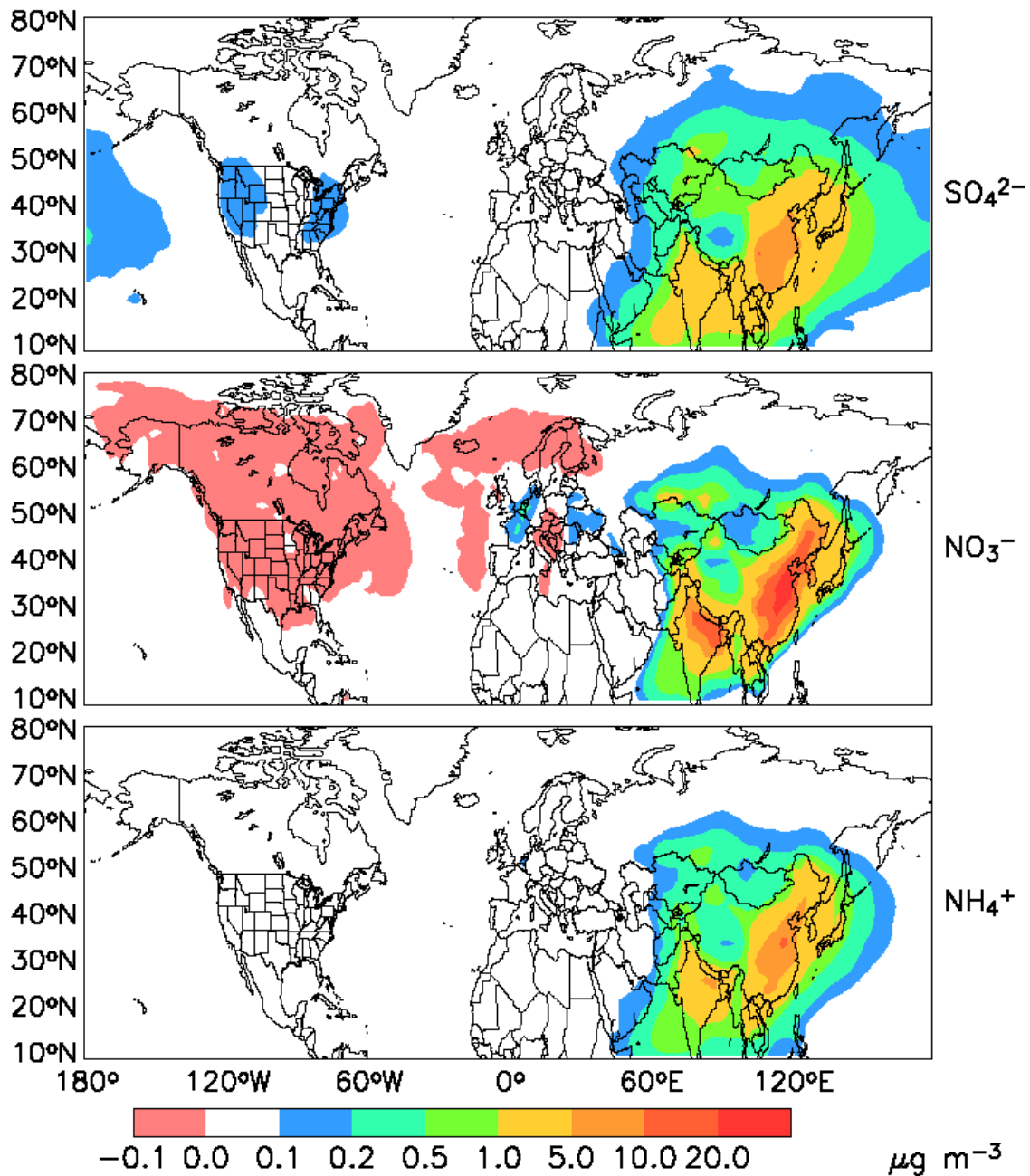


Figure 12a. Enhancements of sulfate-nitrate-ammonium aerosol concentrations in surface air due to anthropogenic emissions from Asia. Values are annual means for 2001 and were obtained by difference between the standard model simulation and a sensitivity simulation with Asian anthropogenic sources shut off.

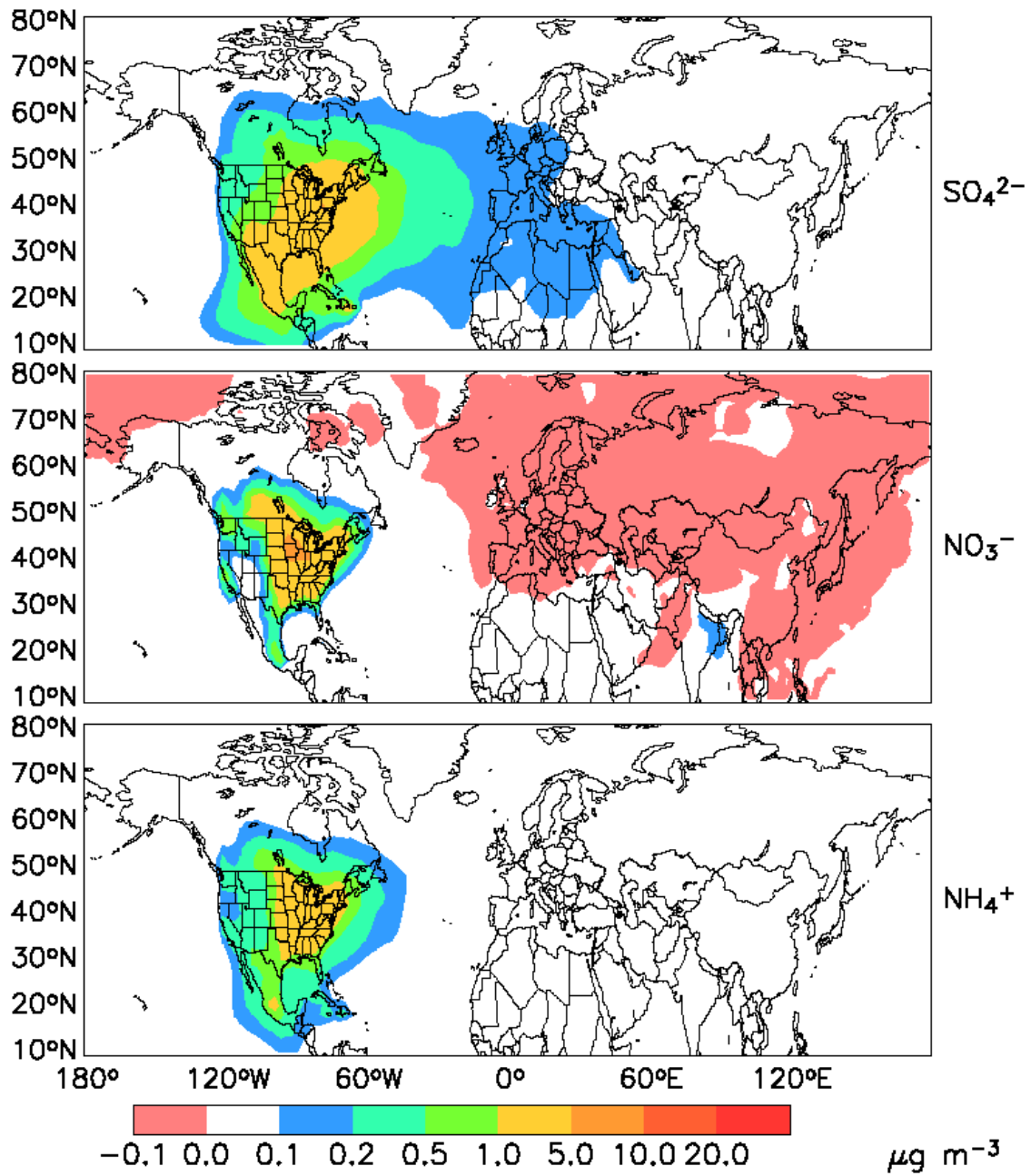


Figure 12b. Same as in Figure 12a but for anthropogenic emissions from North America.

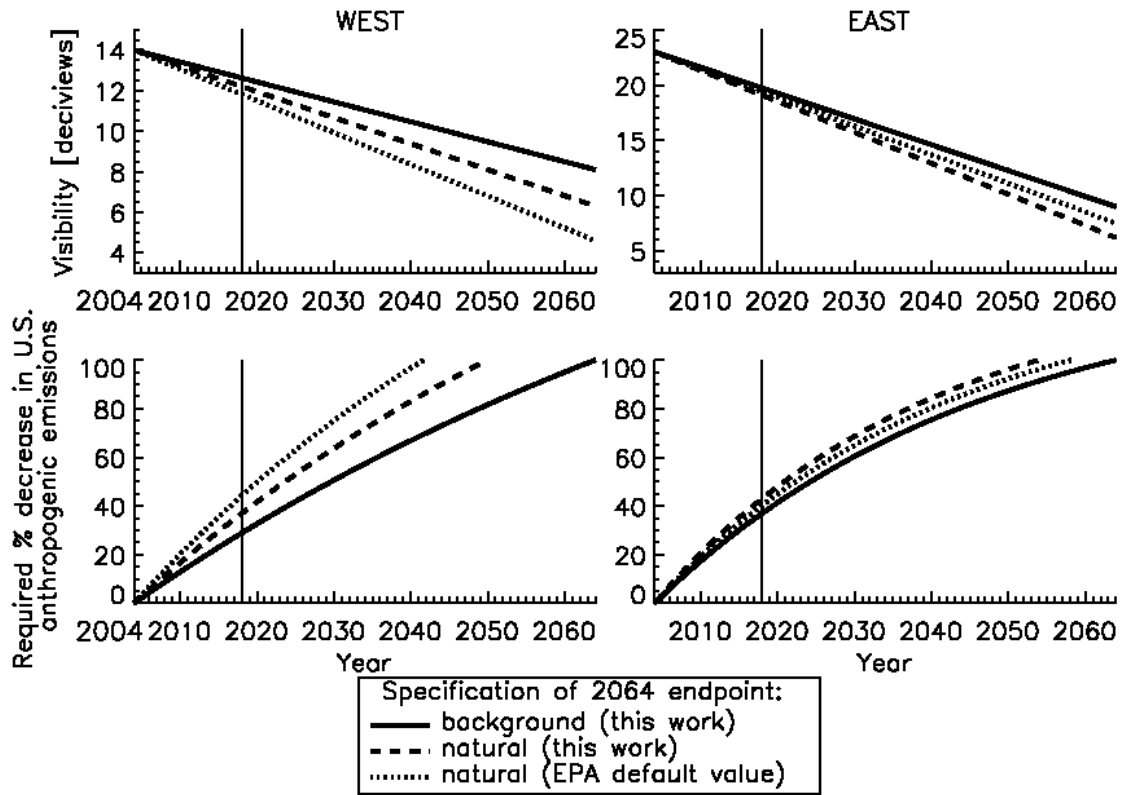


Figure 13. Illustrative example of required visibility improvements (top) and domestic emission reductions (bottom) over the 2004-2064 period for the western and the eastern United States (separated at 95°W) under the EPA Regional Haze Rule [U.S. EPA, 2003a]. The visibility endpoints are as given in Table 3. The required percentage decrease in U.S. anthropogenic emissions corresponding to a given visibility improvement is computed by assuming a linear correspondence between aerosol extinction and emissions. Results are shown for different choices for the 2064 endpoint: (1) EPA natural default visibility (dotted lines), (2) our estimate of natural visibility (dashed lines), and (3) our estimate of background visibility (solid lines). Background includes contributions from both natural and transboundary pollution sources. Year 2018 (thin vertical line) is the target date for phase 1 implementation of the Regional Haze Rule.